2011

Characterization of Novel Akermanite:Poly-E-Caprolactone Scaffolds for Bone Tissue Engineering Aapplications Combined with Human Adipose-Derived Stem Cells

Andre S. Zanetti
Louisiana State University and Agricultural and Mechanical College

CHARACTERIZATION OF NOVEL AKERMANITE:POLY-E-CAPROLACTONE SCAFFOLDS FOR BONE TISSUE ENGINEERING APPLICATIONS COMBINED WITH HUMAN ADIPOSE-DERIVED STEM CELLS

A Dissertation

Submitted to the Graduate Faculty of the
Louisiana State University and
Agricultural and Mechanical College
in partial fulfillment of the
requirements for the degree of
Doctor of Philosophy

in

The Interdepartmental Program in
Engineering Sciences

by
Andre S. Zanetti
D.V.M., Sao Paulo State University, 2006
M.S. in Veterinary Medical Sciences, Louisiana State University, 2009
December, 2011

Acknowledgments

It is a pleasure to thank the many people who made this dissertation possible.

It is difficult to overstate my gratitude to my Ph.D. supervisor, Dr. Daniel J. Hayes. With his passion, his inspiration, and his great efforts to provide available resources, he helped to make the completion of this section of my academic life pleasant and straightforward.

I would like to thank the many people who provided ideal conditions for the development of the research presented in this dissertation: Ted Garthier for his assistance with the lyophilized and the plate reader as well as for letting me use some of his RT-PCR reagents during my pilot study; Julia Y. Chang and Gregory McCandless for the synthesis of akermanite and heat treatment of all ceramic scaffolds used in this dissertation; Marc J Boudreaux for teaching me how to run and analyze qPCR data; Matthew Brown for teaching me how to use the confocal and the fluorescent microscopy at the Biological Sciences Building; Ying Xiao for teaching me how to use the scanning electron microscopy (SEM); Dr. Kenneth Matthews for teaching me how to use the micro-computer tomography machine (μ-CT) in the Physics Department; Dr. Ram Devireddy for letting me use his cell culture facility during my pilot study and for teaching me how to use the cooling machine when we were investigating cryopreservation of scaffolds loaded with human adipose-derived stem cells; and my laboratory colleagues (Lekeith Terrell and Mark Hoppens) for helping me with the fabrication of scaffolds using the unidirectional freezing technique and for assisting me with the analysis of the scaffolds collected from mice, respectively; and for Dr. David Burk for assisting with the histological processing and staining of the scaffolds.

I am indebted to my many graduate student colleagues for providing a stimulating and fun environment in which to learn and grow. I am especially grateful to Jeffrey Cardinale, Britton

Grasperge, Paula Mischler, Sunita Seemanapalli, Rebecca Christofferson, Lekeith Terrell, Niranjan Butchi and Lie Xie.

I am grateful for the College of Engineering Sciences and the Department of Biological Engineering for giving me a home to finish my Ph.D. research project and the administrative assistants (Claudia E. Hawkins, Angela Singleton, Donna T. Elisar and Rhonda D. Shepard) for helping with the deadlines and for assisting me in many different ways.

I would like to thank Dr. Bruce Bunnell and Marjorie McCantes for the human bone marrow-derived stem cells used in the *in vivo* experiment.

I wish to thank Dr. Barry Roberts and Cynthia Kloster for assisting Dr. Daniel J. Hayes and I with the animals and orientation at the Pennington Biomedical Research Center.

I would like to thank Dr. Jeffrey M. Gimble for the adult stem cells and for the countless advices; for sharing his passion to biomedical research; and for believing in my potential during the most difficult times. To him I dedicate most of this work.

I would like also to thank Drs. Cristina Sabliov, Michael J. Keenan and Ram Devireddy for accepting to be part of my Ph.D. research committee.

I wish to thank my entire extended family for providing a loving environment for me. My siblings: Marcello and Fernanda; and my deceased grandparents: Elydia and Americo that, unfortunately, did not physically survive to treasure this moment of happiness with us.

Lastly, and most importantly, I wish to thank my parents, Giuseppe Americo Zanetti and Marilene C. Serrano Zanetti. They born me, raised me, supported me, taught me, and loved me. To them I dedicate this entire dissertation.

This study was supported by the Longwell Family Foundation and the Pennington Biomedical Research Foundation.

Table of Contents

List of Tables

List of Figures

Abstract

The development of porous materials useful as scaffolds for the sustained three-dimensional (3D) growth of human adipose-derived stem cells (hASC) is of particular interest to facilitate healing after musculoskeletal injuries. In this study, a composite porous material obtained by blending akermanite with poly-e-caprolactone (PCL) is proposed as novel alternative to bone tissue regeneration. The objectives of this study are (1) to characterize the akermanite:PCL scaffold properties; (2) to investigate the *in vitro* osteogenic potential of hASC loaded to optimal akermanite:PCL scaffolds; (3) to assess the metabolic activity and osteogenesis of hASC loaded to optimal akermanite:PCL scaffolds after cryopreservation in post-thawed scaffolds; and (4) to evaluate the behavior of optimal akermanite:PCL scaffolds *in vivo* using an immunodeficient murine model for ectopic bone formation. We hypothesized that (1) optimal akermanite:PCL blend has mechanical properties and biocompatibility suitable for tissue engineering applications; (2) hASC loaded to optimal akermanite:PCL scaffolds has higher expression of mature osteogenic marker in scaffolds cultured in osteogenic medium for 21 days; (3) PVP-serum free medium can be used to cryopreserve hASC loaded to optimal akermanite:PCL scaffolds; and (4) hASC preloaded to optimal akermanite:PCL scaffolds would produce meaningful bone-like tissue 8 weeks post-implantation. According to the results, 75:25 akermanite:PCL composite scaffolds displayed increased mechanical (1), biological and osteogenic properties (1-3). Moreover, hASC loaded to 75:25 akermanite:PCL scaffolds and frozen at 40^{o}C/min displayed metabolic activity and osteogenesis comparable to fresh control scaffolds (3). However, *in vivo* implantation of akermanite-base scaffolds (akermanite and akermanite:PCL) led to sudden death within the first 48 hours of this study (4). The acute toxicity observed in all animals assigned to the akermanite scaffolds was associated to a

disturbance of the phosphorus homeostasis *in vivo*. Specifically, akermanite and akermanite:PCL scaffolds harvested 48 hours post-implantation had comparable levels of phosphorous in their composition, indicating acute phosphorous depletion from the serum. Accumulative evidences have suggested that akermanite is biocompatible and can enhance adhesion, proliferation and osteogenic phenotype maintenance of adult/osteoprogenitor stem cells both *in vitro* and *in vivo*. As a conclusion, further studies are needed to address the akermanite dose-dependent toxicity in murine models for akermanite-assisted bone regeneration.

Chapter 1. Human Adipose-Derived Stem Cells and 3D Scaffold Constructs: A Review of the Biomaterials and Models Currently Used to Regenerate Bone

1.1. Introduction

Since the discovery of the human adipose-derived mesenchymal stem cells (hASC) osteogenesis[1], research has substantially progressed toward the use of hASC as stem cell source for bone regeneration. Although some applications would initially involve direct administration of stem cells into the target fracture site, current paradigms describing scaffolds loaded with stem cells are thought to be preferential in guiding bone regeneration by providing support for cell colonization, migration, growth, and differentiation[2]. During the preceding decade, several cell characterization studies have extensively described the differentiation potential and function of hACS both *in vitro* and *in vivo* along with the benefits of scaffold directed hASC osteogenesis (Table 1).

Perhaps, the most compelling evidence supporting the emerging clinical applications of hASC-scaffolds to promote fracture healing in humans was reported in 2004 after a combination of autogenous hASC and bone grafts were used to treat an extensive craniofacial injury in a 7-year-old girl[3]. In the literature, scaffold-based bone tissue engineering in combination with adult stem cells is well established[4-6], however compiled information regarding scaffold use in combination with hASC is still lacking. Therefore, this review will present a historical background on hASC osteogenesis; along with the findings of the current *in vitro* and *in vivo* hASC-scaffolds models as discussed with emphasis on biomaterial properties; finally, a brief discussion on the potential impact of standardization of the current protocols for future hASC-scaffolds applications is also described.

Table 1. Summary of current representative bone tissue engineering models combined with hASC.

		Scaffolds	# Donors (Age)	Cell density	Pathways	OS marker	Study type	Model	Species	Weeks	References
Polymers	*Commercial*	Autologous fibrin blue + (MacroPore PS®)	1 (7 years)	Injection of $3X10^6$ SVF	OS	-	*In vivo*	Calvarial defect	Human	12	3
	Fabricated	PLGA	3 (32-48 years)	Injection of $1X10^6$ hASCs transfected with RunX2 and OSX	OS	OCN, RunX2, OSX, ALP, BSP COL1A1	*In vitro, In vivo*	Ectopic bone formation (subcutaneous)	Nude mouse	2 (*In vitro*), 6 (*In vivo*)	39
		PLGA	4 (20-36 years)	Loading of $1.1X10^6$ hADCSs on top of discs	OS	ALP, BMP-2	*In vitro, In vivo*	Calvarial defect (local injection of 5µM ALN for 1 week)	Sprague-Dawley rat	2 (*In vitro*), 12 (*In vivo*)	40
		mPEG-PCL gel	1 (Young woman)	Mixing $2X10^5$ hADSCs with co-polymer	OS	ALP	*In vitro, In vivo*	Ectopic bone formation (subcutaneous)	Fisher rat	3 (*In vitro*), 2 and 4 (*In vivo*)	38
		Hydrogel	1 (Patient -hAMSCs), 1 (Young child hBMSCs)	Mixing $2.5X10^6$ G.Luc-hAMSCs/hBMSCs	OS	von Kossa	*In vitro, In vivo*	Calvarial defect	Nude mouse	3 (*In vitro*), 12 (*In vivo*)	41
		Atellocollagen	3 (22-30 years)	Loading of $2X10^5$ ATSCs on top of discs	OS	OCN, ALP	*In vitro, In vivo*	Ectopic bone formation (subcutaneous)	Nude mouse	4 (*In vitro*), 4, 6 and 8 (*In vivo*)	42
Natural grafts	*Commercial*	Acellular xenograft (Bio-Oss® and ChronOS®)	7 (mean 32 years)	Loading $8.3X10^6$-$25.0x10^6$ SVF/cm^3 on fibrin hydrogel	OS, AD, ANG	OCN, BSP	*In vivo*	Ectopic bone formation (subcutaneous)	Nude mouse	8	43
	Fabricated	Decellularized bovine bone	4 (? years)	Loading $1.5X10^6$ hASCs on top of discs	OS	OP, COL, BSP	*In vitro*	-	-	5	45
Ceramics	*Commercial*	Titanium (Trabecular Titanium™)	3 (? years)	$1x10^6$ hASCs on top scaffolds	OS	OCN, OP, ALP, COL1	*In vitro*	-	-	4	46
		β-TCP (Symphapore®)	5 (30-40 years)	Loading $3X10^5$ ADSCs/disc	OS	OCN, ALP, OP, FAK	*In vitro*	-	-	4	34
		β-TCP (Symphapore®)	5 (32-40 years)	Loading $2X10^5$ ADSCs-FL/disc	OS	OCN, BSP, ALP	*In vitro*	-	-	4	43
		HA (Engipore®)	7 (mean 32 years)	Loading $8.3X10^6$-$25.0x10^6$ SVF/cm^3 on fibrin hydrogel	OS, AD, ANG	OCN, BSP	*In vivo*	Ectopic bone formation (subcutaneous)	Nude mouse	8	30
		HA (Engipore®)	5 (20-63y)	$8.6X10^5$ SVF/mL by direct perfusion	OS, AD, ANG	BSP	*In vitro, In vivo*	Ectopic bone formation (subcutaneous)	Nude mouse	8	47
		HA (Engipore®)	12 (20-63 years)	Loading $3X10^6$ SVF on top of discs	OS, AD, ANG	OP, ALP	*In vitro, In vivo*	Ectopic bone formation (subcutaneous)	Nude mouse	3 (*In vitro*), 8 (*In vivo*)	48
	Fabricated	Bioactive glass coated with Ca-P	9 (mean 48 years)	Loading $5X10^5$ ASCs on top of discs	OS	ALP	*In vitro*	-	-	2	49
		Biactive glass, β-TCP	9 (mean 48 years)	Loading $5X10^5$ ASCs on top of discs	OS	OP, ALP	*In vitro*	-	-	2	50
		Bioactive glass coated with zinc	9 (mean 48 years)	Loading $5X10^5$ ASCs on top of discs	OS	OP, ALP	*In vitro*	-	-	2	26
		Akermanite, β-TCP	3 (mean 32 years)	$3x10^3$ hASCs/cm^2	OS	OCN, COL1, ALP, Cbaf-1	*In vitro*	-	-	1	30
Ceramics+Polymers	*Commercial*	β-TCP-mPCL coated or not with collagen and fibrin (Osteopore®)	? (30-50 years)	Mixing $3X10^4$ ADSCs/µL of fibrin	OS	OCN, ALP, ON	*In vitro*	-	-	4	33
	Fabricated	Apatite-PLGA	9 (mean 48 years)	Loading $5X10^5$ ASCs on top of discs	OS	ALP	*In vitro*	-	-	2	49
		Bioactive glass-PLA, β-TCP-PLA	6 (mean 44 years)	Loading $3.5X10^5$ ASCs on top of discs	OS	ALP	*In vitro*	-	-	2	52
		β-TCP-PLA	1 (48 years)	Loading of $2X10^4$ hASCs on top of discs	OS	ALP	*In vitro*	-	-	3	15
		β-TCP-PCL	3 (hATMSCs, 20-56 years), 5 (hBMSCs), 3 (haMSCs, 19-35 years), 3 (hUMSCs)	Loading $1.6X10^5$ hATMSCs, hBMSCs, haMSCs or hUMSCs on top of each disc	OS	ON, COL1A1, RunX2, ALP	*In vitro, In vivo*	Ectopic bone formation (subcutaneous)	Nude mouse	4 (*In vitro*), 4 and 8 (*In vivo*)	53
		HA-PLGA coated with BMP-2	3 (mean 32 years)	Loading $2.5X10^6$ ADSCs on top of each disc	OS	BMP-2, OCN, OP, ALP	*In vitro, In vivo*	Ectopic bone formation (subcutaneous)	Nude mouse	4 (*In vitro*), 12 (*In vivo*)	53
		β-TCP-mPCL	? (adult donors)	Loading $5X10^3$ hADSCs /mL	OS	ON, OP, COL1	*In vitro, In vivo*	Ectopic bone formation (subcutaneous)	Nude mouse	4 (*In vitro*), 12 (*In vivo*)	54

*PLGA: poly-lactic-glycolic acid; mPEG-PCL: monopolymer poly(ethylene glycol)-poly-e-caprolactone; β-TCP: β-tricalcium phosphate; HA: hydroxyapatite; Ca-P: calcium phosphate; PLA: poly(l-lactic acid); BMP-2: bone morphogenic protein-2; hAMSCs: human adipose mesenchymal stem cells (MSCs); hBMSC: human bone marrow MSCs; hATMSCs and ATSCs: human adipose tissue MSCs; hfMSCs: human fetal MSCs; haMSCs: human adult MSCs; hUMSCs: human umbilical MSCs;ASCs, hASC and hADSCs: human adipose-derived stem cells; G.Luc: green luciferase protein; SVF: stromal vascular fraction; ADSCs-FL: human adipose-derived fibroblast-like stem cells; OS: osteogenic; AD: adipogenic: ANG: angiogenic; OCN: osteocalcin; OSX: osterix; ALP: alkaline phosphatase; BSP: bone sialoprotein; OP: osteopontin; COL/COL1A1/COL1: collagen type 1; ON: osteonectin; Cbaf-1: core binding alpha factor-1; ALN: alendronate.

1.2. hASC Osteogenesis: A Retrospective Analysis

1.2.1. Isolation, Characterization and Problems with Nomenclature

The term processed lipoaspirate (PLA) cells was first used to describe a subpopulation of progenitor cells isolated from human lipoaspirates in 2001[7]. While the osteogenic potential of PLA cells remained elusive in this report, abnormal adipose tissue mineralization was a well-known pathologic process in several diseases[8]. Moreover, the embryologic origin of adipose tissue offered clues of the presence of a mesenchymal stem cell (MSC) population in PLA cells. Confirmation of the multilineage potential of these PLA cells was provided one year later by the same group[1].

To date, elective subcutaneous liposuction procedures remain the gold standard for human adipose tissue collection[1,7]. The surgical procedure yields anywhere from 300 mL to several liters of lipoaspirate[7,9]. The protocol for isolation of cells from lipoaspirate (or the stromal vascular fraction – SVF) was initially described by Rodbell in three consecutive articles published in the *Journal of Biological Chemistry* in 1966[10-12]. This procedure consisted of homogenization of adipose tissue, consecutive saline washes to remove erythrocytes and other hematopoietic cells, collagenase digestion, and separation of undigested adipose tissue from the pelleted stromal vascular fraction (SVF) containing the ASC. For human lipoaspirate samples, one of the current protocols describes the isolation of 308,849 cells per ml of lipoaspirate[13]. Recently, two automated systems were introduced to accelerate SVF isolation (Cellution® 800/900, Cytori therapeutics; TGI 1000™ cell isolation system, Tissue genesis) but, in general, isolation of hASC for scaffold-based applications remains almost identical to the protocols originally described (Figure 1).

Currently, more than 200,000 elective liposuction procedures are performed annually in the United States and over a million worldwide[14]. Due to ease of harvest and abundance, hASC isolated from lipoaspirates are attractive, readily available adult stem cells that have become increasingly popular for use in many studies (Table 1). Compared to human bone marrow (hBMSC) or umbilical cord stem cells (hUMSC), hASC have similar self-renewal *in vitro*[15]; and the ability of hASC to differentiate in other mesodermal lineages has been demonstrated on several occasions[1,7]. Other studies have indicated that hASC can also be reprogrammed to behave-like cells of ectodermal[16,17] and epidermal[18] lineages. However, despite their apparent pluripotential, hASC lack the potential of embryonic stem cell to differentiate into all embryonic and extraembryonic tissue types[19]. Moreover, expression of surface proteins indicated that hASC differed phenotypically from hBMSC and hUMSC[20]. In general, uncommitted hASC express the surface markers CD29, CD44, CD71, CD90, CD105/SH2, and SH3 but do not express STRO-1 and the hematopoietic markers CD34, CD45 and C117[7,14]. Even though, great strides have been made in the characterization and isolation of pure hASC populations in recent years, establishment of homogeneous cultures is still challenging, particularly because of the lack of universal hASC markers.

Since Zuk et al[1] first reported the PLA cells multipotential, a variety of terms have been used to describe the plastic adherent cell population isolated from collagenase digests of lipoaspirates. A selection of the most common variations of names can be found in Table 1. Efforts have been made by the regenerative medicine community to refine the nomenclature of multipotent cells isolated from adipose tissue. A consensus was reached at the Second Annual International Fat Applied Technology Society Meeting, in 2004, to use the acronym ‘‘ASC’’ for adipose-derived stem cells[21]. Caplan[22] popularized the term mesenchymal stem cell or MSC to specifically refer

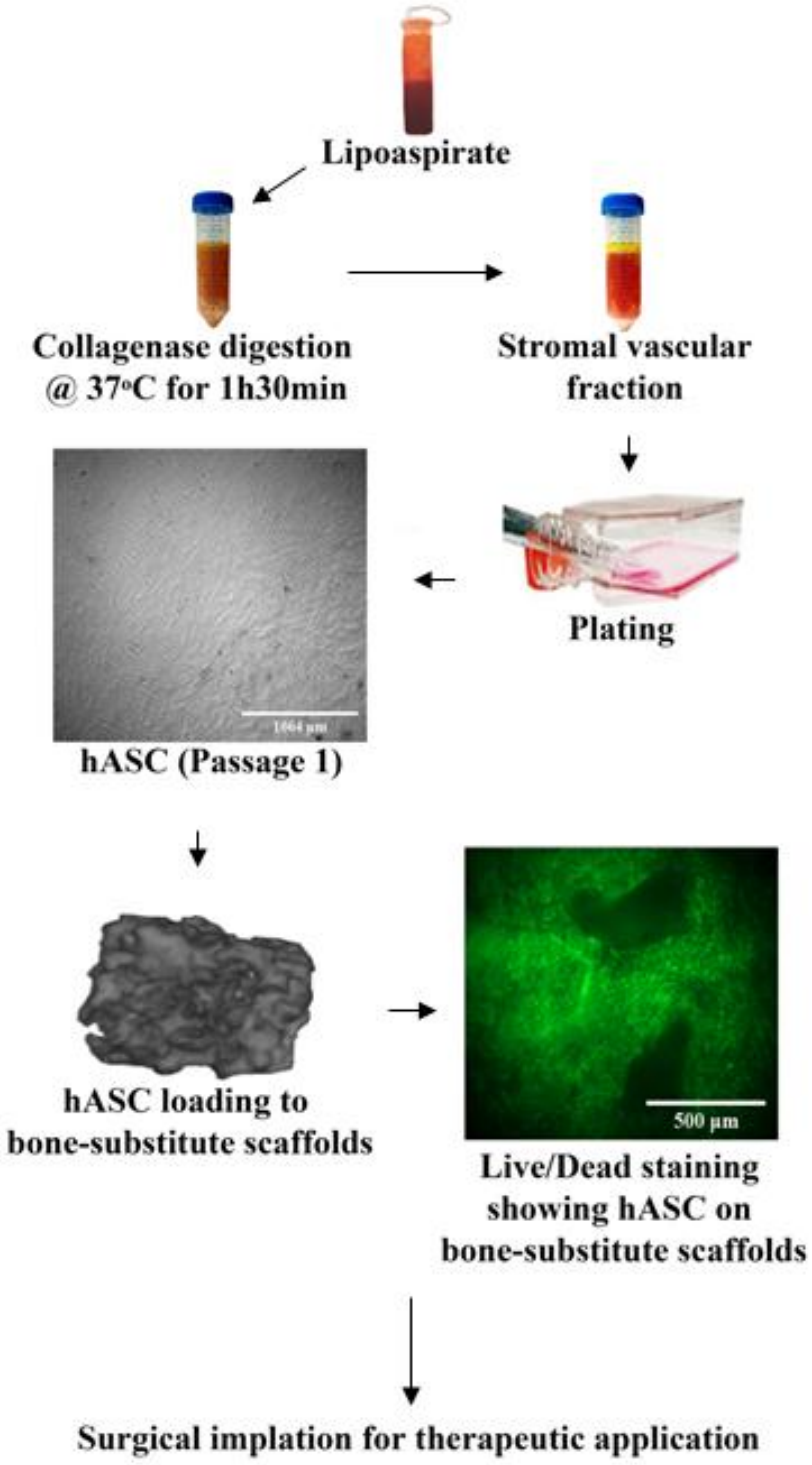

Figure 1. Bone tissue engineering paradigm with human adipose-derived stem cells (hASC). From hASC isolation and expansion to scaffold loading and surgical implantation.

to the non-embryonic subpopulation of cells isolated from bone marrow and periosteum. The Mesenchymal and Tissue Stem Cell Committee (MTSCC) of the International Society for Cellular Therapy concluded that there is not enough scientific information available to accurately support stemness in plastic-adherent populations of cells[23]. Therefore, in 2005 the MTSCC recommended that the use of the term mesenchymal stem cells should be reserved for population of cells with proven self-renewal and multilineage differentiation potentials. For plastic-adhered population of cells that do not meet these criteria, the MTSCC strongly encouraged the replacement of the term 'stem' in MSC to 'stromal'[23]. In agreement with this recommendation, the use of the "ASC" acronym to mean "adipose-derived stromal cells" is also accepted.

1.2.2. Culture Requirements

Following human adipose tissue digestion, the SVF pellets were initially resuspended in control medium (Dulbecco's modified Eagle's medium (DMEM), 10% FBS, 1% antibiotic/antimycotic solution) and plated at high cell densities[1,2]. Today, hASC are usually maintained in medium containing DMEM/Ham's F12, 10% FBS, and 1% penicillin/streptomycin/amphotericin and often supplemented with epidermal growth factor (EGF), fibroblast growth factor (FGF-β) and transforming growth factor (TGF-β)[24]. Additionally, protocols also differ in recommendations for cell seeding density. Evidences suggest that high cell densities impair hASC multipotent properties; therefore, low seeding density and subconfluent passaging are recommended[14,17,18,24]. While bovine serum has raised awareness to the potential transmission of zoonotic diseases to recipients, hASC culture in serum-free medium[25] or low concentrations of human serum supplemented with FGF-β and EGF have also been proposed [24]. Standardization of the hASC culture conditions could facilitate comparisons between different studies.

1.2.3. hASC Osteogenic Differentiation

Deriving bone from hASC requires a well-defined process wherein hASC differentiate into osteoblast precursors (osteoprogenitor, pre-osteoblast), followed by the maturation of osteoblasts and the formation and mineralization of a matrix[6]. In the Zuk et al report[1], mRNA expression of the osteogenic transcription factor core binding alpha factor 1 (Cbaf-1/RunX2) was first detected after 4 days in hASC cultured in osteogenic medium [DMEM, 10% FBS, 0.01 μM 1,25-dihydroxyvitamin D3 (or 0.1 μM dexamethasone), 50 μM ascorbate-2-phosphate, 10 mM β-glycerophosphate, and 1% antibiotic/antimycotic]. Up-regulation of Cbaf-1 in hASC starts to take place as early as day 1 of culture in osteogenic media preparations[26] similar to the finding originally described[1]. Current research indicates that the molecular mechanism of MSC osteoblastogenesis resembles the mechanism observed during the development of the skeleton, where hedgehog[27], Wnt and BMP[28] (bone morphogenic protein) signaling pathways play major roles. In particular, costimulation of the Wnt and BMP pathways produces pronounced osteogenic differentiation of multipotent cells in vitro[28]. BMPs stimulate the transcription of Cbaf-1 and Osterix (OSX), which in turn activates osteoblast-specific genes such as alkaline phosphatase (ALP), osteopontin (OP), osteonectin (ON), bone sialoprotein (BSP), collagen type 1 (COL1) and osteocalcin (OCN) by binding to the osteoblast-specific cis-acting element 2 (OSE2) in the promoter region of these genes[28]. Alkaline phosphatase is an early stage marker for osteogenic differentiation, while COL1 and OCN are only expressed by mature osteoblasts[26]. As little information is available regarding the downstream regulatory events responsible for the commitment of hASC toward the osteogenic pathway, *in vivo* studies have relied on the ability to monitor the expression of one or more of these osteogenic makers in committed hASC during formation of functional bone (Table1).

Bone remodeling is a process of continuous resorption and neosynthesis that determines bone structure and quality during adult life. Bone formation and bone resorption are coupled processes. For instance, mature osteoblasts can modulate osteoclast formation by expressing the negative regulator osteoprotegrin (OPG) or the positive regulator RANKL (receptor activator of NFB ligand)[29]. Imbalances of bone remodeling can result in severe perturbations in skeletal structure and function. For example, osteoporosis results in reduction of bone density in aged people. The disease affects millions worldwide and individuals living with osteoporosis are more at risk of fracture[14]. As hormonal differences are observed between gender and within age groups, hASC osteogenesis is, therefore, predicted to be affected by deficiency or decreased levels of gender steroids[8,30,31]. Studies have shown that hASC-scaffold applications with[32,33] or without[34] BMP-2 controlled delivery systems can enhance the osteogenic potential of hASC isolated from individuals within different age groups, this suggesting that hASC-scaffolds in conjunction with diffusible factors have the potential to become an alternative fracture repair treatment for patients suffering from osteoporosis in the future.

In the past decade, substantial research has been conducted in an effort to better understand the osteogenic fate of the PLA cells isolated in 2001[7]. Human lipoaspirates are readily obtained; the stem cells present in the SVF have great self-renewal potential and have been demonstrated to differentiate into cells of all embryonic germ layers. Even though much of the molecular characterization still remains to be conducted, the expression of known osteogenic markers has been used successfully to monitor hASC osteogenesis (Table 1). Human ASC cultured in scaffold constructs have the potential to differentiate into mature osteoblasts with[32,33] or without[34] growth factor supplementation paving the way for the potential use of hASC-scaffold combinations to treat different diseases.

1.3. hASC and Scaffolds for Bone Tissue Engineering

1.3.1. The Tissue Engineering Decade

Bone tissue engineering has been heralded as the alternative strategy of the twenty-first century to replace or restore the function of traumatized, damaged, or lost bone [35,36]. Over the years, bone grafts have advanced as the gold standard treatment to augment or accelerate bone regeneration. Autogenous cancellous bone grafts have long been used to facilitate bone healing[35] though quantity is limited and surgical procedures for graft harvest are required. Allogeneic bone grafts are costly, require time-consuming bone banking procedures and have the potential for disease transmission[35]. A current research paradigm of bone tissue engineering utilizes hASC isolated after elective lipoaspiration, *in vitro* population expansion and *in vivo* delivery within a scaffold or matrix[2,5,6,37] in a configuration that generates new functional bone (Figure 2). Scaffold-induced hASC osteogenesis has been demonstrated experimentally in a variety of tissue engineering strategies (Table 1). Compared to allogeneic grafts, the risk of donor pathogen transfer to recipients is minimal[37]. Additionally, the self-renewal potential[15], plasticity[15-18], and lack of T cell priming[38] make hASC an attractive alternative to traditional bone grafting techniques.

At present, tissue engineering studies combined with hASC can generally be divided into two categories. These include the *in vitro* characterization of the hASC osteogenic potential in novel or commercially available scaffolds and *in vivo* studies performed in either rats or mice models for calvarial bone defects or subcutaneous ectopic bone formation (Table 1). Several studies describe the combination of hASC with human autografts[3,39], acellular xenografts[39-41], 1st generation of synthetic polymers[38,42-45] or ceramic scaffolds[26,30,34,39,40,46-50] as well as 2nd and 3rd generations of bioabsorbable scaffolds[15,30,32,33,49,51-54].

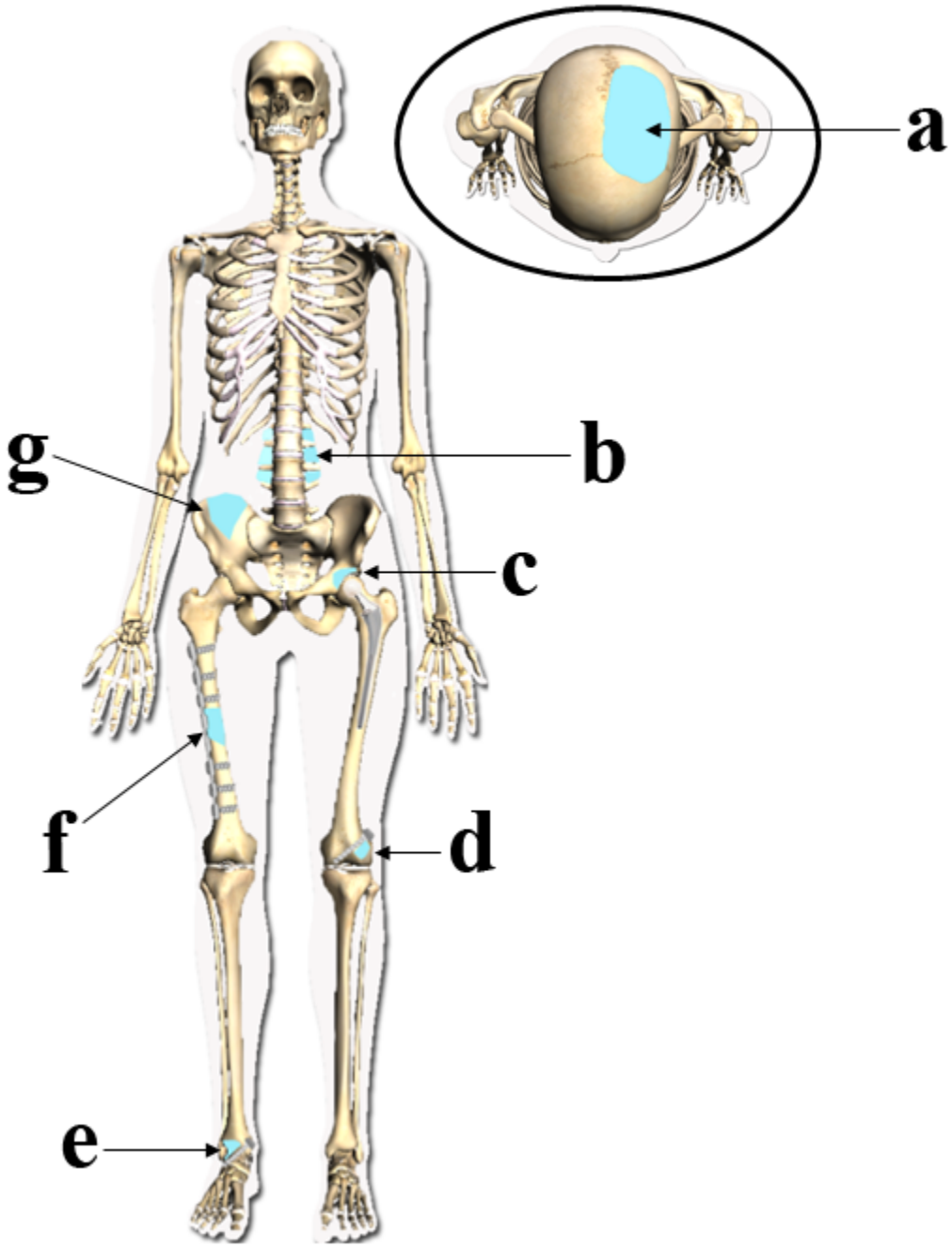

Figure 2. Potential clinical orthopedic applications for the use of bone-substitute scaffolds: (a) calvarial defects, (b) anterior spine fusion, (c) acetabular defects after hip replacement/revision surgery, (d) cystic lesion femur condyle metaphysis, (e) ankle joint arthrodesis, (f) osteolytic/traumatic long bone defects and (g) iliac defects. Adapted from Reichert & Hutmacher[35] and van Gaalen et al.[36].

While current scaffold materials facilitate the attachment of hASC by providing an interconnected pore structure to support cell migration, proliferation, differentiation[2] and in some cases formation of blood vessels[40,47], the major limitations of the 1st generation of bioabsorbable scaffolds used today are their relatively poor mechanical properties and brittle behavior[35,36]. The latest innovation for bioactive and fiber-reinforced biomaterials, is to use both bioactive/bioabsorbable ceramics and bioabsorbable polymeric fiber reinforcement in the same composite structure (referred as 2nd and 3rd generations of bioabsorbable scaffolds)[35,36]. Composite ceramics/polymers are being explored as an alternative to address the mechanical limitations of 1st generation ceramics[35]. The polymer phase allows for tunable rheological properties while the ceramic phase contributes to osteoinduction and osteoconduction. To date, a clear trend towards the use of composite scaffolds can already be observed in some of the current models[15,30,32,33,49,51-54]. It can therefore be predicted that 2nd and 3rd generation composites will be preferred as scaffolding materials for hASC in future clinical trials[24].

1.3.2. Current Biomaterials Used in hASC Bone Tissue Engineering Strategies

- **Biological Materials**

Extracellular matrix (ECM) molecules are naturally occurring materials that have been commonly used as tissue engineering scaffolds combined with hASC [39-41]. Decellularized xenogeneic ECM is well tolerated by human hosts as components of the ECM are generally well conserved among species which may contribute to reduced rates of rejection and associated complications. Among the different xenografts commercially available, deproteinized bovine bone granules (Bio-Oss®) were recently investigated as a substrate for hASC osteogenesis *in vitro*[39] and in an ectopic bone formation model using immunodeficient (nude) mice[40]. Bio-Oss® is a highly porous inorganic material composed of calcium deficient carbonate apatite that was

observed to produce bone after hASC loading both *in vitro*[39] and *in vivo*[40]. In addition to deproteinized grafts, the *in vitro* osteogenic potential of decellularized bovine loaded with hASC after perfusion bioreactor has been demonstrated [41]. The decellularization step is critical process in ECM isolation as xenogeneic and allogeneic cellular antigens can trigger an inflammatory response and/or tissue rejection.

ECM scaffolds are often combined with site specific cells, usually autologous cells from the intended recipient before utilization for tissue repair[3]. The requirement for cells to promote a constructive remodeling response scaffold varies. For bone applications, current models directly load hASC on bone grafts in the presence or absence[39] of a perfusion system[41]. In another approach, hASC were initially loaded on a fibrin hydrogel and then the hASC-fibrin hydrogel was wrapped around an orthopaedic construct[40]. To date, the bone formation potential of hASC combined with ECM scaffolds has been evaluated *in vivo* under non-weight bearing conditions (Table 1). Unmodified ECM scaffolds degrade over time via enzymatic degradation and hydrolysis, changing the strength and mechanical properties of the scaffold after implantation[36]. Therefore, the understanding of the biomechanical properties of the ECM loaded with hASC in weight bearing situations will be critical to future clinical use.

- **Natural Polymers**

Natural polymers were the first to be used in hASC-scaffold studies because they are either components of, or have properties similar to, the natural ECM[3,32,33,45]. For bone tissue engineering applications in combination with hASC, natural polymers are often derived from animal sources. Collagen[33,45], fibrin[3,33,40] and gelatin[32] have been demonstrated to interact favorably with hASC through specific recognition domains present in their structures. Additionally, these protein-based polymers can be degraded by naturally occurring enzymes,

allowing them to be modified, degraded and absorbed *in vivo*[36]. Often when used in scaffolding materials natural polymers can result in a construct with superior mechanical and biological properties[36].

Currently, 19 different types of collagen have been described, with the most abundant being type 1 collagen[36]. Collagen is composed of three polypeptide chains that intertwine with one another to form a triple helix. The polypeptide chains have a repeating sequence of glycine-X-Y, where X and Y are most often found to be proline and hydroxyproline and the chains are held together through hydrogen bounds. Collagen is enzymatically biodegradable, and has a tendency to degrade rapidly *in vivo*, reducing mechanical strength (Table 2).

Fibrin is a fibrous protein naturally produced in the body and that plays a crucial role in wound healing and blood coagulation[8]. It is TGF-β-rich and has been used to augment hASC attachment to scaffold materials[3,33,40]. Fibrin polymerization relies on thrombin to convert fibrinogen into fibrin. Once a gel is formed, studies describe the use of hASC-fibrin composites as a coating for more mechanically robust scaffold constructs[33,40].

Gelatin is a collagen derivative acquired by denaturing the triple-helix structure of collagen into single-strand molecules. It is water-soluble, and entangles easily to form into a gel through changes in temperature and is readily broken down enzymatically by various collagenases. The most commonly described form of a gelatin scaffold is a hydrogel and in this form it has been used to support hASC growth and osteogenic differentiation[32].

The use of collagen, fibrin and gelatin for hASC osteogenesis has been successfully demonstrated. However, collagen in bone engineering application should be used to promote hASC adherence rather than as a monolithic scaffold material as collagen gels have limited

Table 2. Fabrication, degradation and mechanical properties of biomaterials currently used in hASC bone tissue engineering applications.

	Materials	Origin/Fabrication	Degradation	Elastic Modulus (MPa)	Compressive strength (kPa)	References
Ceramics	HA	Bone	Hydrolyses/Cell mediated	50-100	110-660	30,36,39,40,47,51,53
	β-TCP	Sinterization	Hydrolyses/Cell mediated	95-180	100-800	24,34,36,40,49
	Akermanite	Sinterization	Hydrolyses/Cell mediated	57.8-159	530-1130	26
Polymers	PLGA	Crosslink (PGA and PLLA)	Hydrolyses/Enzimatic	2.4	158-257	36,42,43,51,53
	PLLA	Polymerization	Hydrolyses/Enzimatic	3.7	110-275	36,49,52
	PGE	Polymerization	Hydrolyses/Enzimatic	0.5-1.38	200-500	36,38,44
	PCL	Polymerization	Hydrolyses/Enzimatic	11.8	100-250	15,33,36,38,54
	PUV	Polymerization	Hydrolyses/Enzimatic	69-690	138	26,36
	Collagen	ECM	Hydrolyses/Enzimatic	300	8.8	36

*HA: hydroxyapatite; β-TCP: β-tricalcium phosphate; PLGA: poly-lactic-glycolic acid; PLLA: poly(l-lactic acid); PGE: poly(ethylene glycol); PCL: poly-e-caprolactone; PUV: polyurethane; PGA: poly(glycolic acid); ECM: extracellular matrix.

mechanical strength and are susceptible to fast enzymatic degradation which can, therefore, result in unpredictable *in vivo* mechanical properties.

- **Synthetic Polymers**

A variety of biocompatible synthetic polymers are commercially available enabling the design of scaffolds with specific mechanical and biological properties and controllable degradation rates. These polymers can be produced reproducibly in highly purified forms and can be easily processed into devices by casting, extrusion, molding or coating. Much of the research utilizing synthetic polymers in hASC-combined tissue engineering has been focused on hybrid cell/scaffold constructs using degradable polyester polymers such as PLGA[42,43,51,53] which is the copolymer of poly(l-lactic acid – PLLA) and poly(glycolic acid – PGA). Poly-e-caprolactone (PCL)[15,33,38,54] and PLLA[49,52]. Additionally several other polymer systems such as poly(ethylene glycol) (PEG)[38,44], polyurethane (PUV)[26], and silicon[30] have been shown to support hASC proliferation and differentiation (Table 1). The clear advantage of synthetic polymers is that they are highly pure, readily reproducible and have flexible mechanical, chemical and biological properties allowing them to be tailored to suit specific functions. A significant disadvantage of using synthetic polymers is that some, such as PLGA and PLLA, degrade into non-biocompatible products, often acids which can perturb the scaffold microenvironment leading to cell dysfunction or death. At high concentrations of these degradation products, local tissue acidity may increase, resulting in adverse responses such as inflammation or fibrous encapsulation[36].

One of the most frequently cited synthetics for bone scaffolds is poly(l-lactic acid-co-glycolic acid –PLGA). PLGA is the result of the copolymerization of PLLA and PGA. This copolymer is amorphous, and has a decreased degradation rate and mechanical strength compared to PLLA

(Table 2). PLGA typically undergoes bulk degradation by self-catalyzed ester hydrolysis[36]. The degradation rate of PLGA can be controlled by adjusting the ratio of PLLA/PGA in the solution. For example, a 50:50% ratio of PGA and PLLA typically degrades faster than either homopolymers. PLGA has been used alone as a scaffold [42,43] or in combination with apatite[51] and hydroxyapatite (HA)[53] to repair calvarial bone defects in rats[43] or nude mice[51] as well as to investigate ectopic bone formation in nude mice[42,53].

Poly(l-lactic acid) (PLLA) is one of two isomeric forms of poly(lactic acid):D and L. Similar to PGA, PLLA is classified as a linear poly(alpha-hydroxy acid) that is formed by ring-opening polymerization of L-lactide. PLLA is structurally similar to PGA, with the addition of a pendant methyl group[36]. This group increases the hydrophobicity and reduces the melting temperature to 170^{o}-180^{o}C. PLLA typically undergoes bulk, hydrolytic ester-linkage degradation, but decomposes into lactic acid[36]. The additional pendant methyl group hinders the ester bond cleavage of PLLA, resulting in a decreased hydrolytic degradation rate and greater *in vivo* mechanical stability (Table 2). In recent investigations, PLLA has been blended with β-tricalcium phosphate (β-TCP)[49,52] and bioactive glass[49] to assess the in vitro osteogenic potential of hASC in novel biodegradable scaffolds and these results have shown that PLLA-composites can induce osteogenic differentiation of hASC *in vitro*.

Poly(e-caprolactone) is a aliphatic polyester with semi-crystalline properties[36]. PCL is formed through ring-opening polymerization and has repeating units of one ester group and five methylene groups. It is poorly water-soluble with a melting temperature of 58 to 63^{o}C. The degradation of PCL occurs by bulk or surface hydrolysis of ester linkages resulting in a byproduct of caproic acid[38]. PCL degrades slowly in physiological conditions and it can persist *in vivo* for up to 2 years[36]. In studies combined with hASC, PCL has been copolymerized with

collagen[33], fibrin[33], and PEG[38] in an effort to increase the degradation rate of the scaffolds. The ease with which PCL can be copolymerized with a variety of polymers has made it an attractive component of polymeric scaffolds. Moreover, commercial (Osteopore®)[33] and custom-made[15,54] composites blended with β-TCP are also available and they have been shown to produce bone after hASC loading in ectopic bone formation models using nude mice[15,54].

Poly(ethylene glycol) (PEG) is a linear-chained polymer consisted of an ethylene oxide repeating units. Poly(ethylene oxide) PEO has the same backbone as PEG, but a longer chain length and thus a higher molecular weight[36]. PEG is hydrophilic and synthesized by anionic/cationic polymerization. The ability of PEG to swell in aqueous solution has led to its use as a hydrogel, and in some instances as an injectable hydrogel[38,44]. Unfortunately, the linear chain form of PEG leads to rapid diffusion and low mechanical stability (Table 2). Crosslinked PEG networks may be created by attaching functional groups to the ends of the PEG chain and then initiating covalent cross-linking by chemical, thermal or photoactiviation[36]. PEG is resistant to degradation, however, rates of degradation may be increased by copolymerization with hydrolytically or enzymatically degradable polymers[38,44]. The flexibility of PEG modification, whether with cross-linkable groups for network formation or degradable groups for absorbable applications, has led to the interest in PEG for hASC based bone tissue engineering. For example, PEG has been copolymerized with PCL[38] and oligopeptides[44] to form a gel which after hASC loading has been demonstrated to produce ectopic bone in rats[38] and heal calvarial defects in nude mice[44].

Polyurethane (PUV) is an elastomeric polymer that is typically nondegradable[36]. Positive attributes, such as tailorable mechanical strength and biocompatibility have led to the synthesis of degradable polyurethanes with nontoxic diisocyanate derivatives[36] (Table 2). However in

bone tissue engineering applications combined with hASC, PUV has been used only as a template during the fabrication of β-TCP and akermanite scaffold discs[26] which were used to investigate the osteogenic potential of hASC *in vitro*.

- **Bioceramics**

Bone is composed of HA crystals distributed within an organic matrix with porosity and percent mineralization varying among bone types[35]. It is generally agreed that ceramic biomaterials used in bone tissue engineering applications should mimic, as closely as possible, the natural bone architecture to ensure cell attachment and migration within the porous materials. Additionally, they should be absorbed overtime or integrated with the surrounding tissue and eventually be replaced by new or existing host tissue[36]. The concept of bioactivity originated with bioactive glasses by the hypothesis that the biocompatibility of an implant is optimal if it elicits the formation of normal tissues at its surface while establishing a contiguous interface capable of supporting the loads which occur at the site of implantation[35,36]. Bioceramics used in current hASC osteogenic studies included custom-made akermanite[26], β-TCP scaffolds[26,49] and bioactive glass[48-50]; commercially available scaffolds made of β-TCP (Synphare®[34]; ChronOS®[40]), HA (Engipore®)[30,39,40,47], Titanium (Tabrecular Titanium®)[39,46]; polymeric composites made of β-TCP[15,32,49,53,54] and HA[51,53].

Several calcium-phosphate ceramics with varying calcium-to-phosphate ratios have been explored for bone regeneration. Among the Ca-P materials, the apatites are the most commonly studied for osteogenesis due to their chemical and crystalographic similarities to native bone. Apatites form a range of solid solutions as a result of ion substitution[35,36] . The most common apatite used in bone tissue engineering applications is HA[30,39,40,47,51,53]. Studies have shown that hASC seeded on HA form ectopic bone in nude mice[40,47,53], but the inability to attract new

osteoprogenitor cells or cytokines (osteoinduction) to the site of implantation make HA a non-ideal choice for bone tissue engineering strategies[26,35,36].

Synthetic apatites are processed via hydrolysis, hydrothermal synthesis and exchange, sol-gel techniques, wet chemistry, and conversion of natural bone and coral[35,36]. Differences in the structure, chemistry, and composition of apatites arise from differences in processing techniques, time, temperature, and atmosphere. β-tricalcium phosphate, is a synthetic apatite with osteoconductive and osteoinductive properties superior to HA and it has been combined with hASC in several studies[15,32,34,40,49,52,54]. More recently, Liu et al. compared the osteogenic potential of hASC loaded in β-TCP and akermanite scaffolds[26]. According to this study, increased expression of osteogenic markers were observed in akermanite scaffolds compared to β-TCP, loaded with hASC after 10 days. Akermanite ($Ca_2MgSi_2O_7$) is believed to have a stable degradation rate and superior bone deposition compared to β-TCP constructs (Table 2). Moreover, akermanite scaffolds may enhance recruitment and osteogenic commitment of hASC due to the cells affinity for Ca, Mg, and Si ions in the scaffold[26], but, to date, both, akermanite and β-TCP, are still being evaluated as options for bioceramic bone matrices.

Scaffold technology is playing an important role in the success of the current bone tissue engineering strategies. Several different materials have been tested in combination with hASC, but as noted by Lendeckel et al., composite scaffolds may offer a better clinical outcome in terms of mechanical and biological properties[3].

1.3.3. Current Bone Tissue Engineering Models: A Retrospective Analysis on hASC-Scaffolds

Over the past several years, a wide range of bone grafts and synthetic materials became available for scaffold-assisted bone regeneration (Table 1). When considering the current studies for bone applications with hASC, cell cultures and animal models are the most common. Even

though Lendenckel et al. demonstrated that hASC can be clinically used to promote calvarial healing in humans[3], obvious ethical and safety concerns prevent human testing as the first stage in novel scaffold development[35]. Among the animal models available today, inserting biomaterials subcutaneously in rats[38] and nude mice[15,38,40,42,45,47,53,54] are the most common. Calvarial defect models have also been described for the same species[43,44,51]. They can be used to provide first phase (non-load bearing) bone healing models with relative biological inertness due to poor blood supply and limited bone marrow exposure[35].

The first study comparing the in vivo osteogenic potential of hASC (referred as human adipose tissue stem cells or ATSCs) with hBMSC in scaffolds was performed by Hattori et al[45]. After both cell types were seeded on to water soluble collagen honeycomb-shaped scaffolds they were subcutaneously implanted in nude mice. Ectopic bone formation was assessed 4 weeks later in both animal cohorts. According to the results, osteogenic differentiation of ATSCs on scaffolds was similar to that observed in scaffolds loaded with hBMSC after 4 weeks. Two years later, in 2006[54], Jeon et al. investigated the in vivo osteogenic potential of hASC (human adipose-derived precursor cells - ADPC) seeded on β-TCP-PCL composites in a rat model. Experimental groups included: induced—stimulated with osteogenic factors only after seeding into scaffold; preinduced—induced for 2 weeks before seeding into scaffolds; and uninduced cells. Results 12 weeks post-implantation indicated comparable expression levels of osteogenic markers in scaffolds loaded with induced and preinduced groups and both groups had significantly higher marker levels than uninduced controls. In the following year, Scherberich et al. utilized the same composite (β-TCP-PCL) to load SVF cells using a perfusion system[47]. After loading, SVF-scaffolds were subcutaneously implanted in nude mice to investigate if SVF could differentiate toward the osteogenic and angiogenic pathways. Twelve weeks post-implantation,

calcified constructs contained blood vessels functionally connected to the host vasculature. In summary, these first studies demonstrated that hASC loaded to scaffolds have osteogenic potential similar to hBMSC and, besides bone, SVF loaded to scaffolds can also form blood vessels.

Several studies focused on the *in vitro* characterization of the hASC osteogenic potential in novel[26] and commercial scaffolds[33,39] as well as calvarial repair and ectopic bone formation in nude mice[44,53] were performed in 2008. The first calvarial bone defect model for hASC-scaffold osteogenesis was proposed by Degano et al.[44]. In this study, luciferase labeled hASC (human adipose tissue MSC - hAMSCs) and hBMSC loaded to PEG-RGSD, peptide functionalized, scaffolds were implanted in calvarial defects of nude mice and were monitored for 12 weeks. According to these results, hBMSC had better survival rates than hAMSCs, but bone density in calvarial defects bearing scaffolds loaded with both cell types increased significantly more than that of defects without scaffolds.

Liu et al. compared the potential for *in vitro* osteogenesis of hASC on akermanite and β-TCP scaffolds for up to 10 days[26]. Fresh human lipoaspirates were obtained from three healthy patients (mean age, 32 years) after elective liposuction procedure. Passage 3 of each individual was seeding on 10mmX0.8mm akermanite or β-TCP discs at density of $3X10^3$ cells/cm^2 (for attachment and proliferation assays) or $2X10^4$ cells/cm^2 (for osteogenic differentiation assays). Nonseeded discs were similarly treated as blank controls. Density of cells attached to akermanite and β-TCP scaffolds significantly increased after seeding with no significant differences between both scaffold types. Likewise, live/dead staining and lactate dehydrogenase (LDH) release assay indicated that the observed cytotoxicity did not significantly impact cell viability on both akermanite and β-TCP scaffold surfaces. Expression of ALP, OCN and COL1

increased overtime in hASC seeded on both scaffold types and cultured in either control or osteogenic media. Differences between scaffolds were observed only after 10 days of culture, where expression of the osteogenic markers was significantly higher in akermanite scaffolds. According to the authors, the *in vitro* osteoinductive bioactivity of akermantie scaffolds indicated that the material could be used to support bone regeneration.

Another *in vitro* study performed in 2008 characterized the *in vitro* osteogenic potential of hASC isolated from twenty-three donors in both 2D and 3D cultures[39]. The findings indicated that HA (Engipore®), cancellous human bone fragments, deproteinized bovine bone granules (Bio-Oss®), and titanium (Trabecular Titanium®) scaffolds could support the growth of pre-differentiated hASC. Human bone fragments and bovine bone granules were able to induce osteogenic differentiation of control and osteogenic differentiated hASC on 3D scaffolds to a greater extent than in observed in hASC cultured on 2D monolayers. . The authors concluded that further *in vivo* studies are needed to confirm the findings, but the data suggested that culture on 3D scaffolds increases the osteogenic potential of hASC compared to planar culture. In addition to these two *in vitro* studies, Leong et al. detailed an *in vitro* study using mPCL-TCP (Osteopore®) in three-dimensional (3D) tissue culture systems[33]. hASC (or human adipose-derived stem cells – ADSCs) from 3 donors were seeded onto scaffolds treated with fibrin glue and lyophilized collagen. ADSCs within these scaffolds were then induced to differentiate along the osteogenic lineage for 28 days to compare the adhesion, viability, proliferation, metabolism and differentiation as a function of scaffold composition and culture condition. The ADSCs cells were proliferative in both collagen and fibrin mPCL-TCP scaffold systems with a consistently higher cell number in the induced group over the non-induced groups for both scaffold systems. In response to osteogenic induction, these ADSCs expressed elevated OCN, ALP and ON levels

compared to the non-induced groups. Cells were able to proliferate within the pores of the scaffolds and form dense cellular networks after 28 days of culture and induction. The authors concluded that the successful cultivation of osteogenic ADSCs within a 3D matrix comprising fibrin glue or collagen, immobilized within a robust synthetic scaffold is a promising bone tissue engineering technique.

Finally, the first composite scaffolds incorporated with a control-released BMP-2 were also tested in 2008[53]. Jeon et al 2008 fabricated a HA-PLGA incorporated with BMP-2 to investigate the *in vitro* and the *in vivo* osteogenesis of hASC (human adipose-derived stem cells - hADSCs). *In vitro* analysis indicated that hADSCs cultured on BMP-2-loaded HA-PLGA scaffolds for 2 weeks expressed the osteogenic markers ALP, OP, and ON mRNA, while cells on HA-PLGA scaffolds without BMP-2 expressed only ALP. Human ADSCs ectopic bone formation associated with control-released BMP-2-HA-PLGA scaffolds was also investigated 8 weeks after subcutaneous implantation in nude mice. Cohorts included four groups: HA-PLGA scaffolds only, BMP-2-loaded HA-PLGA scaffolds, undifferentiated ADSCs seeded on HA-PLGA scaffolds, and undifferentiated ADSCs seeded on BMP-2-loaded HA-PLGA scaffolds. Eight weeks post-implantation, ASCs loaded to BMP-2-HA-PLGA scaffolds exhibited greater bone formation area and calcium deposition than ASCs loaded to HA-PLGA scaffolds. The authors concluded that HA-PLGA composites integrated with a BMP-2 delivery system can enhance the in vitro and in vivo osteogenic differentiation of hASC without prior *in vitro* exposure to osteogenic media supplements. As a conclusion, the studies performed in 2008 indicated that scaffolds can be used to monitor local in vivo hASC viability and differentiation. Moreover, several *in vitro* studies tested hASC osteogenesis in varying scaffolds often enhanced with

adhesion molecules. Finally, Jeon et al 2008 demonstrated for the first time that BMP-2 can be incorporated to scaffolds to promote controlled osteogenesis of hASC *in vivo*.

Characterization of novel scaffolds for hASC osteogenesis was the major topic for the studies performed in 2009. Girolame et al 2009 described changes in the hASC-scaffold osteogenesis between females of different age groups[30]. This study compared the *in vitro* osteogenic potential of hASC isolated from 26 adult female donors in both monolayer cultures and HA or silicon carbide (SiC-PECVD) scaffolds. The cellular yield of hASC from older donors was significantly greater than that observed from younger donors; however reduced osteogenesis correlated significantly with aging in both monolayer and 3D scaffold culture. Of the scaffolds examined, hASC osteogenesis was up-regulated in the presence of HA, whereas SiC-PECVD produced no significant effect. The authors concluded that in females, age influenced the osteogenic differentiation of hASC in 2D cultures and in 3D scaffolds.

The influence of donor cell origin in scaffolds was evaluated by Zhang et al.[15]. In this study, the authors compared the *in vitro* and *in vivo* osteogenic potential of four types of MSC loaded on β-TCP-PCL scaffolds to investigate if the ontological and anatomical origins of MSC influenced ectopic bone formation. Fetal femurs were collected for isolation of human fetal bone marrow (hfMSCs, n =5) after clinically indicated termination of pregnancy; umbilical cords were collected for isolation of human umbilical cord MSC (hUC-MSCs) following term deliveries (n =3); adipocyte-derived MSCs (hATMSCs) were derived from adipose tissue harvested during elective cosmetic surgery (mean age, 41 years, n = 3); and human adult bone marrow (haMSCs) samples were collected from 3 donors (mean age, 25 years). Donor cells were suspended in fibrin glue before seeding into the porous 5mm x 4mm scaffolds ($1.6X10^5$ cells/scaffold). Culture was maintained in osteogenic medium for 28 days. Samples for DNA quantification and

expression of mRNA levels of osteogenic markers were collected in different time points. MSC were seeded onto mPCL-TCP scaffolds and cultured for 2 weeks in osteogenic medium followed by subcutaneous implantation in nude mice. The effect of donor cells on ectopic bone formation was evaluated in histological and μ-CT analysis 8 weeks post-implantation. After 28 days in culture, hfMSCs consistently showed a higher DNA content in scaffolds, followed by hATMSCs, hUCMSC and haMSC. Expression of osteogenic markers (ALP, RunX2, COL1A1, and ON) and von Kossa staining were also significantly higher in hfMSCs, however, scaffolds loaded with haMSCs demonstrated earlier expression of ON, higher expression of ALP and higher calcium deposition than scaffolds loaded with hUCMSCs and hATMSCs, respectively. Ectopic bone formation in immunodeficient mice 8 weeks after implantation corroborated these findings. Von Kossa staining demonstrated that hfMSCs scaffolds had the largest mineralization area and volume, followed by haMSCs scaffolds, hUCMSCs and hATMSCs indicating that the *in vitro* and *in vivo* osteogenic potential of cells loaded to mPCL-TCP scaffolds is influenced by the donor cells origin.

In the same year, three consecutive *in vitro* studies, investigated the hASC osteogenic potential in bioactive glass (BG) coated with Ca-P[48] or zinc[50], alone or in composites blended with PLLA[49]. In the first study, Haimi et al. evaluated the *in vitro* effect of two different Ca-P treatments of 3D bioactive glass scaffolds on hASC attachment, growth, and osteogenic differentiation[48]. Cells were isolated from adipose tissue samples collected from 10 donors (mean age, 48 years). Passages 3-6 isolated from 2-4 individuals were pooled together and seeded on 14 mmX14mmX5mm scaffolds at density of $5X10^5$ cells/scaffold. After a 3 hour initial incubation, the cell-seeded scaffolds were transferred to long term culture for 2 weeks in control medium. Experimental groups included three types of bioactive glass scaffolds: non-

treated, thick and thin Ca-P treated. After 2 weeks, no significant differences in the cell proliferation, distribution and alkaline phosphatase activity were observed in all three scaffolds. However, within the same time point, OP expression in thin Ca-P-treated scaffolds was significantly higher than the other two scaffold types. The authors concluded that the osteoconductive and osteostimulative properties of bioactive glass scaffolds should be further considered.

In the following paper, Haimi et al. incorporated different concentrations of zinc into porous bioactive glass to evaluate the proliferation and osteogenesis of hASC in these scaffolds[50]. Human ASC were isolated, pooled (3-4 individuals) and seeded at the same density on porous scaffolds as in the previous study. Experimental groups included: BG (control), BG+0.25% zing, BG+1% zinc. In general, after 2 weeks no significant differences in cell viability, proliferation and osteogenic differentiation were observed between experimental groups. However, the ALP activity as well as the DNA content of hASC was significantly increased at 2 weeks compared to that at 1 week in control scaffolds. In summary, this study revealed that zinc had no effect on the proliferation and osteogenesis of hASC. The authors concluded that further investigations are needed to assess the zinc stimulatory potential to hASC as the addition of zinc inhibited the degradation of bioactive glass scaffolds.

Finally, in the last paper, Haimi et al. also compared the *in vitro* osteogenic potential of human ASC loaded into bioactive glass [BG] and β-TCP scaffolds incorporated with PLLA[49]. The hASC were isolated from adipose tissue samples collected after elective liposuction procedure in six donors (mean age, 45 years). Passages 4-7 of different donors (n = 3) were pooled together and seeded on the porous surface of 15mmX3mm scaffold constructs at density of $3.5X10^5$ cells/scaffold and cultured for 2 weeks in control medium. Experimental groups and

controls included: 100% PLLA, β-TCP 10%, β-TCP 20%, BG 10%, and BG 20%. DNA and ALP analysis indicated that after 2 weeks cell number and expression of osteogenic differentiation markers were comparable in all β-TCP-PLLA scaffolds but were significantly higher than the other three scaffold types. As a conclusion, this study raised promises of the use of β-TCP-PLLA composites in bone tissue engineering applications combined with hASC.

Similarly, McCullen et al. also indicated that β-TCP-PLLA composites might directly stimulate the osteogenic differentiation of hASC[52]. In this study, the electrospun composite β-TCP-PLLA was evaluated *in vitro* for viability, proliferation and osteogenic differentiation of hASCs after 18 days. Human adipose-derived adult stem cells (hASC) were isolated after elective liposuction procedures in a 48-year-old Caucasian female. Pre-cultured hASC were seeded at $2X10^4$ cell/cm^2 on 10mmX10mm scaffolds composed of varying loading of β-TCP crystals and PLLA. After overnight incubation, cell-seeded scaffolds were maintained in osteogenic-differentiating medium for 18 days, scaffolds with no cells served as experimental controls. Overall, high β-TCP concentration weakened the tensile strength of the scaffolds but did not affect their stiffness. *In vitro* studies demonstrated that electrospun PLLA w/10% TCP increases hASC proliferation, while electrospun PLLA w/20% TCP accelerates osteogenic differentiation and increases calcium accretion by hASC, compared to neat electrospun PLLA scaffolds. In summary, the conclusion of these four papers together, suggested that bioactive glass might be a viable candidate for promoting osteogenesis in bone tissue engineering applications when combined with hASC, however compared to β-TCP it has a much lower osteogenic potential.

Within the same year, Ahn et al. evaluated the *in vitro* and *in vivo* biocompatibility and osteogenic potential of human adipose tissue–derived stem cells (hADSCs) used in conjunction

with an injectable mPEG-PCL diblock copolymer[38]. Human ADSCs were isolated after collection of subcutaneous adipose tissue of a female donor. For the *in vitro* study, $3X10^4$ cells were seeded on gels composed of mPEG-PCL diblock copolymer (20 wt%). For comparison, an equivalent number of hADSCs was seeded on 24-well plates and maintained in culture for 1 week. For the *in vivo* study, experimental groups included: G (gel only), GF (gel+osteogenic factor), GC (gel+$2X10^5$ hADSCs), and GCF (gel+$2X10^5$ hADSCs+osteogenic factor). Gels containing each experimental group were subcutaneously injected in Fisher rats (4 groups of 3 rats each) and ectopic bone formation was observed 2-4 weeks post-injection. After 7 days in culture, viability of plated cells was higher than in gels composed of mPEG-PCL. Moreover, within this time point, most hADSCs seemed to be located inside the gels rather than surface associated. After 4 weeks, von Kossa staining revealed increased mineralization in gel implants containing both hADSCs and osteogenic factors compared to controls. Inflammation associated with host macrophages co-localization was attributed to gel-specific graft rejection of the mPEG-PCL copolymer gel only, whereas the inflammatory response of gels embedded with hADSCs were much reduced.

In conclusion, studies performed in 2009, indicated that the osteogenic potential of hASC is lower compared to hfMSCs in scaffolds and is also significantly affected by donor age. Moreover, hASC have better differentiation on composite scaffolds than 1st generation ceramic scaffolds.

Studies conducted in 2010 evaluated the in vitro hASC osteogenesis in custom-made xenografts[40,41], PLGA scaffolds alone[43] or blended with apatite[51] as well as 1st generation commercially available bioceramics made of HA[40], β-TCP[34,40] and titanium[46]. Gastaldi et al. investigated the *in vitro* osteogenic potential of hASC loaded on 12mm x 6mm trabecular

titanium scaffolds (Trabecular Titanium^{TM})[46]. Passage 3 of freshly isolated hASC harvested from healthy patients undergoing orthopedic surgery were seeded at density of $1X10^6$ cells/scaffold and cultured in osteogenic or control medium for 28 days with data collected at different time points. Expression of the osteogenic markers ALP, COL1, OCN and OP as well as calcium deposition were higher in scaffolds cultured in osteogenic medium than in scaffolds cultured in control medium. The highest ALP and COL1 expression were observed in scaffolds cultured in osteogenic medium after 21 days, while the highest expression of OCN and OP were observed after 28 days in scaffolds cultured in osteogenic medium. The conclusions suggest that titanium/hASC construct could be used as an alternative in bone tissue engineering applications.

In another in vitro study, Marino et al. evaluated the osteogenic potential of human adipose stem cells (fibroblast-like adipose tissue-derived stromal cells—ADSC-FL) isolated from 5 donors (mean age, 36 years) and seeded onto commercially available 10mm x 2mm porous β-TCP discs (Synhapor^{TM}, $2X10^5$ cells/disc) and cultured in control or osteogenic media for several different time points[34]. The findings indicated that β-TCP alone could trigger osteogenic differentiation of ADSC-FL. Alkaline phosphatase, OCN, and OP expressions were observed in cells cultured in both control and osteogenic media with expression of OCN and OP being higher after 14 and 28 days in cells cultured in osteoinductive medium.

Similarly, Frohlich et al. also observed that perfusion culture of hASC on bovine decellularized bone scaffolds in the presence of osteogenic supplements contributed to the uniform distribution of cells and bone matrix within the constructs[41]. In this study, the authors used a perfusion bioreactor system to load hASC onto a bovine decellularized bone scaffold. Subcutaneous adipose tissue was obtained from four female donors undergoing elective procedures. Passage 3 of freshly isolated hASC were loaded at a cell density of $1.5X10^6$

cells/40μL onto 0.37–0.45 mg/mm^3 scaffolds using a perfusion bioreactor connected to a peristaltic pump (Ismatec, flow rate - 1.8 mL/min). Immediately after incubation (1 hour), some seeded scaffolds were collected to assess the loading efficiency while other scaffolds were transferred in parallel to both static or perfusion cultures to assess the osteogenic differentiation of seeded scaffolds after 5 weeks in both control and osteogenic medium. Treatment groups included: static-control, static-osteogenic, perfused-control, and perfused-osteogenic. Biochemical analysis revealed that ALP expression was higher in scaffolds cultured in osteogenic than in control medium after 4 weeks. Calcium deposition as a mean of alizarin red and von kossa staining also corroborate these findings. Moreover, uneven distribution of collagen, OP (after 2 and 5 weeks) and BSP (after 5 weeks) were observed in the statically cultured constructs supplemented with osteogenic medium, while uniform spatial distribution of all three proteins were observed in constructs cultured in the perfusion bioreactor. In summary, these in vitro studies demonstrated that the composition of the scaffolds can modulate the osteogenic differentiation of hASC. Moreover, perfusion bioreactor culture system improved the homogenenity of osteogenesis and positively correlated with increased bone mineralization within scaffolds after 5 weeks.

The osteogenic effect of hASC loaded to different scaffold materials was also observed in 2010 in three different *in vivo* studies. In the first study, Muller et al. investigated the osteogenic and vasculogenic potentials of fibrin gels embedded with freshly isolated human SVF cells and seeded on commercially available ceramic scaffolds to assess the feasibility of an intraoperative approach to enhance bone healing in a setting compatible to clinical situations[40]. Subcutaneous adipose tissue was obtained from 11 individuals undergoing (10 female, 1 male; mean age 32 years) elective abdominal wall plasty (n=5), breast reduction (n=3), or liposuction of the thigh

(n=2) and the abdominal wall (n=1), respectively. Freshly isolated SVF containing variable fractions of mesenchymal and endothelial progenitors were loaded in 4mmX8mm β-TCP (ChronOS®) and HA (Engipore®) cylinders ($8.3X10^6$ - $39.2X10^6$ nucleated cells/cm^3), or 4mmX5mmX6mm acellular xenograft (Bio-Oss®) blocks ($8.3x10^6$ - $25.0x10^6$ nucleated cells/cm^3) and a fibrin hydrogel was adhered to each construct to serve as a cell carrier before subcutaneously implantation in nude mice. Eight weeks after implantation, the authors concluded that no major qualitative differences in the formation of dense matrix or blood vessels were observed between the scaffold groups. Even though dense collagen matrix was observed in samples stained with H&E and Masson's trichrome, no effective *de novo* bone formation could be observed, suggesting that SVF alone without short term osteoinductive stimulation poorly modulated osteogenic differentiation on scaffolds. In the second study, Levi et al. loaded hASC to apatite-PLGA composites and surgically implanted them into calvarial defect in nude mice[51]. Human ASC were harvested from female lipoaspirate. Critical-sized (4 mm) calvarial defects were created in the parietal bone of adult male nude mice. Defects were either left empty, treated with an apatite coated PLGA scaffold alone, or a scaffold with hASC. Cells were shown to persist within a defect site for two weeks (shown by sex chromosome analysis and quantified using Luciferase+ ASCs). Finally, recombinant BMP-2 (rBMP-2) was observed to increase hASC osteogenesis in vitro and osseous healing *in vivo*. The authors concluded that hASC ossified critical sized mouse calvarial defects without the need for pre-differentiation and that recombinant differentiation factors such as BMP-2 may be used to supplement hASC mediated repair. These two studies, indicated that SVF processing and implantation can be performed within real clinical setting situations. Moreover, repair of calvarial defect strongly suggested that

hASC-scaffolds can be used in the treatment of human skeletal defects as previously demonstrated[3].

The last *in vivo* study performed in 2010 investigated if alendronate (Aln), a bisphosphonate commonly used to treat osteoporotic patients, could enhance the in vitro and in vivo human adipose-derived stem cells (hADSCs) osteogenesis[43]. Wang et al. isolated hADSCs from the adipose tissue collected in 4 patients (age range, 20-36 years) admitted for elective hip replacement surgery. For the *in vitro* study, untreated hADSCs (control) or cells treated with increasing doses of Aln were cultured for 5 days in osteogenic medium. Immediately after, hADSCs (control and Aln-treated) were transferred into osteogenic medium and cultured for 14 days. For the *in vivo* study, porous PLGA discs (2mmX2mm) were pre-wetted, loaded with $1X10^6$ cells (one donor only) and incubated overnight before discs were placed in surgically created 7-mm calvarial defects in male Spraguee Dawley rats for 12 weeks post-implantation. Animals were separated in four groups with local injections of PBS or Aln (5 µM) performed 4 days post-implantation: PLGA alone + PBS; PLGA alone + Aln; hADSC/PLGA + PBS; and hADSC/PLGA + Aln. The findings of the in vitro study indicated that BMP-2 expression, ALP activity and alizarin red staining were enhanced in hADSCs pre-cultured with 5 µM Aln. Even though different degrees of bone in-growth were observed in all treatment groups, maximal new bone formation in critical-sized calvarial defects and BMP-2 expression were observed after 12 weeks in rats treated with local injection of Aln after implantation of hASDC-PLGA scaffold discs. The authors conclude that a combination of local, short-term Aln treatment with hADSCs and biodegradable PLGA enhanced the bone repair of a calvarial defect.

Studies performed in 2010, indicated that hASC-scaffold osteogenesis may be influenced by the scaffold composition. Moreover, complete cell processing to implantation can be performed

within real clinical setting situations. Finally, in osteoporotic patients, fracture treatment could one day be enhanced by combining local, short-term Aln treatment with hASC-scaffolds.

In 2011, during the preparation of this publication, only two published studies have combined hASC with scaffolds[32,42]. Weinand et al. compared the osteogenic potential of hASC to hBMSCs in third-generation gelatin/β-TCP scaffolds incorporated with controlled-release BMP-2[32]. Four different group combinations were evaluated in vitro at several time points. Density compared to native bone was observed at 6 weeks in scaffolds incorporated with controlled-release BMP-2. Gene expression of osteogenic markers as well as von kossa staining indicated similar bone formation in all group combinations (hBMSC, hASC, osteogenic or control media) in gelatin/beta-TCP scaffolds incorporating controlled-release BMP-2. The authors concluded that hASC and hBMSC treated with osteogenic or control media have similar osteogenic potential.

Lee et al. looked at the *in vitro* and *in vivo* osteogenesis of hASC transfected with osteogenic transcription factors to investigate if electroporation could be safely used as an alternative to viral transfection methods in bone tissue engineering applications[42]. Passage 2 of hASC lipoaspirated from three patients (mean age, 41 years) were electroporated with Runx2, Osterix, or both genes. The in vitro osteogenesis of transfected cells (passage 3) cultured in osteogenic medium was observed after 14 days in two groups: cells only or cells injected into 5mmX2mm PLGA scaffolds ($1X10^6$ cells/scaffold). Scaffolds were also subcutaneously implanted in nude mice to investigate if transfected cells promoted ectopic bone formation 6 weeks after implantation. In this case, groups composed of PLGA scaffolds only, PLGA-untransfected ASCs and PLGA-transfected ASCs treated with EGFP-C1 were used. Compared to untransfected cells (control), Runx2, Osterix, or both as well as the osteogenic markers ALP, COL1, OCN and

BSP were overexpressed after 7 and 14 days in transfected cells. Von Kossa staining of PLGA scaffolds loaded with hASC transfected with Runx2, Osterix, or both genes also showed greater mineralization than in scaffolds loaded with control cells after 14 days of culture in osteogenic medium. Six weeks post-implantation, mineralization of scaffolds loaded with hASC transfected with Runx2, Osterix, or both genes was also observed in nude mice using μ-CT and Masson's trichrome staining. The findings indicated ectopic bone formation was greater in mice implanted with scaffolds loaded with electroporated hASC than in mice implanted with scaffolds with untreated control cells, while no mineralization was observed in mice implanted with scaffolds only. The authors concluded that electroporation-mediated transfer of Runx2 or Osterix genes enhanced the *in vitro* and *in vivo* osteogenenic differentiation of hASC. These studies together, have so far indicated that hASC osteogenesis can be modulated in a scaffold microenvironment.

From all the studies performed in the decade following the first clinical evidence that hASC-scaffolds can be used in humans[3], two important points can be made. The first and most obvious is that hASC osteogenesis in scaffolds has been demonstrated in both *in vitro* and *in vitro* studies using a variety of bioabsorbable materials. Rats and nude mice models for non-weight bearing bone formation have led the way to assess hASC osteogenesis *in vivo*. While 1st generation scaffolds facilitate the attachment of hASC and subsequent cell proliferation, differentiation and in some cases neovascularization; their poor mechanical properties and brittle behavior are non-ideal for future scaffold-assisted bone regeneration with hASC. Composite scaffolds loaded with hASC have been shown to have better mechanical and biological properties and therefore may be preferred as scaffolding materials for hASC in future clinical trials. The second point, and maybe the most important for the future of hASC-scaffold therapy, is also clear in the current reports. Even though the field is still new, the lack of standardization in applied techniques (such

as scaffold fabrication, cell passages, loading techniques and medium preparations) makes the comparison between different studies difficult. Perhaps, such agreements will be reached in the near future allowing for more facile comparisons between different studies. With this important step, the use of hASC-scaffolds for bone regeneration would take a major step toward clinical trials and potential regulatory approval.

1.4. Conclusions

Since the first discovery of the hASC osteogenesis, research substantially progressed toward the use of hASC as stem cell source to regenerate bone. Current strategies primarily aim the *in vitro* characterization of the hASC osteogenic potential in novel or commercially available scaffolds combined or not with *in vivo* studies performed under non-weight bearing conditions in either rats or mice models for calvarial bone defects or subcutaneous ectopic bone formation. While 1st generation scaffold materials have been demonstrated to facilitate the attachment and hASC differentiation, their major limitations today are their relatively poor mechanical properties and brittle behavior. Due to the increased mechanical and biological properties 2nd and 3rd generation composites will be preferred as scaffolding materials for hASC in future tissue engineering applications. However, for scaffold-assisted bone tissue engineering combined with hASC become a reality, standardization of the current protocols is needed.

1.5. References

1. Zuk PA, Zhu M, Ashjian P, De Ugarte DA, Huang JI, Mizuno H, Alfonso ZC, FraserJK, Benhaim P, Hedrick MH. Human adipose tissue is a source of multipotent stem cells. Mol. Biol. Cell 2002;13:4279–4295.

2. Lawrence BJ, Madihally SV. Cell colonization in degradable 3D porous matrices. Cell Adh Migr 2008;2:9-16.

3. Lendeckel S, Jodicke A, Christophis P, Heidinger K, Wolff J, Fraser JK, Hedrick MH, Berthold L, Howaldt HP. Autologous stem cells (adipose) and fibrin glue used to treat

widespread traumatic calvarial defects: case report. J. Craniomaxillofac. Surg 2004;32:370–373.

4. Chim H, Hutmacher DW, Chou AM, Oliveira AL, Reis RL, Lim TC, Schantz JT. A comparative analysis of scaffold material modifications for load-bearing applications in bone tissue engineering. Int J Oral Maxillofac Surg 2006;35:928-934.

5. Tapp H, Hanley EN, Patt JC, Gruber HE. Adipose-derived stem cells: characterization and current application in orthopaedic tissue repair. Exp Biol Med 2009;234:1-9.

6. Levi B, Longaker MT. Concise review: adipose-derived stromal cells for skeletal regenerative medicine. Stem Cells 2011;29:576-582.

7. Zuk PA, Zhu M, Mizuno H, Huang J, Futrell JW, Katz AJ, Benhaim P, Lorenz HP, Hedrick MH. Multilineage cells from human adipose tissue: implications for cell-based therapies. Tissue Eng. 2001;7:211–228.

8. Kumar V, Abbas AK. Robbins and Cotran Pathologic basis of diseases; 2010. pp1425.

9. Katz AJ, Llull R, Hedrick MH, Futrell JW. Emerging approaches to the tissue engineering of fat. Clin Plast Surg 1999;26:587–603.

10. Rodbell M. Metabolism of isolated fat cells. II. The similar effects of phospholipase C (Clostridium perfringens alpha toxin) and of insulin on glucose and amino acid metabolism. J Biolog Chem 1966;241:130-139.

11. Rodbell M. The metabolism of isolated fat cells. IV. Regulation of release of protein by lipolytic hormones and insulin. J Biolog Chem 1966;241:3909-3917.

12. Rodbell M, Jones AB. Metabolism of isolated fat cells. 3. The similar inhibitory action of phospholipase C (Clostridium perfringens alpha toxin) and of insulin on lipolysis stimulated by lipolytic hormones and theophylline. J Biolog Chem 1966;241:140-142.

13. Mitchell JB, McIntosh K, Zvonic S, Garrett S, Floyd ZE, Kloster A, Di Halvorsen Y, Storms RW, Goh B, Kilroy G, Wu X, Gimble JM. Immunophenotype of human adipose-derived cells: temporal changes in stromal-associated and stem cell-associated markers. Stem Cells 2006;24:376-385.

14. Yoshimura K, Shigeura T, Matsumoto D, Sato T, Takaki Y, Aiba-Kojima E, Sato K, Inoue K, Nagase T, Koshima I, Gonda K. Characterization of freshly isolated and cultured cells derived from the fatty and fluid portions of liposuction aspirates. Journal of cellular physiology 2006;208:64-76.

15. Zhang ZY, Teoh SH, Chong MS, Schantz JT, Fisk NM, Choolani MA, Chan J. Superior osteogenic capacity for bone tissue engineering of fetal compared with perinatal and adult mesenchymal stem cells. Stem Cells 2009;27:126-137.

16. Kang SK, Putnam LA, Ylostalo J, Popescu IR, Dufour J, Belousov A, Bunnell BA. Neurogenesis of Rhesus adipose stromal cells. J Cell Sci 2004;117:4289–4299.

17. Kingham PJ, Kalbermatten DF, Mahay D, Armstrong SJ, Wiberg M, Terenghi G. Adipose-derived stem cells differentiate into a Schwann cell phenotype and promote neurite outgrowth in vitro. Exp Neurol 2007;207:267–274.

18. Trottier V, Marceau-Fortier G, Germain L, Vincent C, Fradette J. IFATS collection: using human adipose-derived stem/stromal cells for the production of new skin substitutes. Stem Cells 2008;26:2713–2723.

19. Fortunel NO, Otu HH, Ng HH, Chen J, Mu X, Chevassut T, Li X, Joseph M, Bailey C, Hatzfeld JA, Hatzfeld A, Usta F, Vega VB, Long PM, Libermann TA, Lim B. Comment on " 'Stemness': transcriptional profiling of embryonic and adult stem cells" and "a stem cell molecular signature". Science 2003;302:393,author reply 393.

20. Dominici M, Le Blanc K, Mueller I, Slaper-Cortenbach I, Marini F, Krause D, et al. Minimal criteria for defining multipotent mesenchymal stromal cells. The International Society for Cellular therapy position statement. Cytotherapy 2006;8:315–317.

21. Miranville A, Heeschen C, Sengenes C, Curat CA, Busse R, Bouloumie A. Improvement of postnatal neovascularization by human adipose tissue-derived stem cells. Circulation 2004;110:349-355.

22. Caplan AI. Mesenchymal stem cells. J Orthop Res 1991;9:641-650.

23. Horwitz EM, Le BK, Dominici M, Mueller I, Slaper-Cortenbach I, Marini FC, Deans RJ, Krause DS, Keating A. Clarification of the nomenclature for MSC: The International Society for Cellular Therapy position statement. Cytotherapy 2005;7:393-395.

24. Gimble JM, Bunnell BA, Guilak F, Smith SR, Katz AJ. Isolation and Growth of Stem Cells. In: Pallua. Tissue Engineering; 2011. pp643.

25. Thirumala S, Gimble JM, Devireddy RV. Cryopreservation of stromal vascular fraction of adipose tissue in a serum-free freezing medium. J Tissue Eng Regen Med 2010;4:224-232.

26. Liu Q, Cen L, Yin S, Chen L, Liu G, Chang J, Cui L. A comparative study of proliferation and osteogenic differentiation of adipose-derived stem cells on akermanite and beta-TCP ceramics. Biomaterials 2008;29:4792-4799.

27. James AW, Leucht P, Levi B, Carre AL, Xu Y, Helms JA, Longaker MT. Sonic Hedgehog influences the balance of osteogenesis and adipogenesis in mouse adipose-derived stromal cells. Tissue Eng Part A 2010;16:2605-2616.

28. Milat F, Ng KW Is Wnt signalling the final common pathway leading to bone formation? Molecular and cellular endocrinology 2009;310:52-62.

29. Engin F, Lee B. NOTCHing the bone: insights into multi-functionality. Bone 2010;46:274-280.

30. De Girolamo L, Lopa S, Arrigoni E, Sartori MF, Baruffaldi Preis FW, Brini AT.Human adipose-derived stem cells isolated from young and elderly women: their differentiation potential and scaffold interaction during in vitro osteoblastic differentiation. Cytotherapy 2009;11:793-803.

31. Im GI, Shin YW, Lee KB. Do adipose tissue-derived mesenchymal stem cells have the same osteogenic and chondrogenic potential as bone marrow-derived cells? Osteoarthritis Cartilage 2005;13:845-853.

32. Weinand C, Nabili A, Khumar M, Dunn JR, Ramella-Roman J, Jeng JC, Jordan MH, Tabata Y. Factors of Osteogenesis Influencing Various Human Stem Cells on Third-Generation Gelatin/beta-Tricalcium Phosphate Scaffold Material. Rejuvenation Res 2011;32:3166-3177.

33. Leong DT, Nah WK, Gupta A, Hutmacher DW, Woodruff MA. The osteogenic differentiation of adipose tissue-derived precursor cells in a 3D scaffold/matrix environment. Curr Drug Discov Technol 2008;5:319-327.

34. Marino G, Rosso F, Cafiero G, Tortora C, Moraci M, Barbarisi M, Barbarisi A. Beta-tricalcium phosphate 3D scaffold promote alone osteogenic differentiation of human adipose stem cells: in vitro study. J Mater Sci Mater Med 2010;21:353-363.

35. Reichert JC, Hutmacher DW. Bone tissue engineering. In: Pallua. Tissue Engineering; 2011. pp643.

36. Gaalen S, Kruyt M, Meijer G, Mistry A, Mikos A, Beucken J, Jansen J, Groot K, Cancedda R, Olivo C, Yaszemski M, Dhert W. Tissue Engineering of Bone. In: Clemens van Blitterswijk . Tissue Engineering; 2008. pp740.

37. Sandor GKB, Suuronen R. Combining Adipose-Derived Stem Cells, Resorbable Scaffolds and Growth Factors: An Overview of Tissue Engineering. J Canad Dent Assoc 2008;74:167-170.

38. Ahn HH, Kim KS, Lee JH, Lee JY, Lee IW, Chun HJ, Kim JH, Lee HB, Kim MS. In vivo osteogenic differentiation of human adipose-derived stem cells in an injectable in situ-forming gel scaffold. Tissue Eng Part A 2009;15:1821-1832.

39. De Girolamo L, Sartori MF, Arrigoni E, Rimondini L, Albisetti W, Weinstein RL, Brini AT. Human adipose-derived stem cells as future tools in tissue regeneration: osteogenic differentiation and cell-scaffold interaction. Int J Artif Organs 2008;31:467-479.

40. Muller AM, Mehrkens A. Towards an intraoperative engineering of osteogenic and vasculogenic grafts from the stromal vascular fraction of human adipose tissue. Eur Cell Mater 2010;19:127-135.

41. Frohlich M, Grayson W, Marolt D, Gimble J, Velikonja NK, Vunjak-Novakovic G. Bone grafts engineered from human adipose-derived stem cells in perfusion bioreactor culture. Tissue Eng Part A 2010;16:179-189.

42. Lee JS, Lee JM. Electroporation-mediated transfer of Runx2 and Osterix genes to enhance osteogenesis of adipose stem cells. Biomaterials 2011:32:760-768.

43. Wang CZ, Chen SM, Chen CH, Wang CK, Wang GJ, Chang JK, Ho ML. The effect of the local delivery of alendronate on human adipose-derived stem cell-based bone regeneration." Biomaterials 2010;31:8674-8683.

44. Dégano IR, Vilalta M, Bagó JR, Matthies AM, Hubbell JA, Dimitriou H, Bianco P, Rubio N, Blanco J. Bioluminescence imaging of calvarial bone repair using bone marrow and adipose tissue-derived mesenchymal stem cells. Biomaterials 2008;29:427-437.

45. Hattori H, Sato M, Masuoka K, Ishihara M, Kikuchi T, Matsui T, Takase B, Ishizuka T, Kikuchi M, Fujikawa K, Ishihara M. Osteogenic potential of human adipose tissue-derived stromal cells as an alternative stem cell source. Cells Tissues Organs 2004;178:2-12.

46. Gastaldi G, Asti A, Scaffino MF, Visai L, Saino E, Cometa AM, Benazzo F. Human adipose-derived stem cells (hASCs) proliferate and differentiate in osteoblast-like cells on trabecular titanium scaffolds." J Biomed Mater Res A 2010;94:790-799.

47. Scherberich A, Galli R, Jacquiery C, Farhadi J, Martin I. Three-dimensional perfusion culture of human adipose tissue-derived endothelial and osteoblastic progenitors generates osteogenic constructs with intrinsic vascularization capacity." Stem Cells 2007;25:1823-1829.

48. Haimi S, Moimas L, Pirhonen E, Lindroos B, Huhtala H, Raty S, Kuokkanen H, Sandor GK, Miettinen S, Suuronen R. Calcium phosphate surface treatment of bioactive glass causes a delay in early osteogenic differentiation of adipose stem cells." J Biomed Mater Res A 2009;91:540-547.

49. Haimi S, Suuriniemi N. Growth and osteogenic differentiation of adipose stem cells on PLA/bioactive glass and PLA/beta-TCP scaffolds." Tissue Eng Part A 2009;15:1473-1480.

50. Haimi S, Gorianc G. Characterization of zinc-releasing three-dimensional bioactive glass scaffolds and their effect on human adipose stem cell proliferation and osteogenic differentiation. Acta Biomater 2009;5:3122-3131.

51. Levi B, James AW, Nelson ER, Vistnes D, Wu B, Lee M, Gupta A, Longaker MT. Human adipose derived stromal cells heal critical size mouse calvarial defects. PLoS One 2010;5:e11177.

52. McCullen SD, Zhu Y. Electrospun composite poly(L-lactic acid)/tricalcium phosphate scaffolds induce proliferation and osteogenic differentiation of human adipose-derived stem cells. Biomed Mater 2009;4:035002.

53. Jeon O, Rhie JW, Kwon Ik, Kim JH, Kim BS, Lee SH. In vivo bone formation following transplantation of human adipose-derived stromal cells that are not differentiated osteogenically. Tissue Eng Part A 2008;14:1285-1294.

54. Leong DT, Abraham MC, Rath SN, Lim TC, Chew FT, Hutmacher DW. Investigating the effects of preinduction on human adipose-derived precursor cells in an athymic rat model." Differentiation 2006;74:519-529.

Chapter 2. Characterization of Novel Akermanite:Poly-E-Caprolactone Scaffolds for Human Adipose-Derived Stem Cells Bone Tissue Engineering

2.1. Introduction

Scaffold-assisted bone tissue engineering has been described as the alternative strategy to regenerate bone in the twenty-first century (Gaalen et al., 2008) because scaffolds can provide support for cell colonization, migration, growth, and differentiation in the fracture site (Lawrence and Madihally, 2010). Of the adult pluripotent cells sources used in scaffold assisted-bone tissue engineering strategies, human adipose-derived stromal cells (hASC) are of particular interest because hASC can be obtained readily through minimally invasive procedures and scaffolds loaded with autologous hASC have been clinically demonstrated to be an effective treatment to promote bone growth and tissue repair in humans (Lendeckel et al., 2004). To date, the scaffold-hASC osteogenic potential has been investigated using a variety of tissue engineering techniques. Recent studies have combined hASC with human autografts (Lendeckel et al., 2004; De Girolamo et al., 2008), acellular xenografts (De Girolamo et al., 2008; Muller and Mehrkens, 2010; Frohlich et al., 2010), synthetic polymers (Hattori et al., 2004; Dégano et al., 2008; Wang et al., 2010; Lee and Lee, 2011), ceramics (Scherberich et al., 2007; Dégano et al., 2008; De Girolamo et al., 2008; Liu et al., 2008; De Girolamo et al., 2009; Haimi et al., 2009; Haimi and Suuriniemi, 2009; Haimi and Gorianc, 2009; Marino et al., 2010; Gastaldi et al., 2010; Muller and Mehrkens, 2010) and composite scaffolds (Leong et al., 2006; Jeon et al., 2008; Leong et al., 2008; De Girolamo et al., 2009; Haimi and Suuriniemi, 2009; McCullen and Zhu, 2009; Zhang et al., 2009; Levi et al., 2010; Wang et al., 2010; Weinand et al., 2011). While clinical trials to exploit the benefits of scaffold-hASC for orthopedic applications are not underway in humans (Gimble et al., 2010; Gimble et al., 2011), the search for improved osteogenic scaffold materials continues.

Ideal scaffold materials for future hASC bone tissue engineering strategies should be biocompatible, absorbable, easy to handle, capable of supporting hASC growth and osteoinductive with predictable mechanical and degradation properties during the healing process (Reichert and Hutmacher, 2011). Autogenous bone grafts provide an osteoconductive matrix where self-osteoprogenitor cells can undergo osteogenesis through the synthesis and release of osteoinductive growth factors (Lendeckel et al., 2004; De Girolamo et al., 2008). However, the avaiability and the need for a secondary operative procedure are major limitations (Reichert and Hutmacher, 2011). Allogeneic grafts are more easily obtained (De Girolamo et al., 2008; Muller and Mehrkens, 2010; Frohlich et al., 2010), but cost, and concerns about disease transmission or implant rejection are remain concerns (Reichert and Hutmacher, 2011). Several types of bone-substitute scaffolds used in combination with hASC have demonstrated osteoconductive and osteoinductive properties (Leong et al., 2006; Scherberich et al., 2007; De Girolamo et al., 2008; Jeon et al., 2008; Leong et al., 2008; Liu et al., 2008; De Girolamo et al., 2009; Haimi et al., 2009; Haimi and Suuriniemi, 2009; Haimi and Gorianc, 2009; Marino et al., 2010; McCullen and Zhu, 2009; Zhang et al., 2009; Gastaldi et al., 2010; Levi et al., 2010; Muller and Mehrkens, 2010; Wang et al., 2010; Weinand et al., 2011).

Among the materials currently used in hASC bone tissue engineering strategies, β-tricalcium phosphate (β-TCP) is the most common (Leong et al., 2006; Leong et al., 2008; Liu et al., 2008; Marino et al., 2010; McCullen and Zhu, 2009; Zhang et al., 2009; Wang et al., 2010; Weinand et al., 2011). β-TCP is a biocompatible synthetic apatite ($Ca_3P_2O_8$) with osteoconductive and osteoinductive properties superior to natural bone hydroxyapatite (HA) (Gaalen et al., 2008; Wang et al., 2010). However, β-TCP has poor compressive strength (Miranda et al., 2008) and a high degradation rate (Bouler et al., 2000) making β-TCP a less than ideal choice for future

scaffold-hASC clinical trials. Recently, Liu et al. (2008) compared the osteogenic potential of hASC loaded to β-TCP with another biocompatible synthetic apatite (akermanite). The findings of this study indicated increased expression of osteogenic markers in hASC cultured on akermanite scaffolds. Akermanite ($Ca_2MgSi_2O_7$) is believed to have a stable degradation rate and result in superior bone deposition compared to β-TCP (Liu et al., 2008). Moreover the Ca, Mg, and Si ion extracts of akermanite scaffolds have been linked to hASC osteogenesis via up-regulation of extracellular signal-related kinase (ERK), a member of the mitogen-activated protein kinases (MAPKs) signaling pathway (Gu et al., 2011). These findings together with the improved mechanical and degradation properties (Liu et al., 2008) make akermanite a potential candidate for future hASC-bone tissue engineering strategies.

While current hASC osteogenesis strategies have been successfully demonstrated in either HA (Scherberich et al., 2007; Dégano et al., 2008; De Girolamo et al., 2009; Wang et al., 2010), β-TCP (Liu et al., 2008; Haimi and Suuriniemi, 2009; Zhang et al., 2009; Marino et al., 2010; Wang et al., 2010) and akermanite (Liu et al., 2008; Gu et al., 2011) ceramic scaffolds, the major limitations of 1st generation bone-substitute scaffolds used today are their relatively poor mechanical properties and brittle behavior (Reichert and Hutmacher, 2011). The latest innovation for bioactive and fiber-reinforced bioabsorbable composites is to use both bioactive and/or bioabsorbable ceramics and bioabsorbable polymeric fiber reinforcement in the same composite structure (Reichert and Hutmacher, 2011). Current models for hASC bone tissue engineering have combined HA (Jeon et al., 2008; Levi et al., 2010) and β-TCP (Leong et al., 2006; Leong et al., 2008; Haimi and Suuriniemi, 2009; McCullen and Zhu, 2009; Zhang et al., 2009; Weinand et al., 2011) with poly(l-lactic acid-co-glycolic acid –PLGA) (Jeon et al., 2008; Levi et al., 2010), poly(lactic acid - PLA) (Haimi and Suuriniemi, 2009; McCullen and Zhu,

2009), gelatin (Weinand et al., 2011) and poly-e-caprolactone (PCL) (Leong et al., 2006; Leong et al., 2008; Zhang et al., 2009) but, to date, no attempts to develop an akermanite composite have been made.

From a clinical stand point, moldable bone-substitute scaffolds are highly desirable (Kneser et al., 2006). Among the synthetic polymers currently used as composite scaffolds in hASC applications, PCL is an attractive candidate for the development of moldable akermanite scaffolds because it is biocompatible, poorly water-soluble, has a slow degradation rate, low melt viscosity and a glass transition temperature well below physiologic temperature (Leong et al., 2006; Gaalen et al., 2008; Leong et al., 2008; Zhang et al., 2009) allowing for facile molding. The objective of this study was to explore akermanite and PCL porous composite material as an alternative to pure ceramic or HA/β-TCP composites for support of hASC-combined bone tissue regeneration strategies. The hypothesis of this study was that an akermanite:PCL composite would have greater compressive strength and comparable biocompatibility and osteoinductive potential to control ceramic scaffolds.

2.2. Materials and Methods

2.2.1. Synthesis of Akermanite

Akermanite, $Ca_2MgSi_2O_7$, was synthesized by ceramic methods with calcium carbonate (1.237 g, 12.4 mmol), magnesium carbonate (0.521 g, 6.2 mmol), and silicon dioxide (0.742 g, 12.4 mmol) as the starting materials. These materials were mixed and ground up thoroughly using an agate mortar and pestle. The 2.5 g white powder mixture was then pressed into a pellet with hydraulic press (with approximately 1 metric ton of applied pressure) and then heated up multiple times in an open to air boat-shaped alumina crucible using a programmable box furnace to achieve the following net reaction:

$2\ CaCO_3 + MgCO_3 + 2\ SiO_2 \rightarrow Ca_2MgSi_2O_7 + 3\ CO_2\ (g)$

The initial heat treatment was carried out at 950°C (after increasing the furnace chamber temperature from room temperature at rate of 100°C/h) for 48 hours. This intermediate reaction, which involves the conversion of the carbonate starting materials to oxides, was then allowed to cool down back to room temperature by heat loss through the top exhaust port of the furnace. The pellet was then weighed to confirm the mass loss of approximately 0.8 g (or 18.5 mmol) of carbon dioxide. Subsequent heat treatments involved additional grinding, pellet pressing, and heating the crude product at the dwell temperature of 1300°C (after ramping up the temperature from room temperature at rate of 100°C/h) for 48 hours. Each 48 hour heat treatment was followed by cooling back to room temperature by furnace exhaust. The number of heat treatments at 1300°C required was dictated by proof of desired product purity (as judged by powder X-ray diffraction) and typically varied with each batch from 2 to 3 times.

2.2.2. Characterization of Akermanite by Powder X-Ray Diffraction

Powder X-ray diffraction was performed for phase identification and sample purity confirmation on a Bruker D8 Advance powder diffractometer equipped with Cu Kα radiation source ($\lambda = 1.54178$ Å) and a germanium incident beam monochromator. Intensities of diffracted X-rays were recorded at room temperature in 0.02° step size over a 2θ range of 15-60°. Experimental powder patterns of synthesized products were compared to single crystal data obtained from the Inorganic Crystal Structure Database (ICSD) in order to confirm sample purity and, if necessary, to identify possible impurities. A list of crystallographic data used for comparison is the following: CaO, ICSD 26959 (Gerlach, 1922); MgO, ICSD 29127 (Bragg, 1920); $Ca_3MgSi_2O_8$, merwinite, ICSD 26002 (Moore and Araki, 1972); and $Ca_2MgSi_2O_7$, akermanite, ICSD 26683 (Warren, 1930).

2.2.3. Synthesis of Ceramic Scaffolds

Akermanite and 60%β-tricalcium phosphate:40%hydroxyapatite (60:40 β-TCP:HA) powders (3 g) were suspended in polyvinyl alcohol aqueous solution (10 wt %) and stirred in a glass beaker to obtain a well-dispersed slurry (Liu et al., 2008). Polyurethane foam templates were cut into the desired shapes (10mmX10mm and 10mmX4mm) to replicate a porous scaffold. Then, the prepared foam templates were immersed in a glass beaker containing akermanite or 60:40 β-TCP:HA slurry and compressed with glass stick to force the slurry to migrate into the pores of the foams which were then incubated at 60°C for 1 day. After drying, the scaffolded materials (either akermanite or a 60:40 β-TCP:HA mixture) were placed in an open to air boat-shaped alumina crucible and heated in a programmable box furnace to 500°C (at rate of 50°C/h) and allowed to dwell at this temperature for 5 hours. After allowing the furnace to cool to room temperature, the scaffolds were then heat treated at 1300°C (at rate of 60°C/h) for 3 hours and cooled to room temperature by furnace exhaust.

2.2.4. Fabrication of PCL and Akermanite:PCL Scaffolds

A 10% PCL solution in 8 ml of 1-4, dioxane was prepared and akermanite was added at weight (g) ratio of 0,0:0,8 (PCL); 0.2:0.6; 0.4: 0.4; 0,6:0.2 (25:75; 50:50; 75:25 akermanite:PCL wt.%) in a glass bottle. The mixtures were molded into 10mmX4mm polydimethylsiloxane (PDMS) templates or in 17mmX10mm glass cylinder vials. Composites (akermanite:PCL) and pure PCL solutions were immediately frozen with liquid nitrogen with a drop ratio of 1 inch/hour using a unidirectionally thermally induced phase separation technique over 2 hours (10mmx10mm cylinders) or frozen at -20^{o}C overnight (10mmX4mm discs). Post freezing the samples were immediately incubated in a freeze-drier for 48 hours. PCL or akermanite:PCL scaffolds were prepared for SEM, compression testing, degradation rate and cytotoxicity studies.

2.2.5. Scaffolds Ultrastructure Characteristics

The morphology of the resulting specimens was observed by scanning electron microscopy (SEM; JSM-6610). For SEM observations, the scaffolds were mounted on aluminum specimen stubs with gold-palladium using an SPI-module Sputter Coater at 7 mA for 2 min and immediately examined under SEM at 10 kV. Scanning electron micrographs were evaluated with MetaMorph® Software package for Olympus. The porosity of the scaffolds was determinate in triplicates by subtracting the total scanned electron micrograph area from the void space. The pore size of the scaffolds was measured in triplicates (5 measurements/scanner electron micrograph) for each scaffold type.

To analyze the cellular distribution in the scaffolds, hASC-scaffolds were fixed in 2% gluteraldehyde and 0.1M phosphate buffer (PB, pH 7.45) at 48^{o}C for 1 h. The same buffer (PB, pH 7.45) was used twice to wash the samples, followed by dehydration series in ethanol (50%, 70%, 90%, 95%, and 100%) before the samples were dried for mounting and coating as described above.

2.2.6. Mechanical Test

Three specimens per scaffold type with geometry of 10mmX10mm were compressed at room temperature using a hydraulic-mechanical testing machine (Instron-Model 5696) at testing rate of 5 mm/min and maximum compression strain of 90%.

2.2.7. Degradation Rate in Stromal Medium

In vitro degradation of scaffolds cultured (1 scaffold/15 mL centrifuge tube) in 5 ml of stromal medium (Dulbecco's modified Eagle's medium (DMEM), 10% FBS, 1% triple antibiotic solution) was performed in triplicates after 7, 14 and 21 days. Weight of dried scaffolds was collected from each scaffold at time point 0. Briefly, weight loss was determined by incubation,

at 37°C in stromal medium, agitation on an orbital shaker incubator (Thermo Scientific) at each time point. Before each measurement, scaffolds were trypsinized, rinsed in distilled water and freeze-dried for 48 hours. The media extracts of the scaffolds were stored at 4°C for viability assays.

2.2.8. Isolation of hASC and Culture

Liposuction aspirates from subcutaneous adipose tissue were obtained from male (n = 1) and females (n = 2) subjects undergoing elective procedures. All tissues were obtained with informed consent under a clinical protocol reviewed and approved by the Institutional Review Board at the Pennington Biomedical Research Center. Isolation of hASC was performed as described elsewhere (Gimble et al., 2011). The initial passage of the primary cell culture was referred to as ‘‘Passage 0’’ (p0). The cells were passaged after trypsinization and plated at a density of 5,000 cells/cm^2 (‘‘Passage 1’’) for expansion on T125 flasks until 80% of confluence was reached. Passage 2 of each individual was used for cell viability after acute exposure to the scaffold medium extracts and on scaffolds after loading using a spinner flask.

2.2.9. MTT Assay and hASC-Cytotoxicity to Medium Extracts

The cellular viability of on scaffold cultures were determined using the cytotoxicity assay (MTT proliferation kit). The media extracts from scaffolds after 7, 14 and 21 days of culture were filtered and then pipetted (100 μL/well) into a 96-well plate previously sub-cultured with hASC (3,000 cells/well) and incubated in a CO_2 incubator at 37°C containing 5% CO_2 for 24 hours. After the 24-hours incubation period, 10 μL of the MTT reagent was added to the each well and re-incubated at 37°C in 5% CO_2 for 4 h. Then, MTT detergent (100 μL) was added to each well and samples were incubated at 37°C in 5% CO_2 overnight. Cell viability was measured

at wavelength of 590 nm using a plate reader. Each experiment was performed in triplicates for hASC plated from each of the three donors (3 wells/donor).

2.2.10. hASC Loading on Scaffolds and Culture

Passage 2 of each donor (n = 3) was individually loaded to each scaffold type (10 scaffolds/type/donor) using a custom-made spinner flask bioreactor at loading density of 1,300 cells/mL for 2 hours. Immediately after, scaffolds were transferred into 48-well plates and maintained in stromal medium for 21 days. SEMs and live/dead staining (Cell viability®, Invitrogen – using a Leica DM RXA2 Deconvolution System) were performed at 7, 14 and 21 days to assess hASC attachment and viability on scaffolds.

2.2.11. Quantification of DNA on Scaffolds

Total DNA content was used to determine the number of cells on each scaffold as previously described (Liu et al., 2008). Briefly, scaffolds were crushed and then incubated with 0.5 mL proteinase K (0.5 mg/mL) at 56ºC overnight. The mixture was centrifuged at 108 g for 5 minutes and then 50 µl aliquots were mixed with 50 µl Picogreen dye solution (0.1 g/mL, Invitrogen) in 96-well plates. Samples were excited at 480 nm and total DNA concentration was compared to a standard curve generated from serial dilutions of hASC. Scaffold without cells were used to subtract the background fluorescence emission from all readings.

2.2.12. Reverse Transcriptase-Polymerase Chain Reaction (RT-PCR)

Total RNA was extracted from cells and cell-scaffold using the Trizol reagent (Sigma). RT-PCR was performed using OneStep RT-PCR kit (Qiagen) and interleukin-6 (Il-6) forward (5'-CAGAAAACAACCTGAACCTTCCA -3') and reverse (5'-GGCAAGTCTCCTCATTGAATCC -3') to assess proinflammatory upregulation in hASC exposed to the medium extracts and on cells loaded to the scaffolds; and alkaline phosphatase

(ALP) forward (5'- AATATGCCCTGGAGCTTCAGAA -3') and reverse (5'-CCATCCCATCTCCCAGGAA -3') and osteocalcin (OCN) forward (5'-GCCCAGCGGTGCAGAGT -3') and reverse (5'- TAGCGCCTGGGTCTCTTCAC -3') to assess the osteogenic differentiation of hASC loaded to scaffolds at different time points. Reactions were performed with a MJ Mini Thermal Cycler (BioRad). Water (negative), LPS-treated cells (500 μg/mL) and hASC culture in osteogenic medium for 21 days were used as controls. Samples were normalized (ΔCt) against the house keeping gene 18SrRNA. Semi-quantitative analysis of the gels was performed in duplicates by measuring the mean and intensity of each band with Photoshop. The relative expression of the bands was calculated by dividing the absolute intensity of each target gene by the absolute intensity of the 18SrRNA bands.

2.2.13. Statistical Analysis

All results were expressed as mean±SEM. Normality of the data was confirmed using the Shapiro-Wilk test ($P < 0.001$). Data was analyzed with one or two-way analysis of variance (ANOVA), followed by Tukey's minimum significant difference (MSD) post hoc test for pairwise comparisons of main effects. For all comparisons, a P-value < 0.05 was considered significant.

2.3. Results

2.3.1. Synthetic Akermanite Purity Confirmation

Representative powder x-ray diffraction patterns are provided in Figure 3 for akermanite ceramic. The result after the initial heat treatment at 950°C (Figure 3a) shows diffraction peaks corresponding to the products of decarbonation, calcium oxide ($2\theta = 32.26°$, 37.44°, and 53.96° which can be indexed as hkl = 1 1 1, 0 0 2, and 0 2 2, respectively) and magnesium oxide (2θ =

42.96° which can be indexed as *hkl* = 0 0 2). Also the formation of the merwinite phase, $Ca_3MgSi_2O_8$, can be observed by presence of major diffraction peaks (2θ = 33.42°, 33.56°, 33.82°, and 47.60° which can be indexed as *hkl* = 0 1 3, 4 1 1, 0 2 0, and -4 2 2, respectively). Typically, the next heat treatment carried out at 1300°C results in the presence of two predominant mineralogical phases, akermanite and merwinite (Figure 3b). After 2-3 successive heat treatments at 1300°C, the merwinite phase was eventually removed (or below the limits of detection) and a pure sample akermanite was prepared for scaffold formation (see Figure 3c for proof akermanite purity).

2.3.2. Ultrastructure Characterization of the Scaffolds

The scanning electron micrographs of the scaffolds revealed the formation of porous structures with varying porosity and pore size (Figures 4AB). Scaffolds composed of PCL (Figure 4d) and different akermanite:PCL combinations (25:75, 50:50 and 75:25 - Figures 4e-f, respectively) had the highest porosities which averaged 89% (89.09±2.73) and were at least 1-fold greater than the porosities reported for CellCeramic™ (82.50±0.50 - Figure 4a), 60:40 β-TCP:HA (58.00±3.00 - Figure 4b) and akermanite (55.00±4.00 - Figure 4c) ($P < 0.05$). CellCeramic™ scaffolds had the greatest pore size (280 μm ±37.44), followed by 75:25 (118.20 μm ±8.82) and 25:75 (103.60 μm ±7.28) akermanite:PCL scaffolds as well as akermanite (98.57±18.92), all of which had pores significantly greater than those observed in PCL (73.2±2.417) and 60:40 β-TCP:HA (55.99±7.486) scaffolds.

2.3.3. Compression Test

At maximum strain, 25:75 akermanite:PCL scaffolds displayed the highest strength (9831 Kpa±1200), followed by the other two akermanite:PCL scaffolds (75:25, 4592±407.90; 50:50,

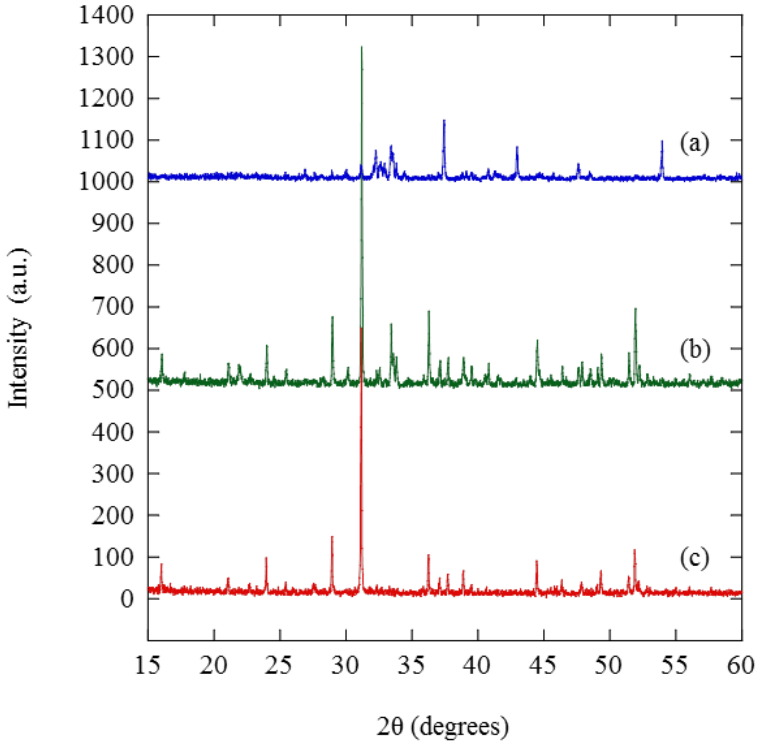

Figure 3. Powder x-ray diffraction patterns for akermanite ceramic. In (a) the formation of decarbonation, calcium oxide and magnesium oxide and merwinite are shown after the initial heat treatment at 950°C. In (b), the predominant presence of akermanite and merwinite after heat treatment at 1300°C. Finally in (c), the presence of pure akermanite is shown at 2-3 successive heat treatments at 1300°C.

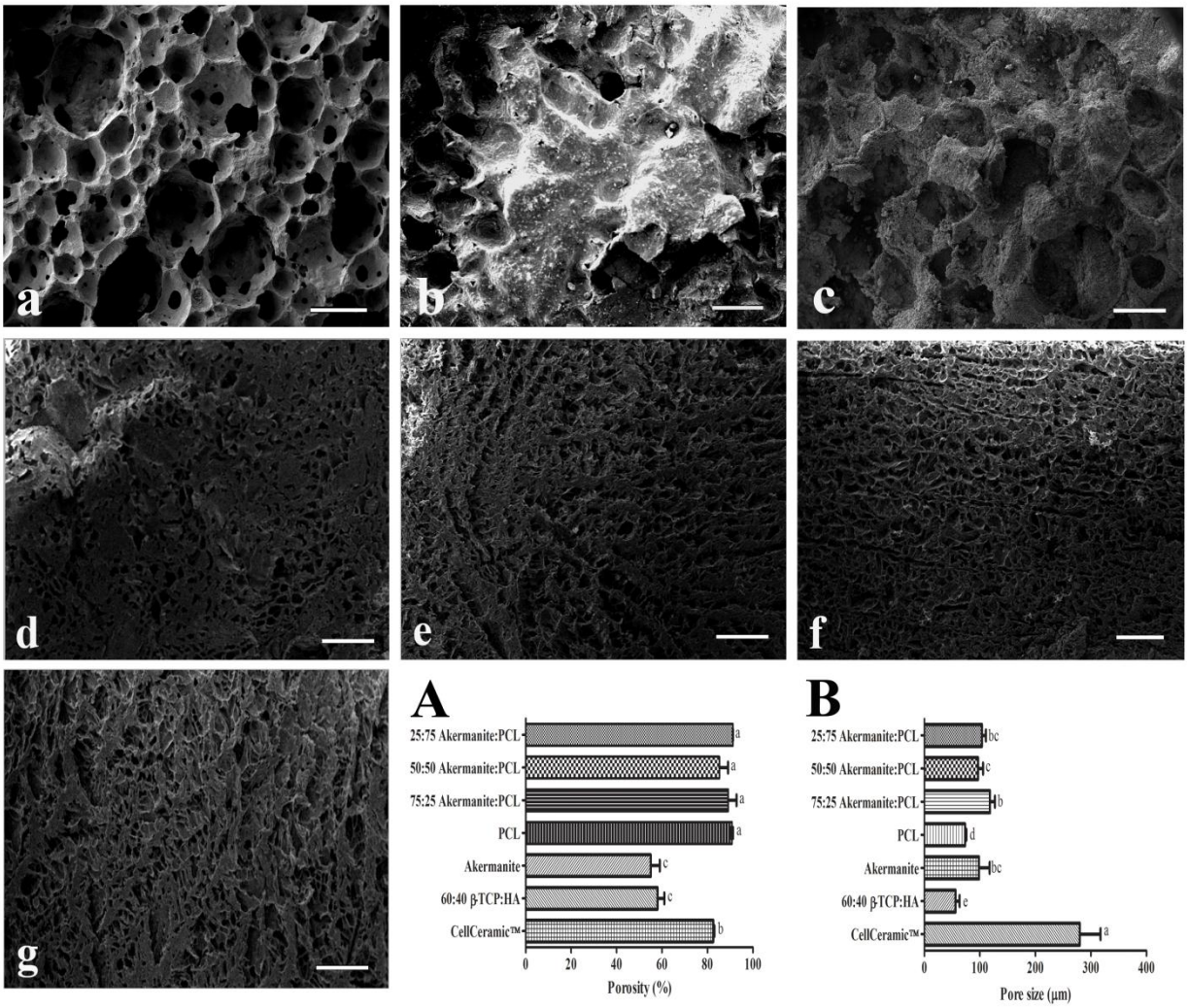

Figure 4. Porosity (A) and pore size (B) of CellCeramic^{TM} (a), 60:40 β-TCP:HA (b), akermanite (c), PCL (d) and the akermanite:PCL combinations (75:25; 50:50; 25:75 – e-f, respectively). Scale bar 500 μm.

4320±1459) and PCL (4387±43.55) which had similar compression strength but were statistically stronger than akermanite (1598±415) scaffolds. Among the scaffolds, 60:40 β-TCP:HA (743.90±43.55) and CellCeramic™ (607.70±7.65) had the lowest strengths (Figure 5).

2.3.4. *In vitro* Scaffold Degradation

Figure 6 shows the degradation of the scaffolds in stromal medium as a function of the dry mass lost (%) over a 21 days period. In general, 60:40 β-TCP:HA (91.34±0.51), CellCeramic™ (90.34±0.50) and akermanite (89.97±0.17) lost the most mass after 7 days, followed by PCL (93.28±0.40) and the three akermanite:PCL combinations (25:75 - 97.98±0.45; 50:50 - 97.34±0.33; 75:25 - 96.14±0.12). After 14 days, akermanite scaffolds dissolved the most in stromal medium (74.42±0.482), with comparable loses in CellCeramic™ (81.33±0.11) and 60:40 β-TCP:HA (83.24±0.12) which degraded more than PCL (89.34±0.367) and two akermanite:PCL scaffolds (50:50, 89.78±0.11; 75:25, 89.34±0.57). Within this time point, scaffolds composed of 25:75 akermanite:PCL had the lowest mass loss.

The percentage of dry weight lost after 21 days was the greatest in CellCeramic™ (73.26±0.59), 60:40 β-TCP:HA (76.19±0.49) and akermanite (72.76±0.17) scaffolds, followed by comparable loses in the 75:25 (82.76±0.29) and 50:50 (83.40±0.33) akermanite:PCL scaffolds. At the end of this experiment, PCL (87.01±0.17) and 25:75 (88.62±0.51) akermanite:PCL scaffolds had the lowest dry mass losses.

The percentage of dry weight lost after 21days was the greatest in CellCeramic™ (73.26±0.59), 60:40 β-TCP:HA (76.19±0.49) and akermanite (72.76±0.17) scaffolds, followed by comparable loses in the 75:25 (82.76±0.29) and 50:50 (83.40±0.33) akermanite:PCL scaffolds. At the end of this experiment, PCL (87.01±0.17) and 25:75 (88.62±0.51) akermanite:PCL scaffolds had the lowest dry weight losses.

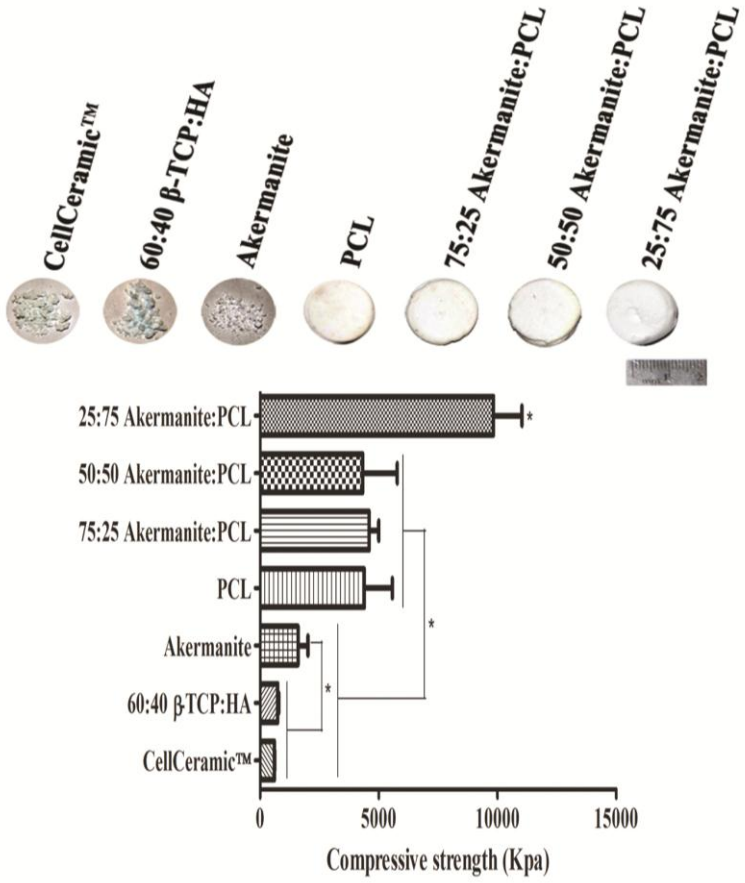

Figure 5. Compression strength in cylindrical discs (10mmX10mm). The images are depicting the deformed scaffolds immediately after maximum strain.

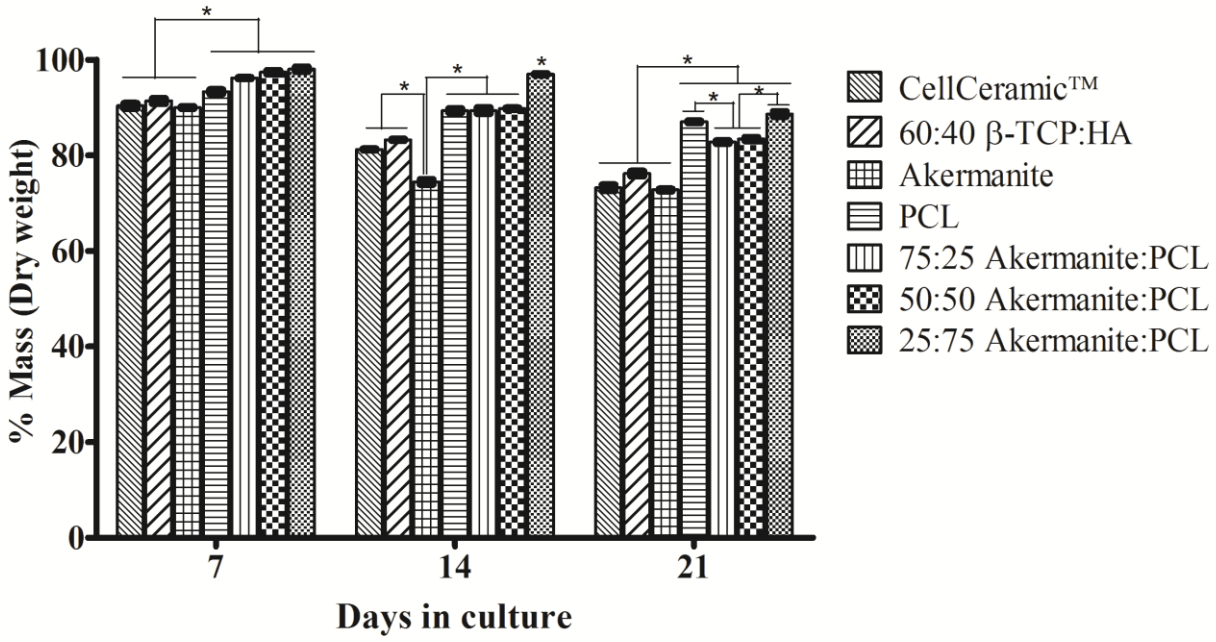

Figure 6. Percentage of dry weight loss in scaffolds immersed in stromal media and incubated in a shaker at 37°C over a 21 days period. The asterisks indicate significant differences in the dry weight percentage of tested scaffolds within the same time point.

2.3.5. Viability of hASC After Acute Exposure to the Media Extracts of Different Scaffolds (The MTT Assay)

The hASC 24 hours exposure to the media extracts collected from the tested scaffolds after 7, 14 and 21 days revealed distinct metabolic activity patterns (Figure 7A) and cell behaviors (Figure 7a-u) as a function of scaffold composition. For the media extracts collected after 7 days, the hASC metabolic activity was the highest in cohorts subjected to akermanite (0.22±0.01 - Figure 7m) and the akermanite:PCL combinations (75:25, 0.22±0.01 - Figure 7g; 50:50, 0.21±0.01 - Figure 7d; 25:75, 0.19±0.01 - Figure 7a) which were significant greater than the metabolic activity observed in hASC exposed to PCL (0.11±0.01- Figure 7j), followed by 60:40 β-TCP:HA (0.04±0.01- Figure 7p) and CellCeramic^{TM} (0.01±0.01- Figure 7s) ($P < 0.05$). After 14 days, the metabolic activity of the hASC as a function scaffold content revealed comparable metabolic patterns in hASC exposed to akermanite (0.18±0.01- Figure 7n) and 25:75 akermanite:PLC (0.18±0.01- Figure 7b), however these values were significantly greater than the values observed in hASC exposed to 75:25 (0.12±0.02- Figure 7h) and 50:50 (0.11±0.02- Figure 7e) akermanite:PCL media extracts, CellCeramic^{TM} (0.10±0.01- Figure 7t) and PCL (0.10±0.01 - Figure 7k). After 14 days, the metabolic activity of hASC exposed to 60:40 β-TCP:HA (0.04±0.01 - Figure 7q) media extracts was the lowest among the tested scaffolds ($P < 0.05$).

The metabolic activity of hASC exposed media extracts collected after 21 days was the highest in hASC exposed to akermanite (0.20±0.01 - Figure 7o) and 25:75 akermantie:PCL (0.20±0.01 - Figure 7c) which were significantly greater than PCL (0.16±0.01 - Figure 7l), CellCeramic^{TM} (0.11±0.01 - Figure 7u), 60:40 β-TCP:HA (0.08±0.01 - Figure 7r) and two of the akermanite:PCL combinations (75:25, 0.04±0.01 - Figure 7i; 50:50, 0.03±0.01 - Figure 7f).

In general, hASC detachment during acute exposure to scaffolds media extracts at different time points was not observed in cohorts exposed to PCL (Figures 7j-l), akermanite (Figures 7m-

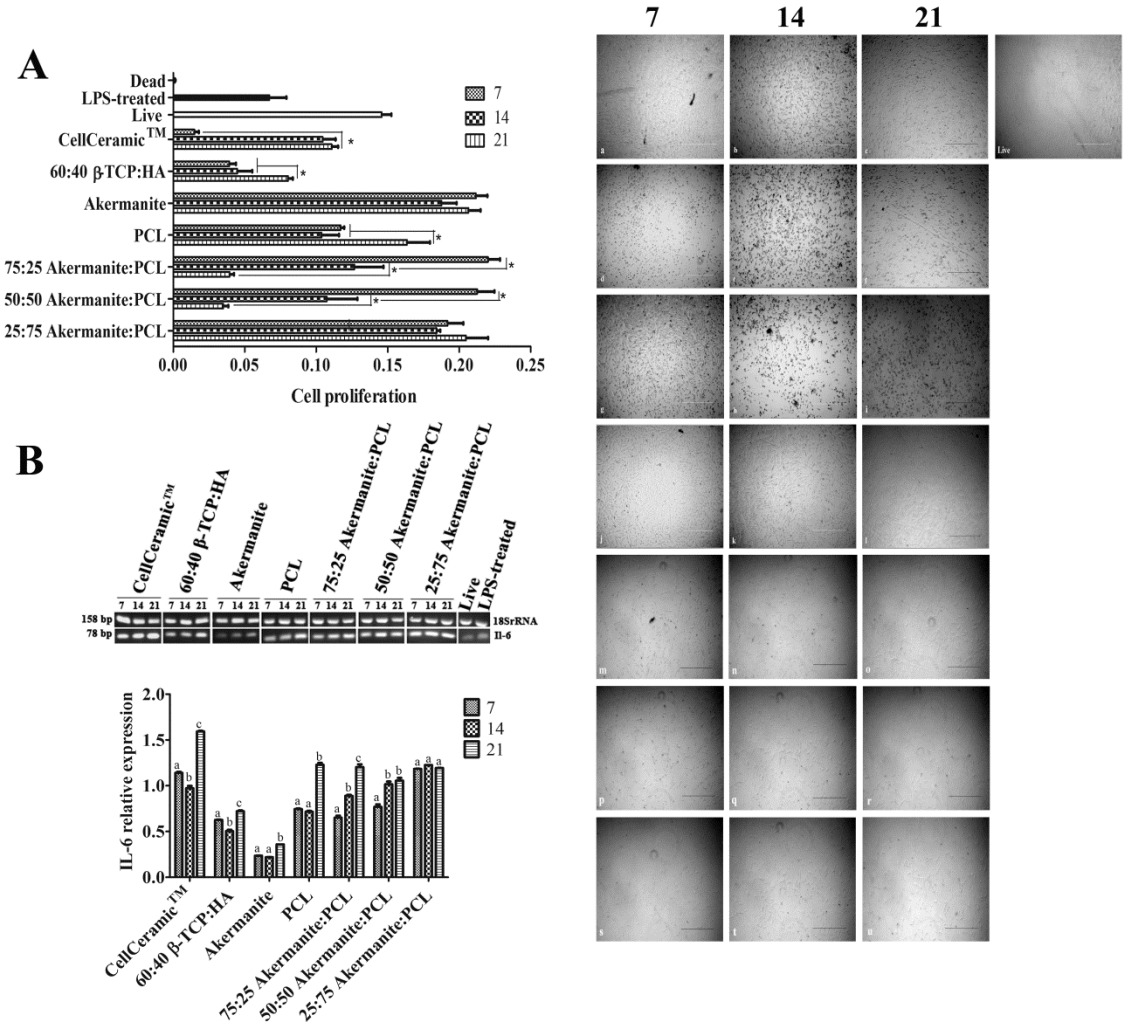

Figure 7. Viability of hASC (n = 3 donors) after acute exposure (24 hours) to the media extracts of different scaffolds. In A, the cell proliferation of hASC, determinate by the MTT assay, indicate the hASC metabolic activity after expose to different media extracts. In B, the gels and the semi-quantitative analysis of the Il-6 relative expression are depicted after hASC acute exposure to different media extracts at 7, 14 and 21 days. The asterisks indicate significant differences in the metabolic activity and the Il-6 relative expression within different time points for each one of the scaffold media extracts. Inserts indicate the hASC behavior after acute exposure to scaffold media extracts at 7, 14 and 21 days. Briefly, 25:75 akermanite:PCL (a-c), 50:50 akermanite:PCL (d-f), 75:25 akermanite:PCL (g-i), PCL (j-l), akermanite (m-o), 60:40 β-TCP:HA (p-r) and CellCeramic^{TM} (s-u). Scale bars 1040 μm, 2X.

o), 60:40 β-TCP:HA (Figures 7p-r) and CellCeramic™ (Figures 7s-u). However, increased number of detached hASC were observed after acute exposure to the three akermanite:PCL combinations tested in this study (Figures 7a-i). In the media extracts collected after 7 days, hASC detachment was not observed in hASC exposed to 25:75 akermanite:PCL media extracts (Figure 7a), however hASC detachment was observed in the cohorts exposed to 50:50 (Figure 5d) and 75:25 (Figure 7g) akermanite:PCL media extracts, respectively. In hASC exposed to the akermanite:PCL media extracts after 14 days of culture, increased numbers of detached hASC were observed in all three akermanite:PCL combinations (Figures 7b,e,h). Likewise, hASC exposure to the media extracts of akermanite:PCL scaffolds cultured for 21 days yielded highest number of detached cells, especially in hASC exposed to 75:25 akermanite:PCL media extracts (Figure 7i).

2.3.6. Semi-Quantitative RT-PCR Analysis After hASC Acute Exposure to Media Extracts

The relative expression of Il-6 mRNA changed significantly over time in hASC exposed to all media extracts, with the exception cells exposed to the 25:75 akermanite:PCL media extracts (Figure 7B). After 7 days, the relative expression of Il-6 was highest in hASC exposed to the media extracts collected from CellCeramic™ (1.14±0.01) and 25:75 akermanite:PCL (1.18±0.01) with no significant differences observed between them, followed by significant differences between 50:50 akeramanite:PCL (0.77±0.02) and PCL (0.74±0.01) which were comparable between each other but significantly greater than 75:25 akermanite:PCL (0.65±0.01) and 60:40 β-TCP:HA (0.62±0.01) which were statistically greater than the Il-6 expression observed in hASC exposed to the akermanite (0.23±0.01) media extracts.

In the hASC exposed to media extracts collected after 14 days of culture, the Il-6 expression was the highest in hASC exposed to the 25:75 akermanite:PCL media extracts (1.22±0.01), with

comparable Il-6 expression between 50:50 akermanite:PCL (1.01±0.02) and CellCeramic™ (0.97±0.01) media extracts which were both statistically greater than 75:25 akermanite:PCL (0.89±0.01), PCL (0.71±0.01) and 60:40 β-TCP:HA (0.50±0.01). Within the same time point, the Il-6 expression was the lowest in hASC exposed to akermanite media extracts (0.22±0.01).

For the media extracts of scaffolds collected after 21 days, the Il-6 expression was the highest in hASC exposed to CellCeramic™ (1.59±0.01), followed by comparable Il-6 expression between hASC expose to PCL (1.23±0.01), 75:25 (1.20±0.02) and 25:75 (1.19±0.01) akermanite:PCL media extracts which were significantly greater than 50:50 akermanite:PCL (1.05±0.02) and 60:40 β-TCP:HA (0.72±0.01). The lowest Il-6 expression in hASC exposed to scaffolds media extracts collected after 21 days of culture was observed in hASC exposed to akermanite media extracts (0.36±0.01).

2.3.7. Viability of hASC on Scaffolds

Spinner flask bioreactor yielded in average a loading efficiency of 67% (66.71±5.16) with no significant differences between scaffold types. In the summary provided in Figure 8, the viability of hASC loaded to akermanite:PCL scaffolds 25:75 (Figure 8a), 50:50 (Figure 6d) and 75:25 (Figure 8g) measured by the Live/Dead staining after 7 days was lowered than in the control ceramic scaffolds (akermanite - Figure 8m; 60:40 β-TCP:HA - Figure 8p; CellCeramic™ - Figure 8s) but greater than in PCL alone (Figure 8j), with increased number of viable hASC in 75:25 akermanite:PCL scaffolds. After 14 and 21 days of culture, increased number of viable hASC was observed in akermanite (Figure 8n-0), 60:40 β-TCP:HA (Figure 8q-r), CellCeramic™ (Figure 8t-u) and 75:25 akermanite:PCL (Figure 8h-i) compared to PCL (Figure 8k-l) and the other akermanite:PCL scaffolds (25:75 and 50:50, Figures 8b-c and e-f, respectively).

2.3.8. DNA Quantification on Scaffolds (The Picogreen Assay)

Considering the hASC proliferation on different scaffolds (Figure 9A), after 7 days the highest DNA content was observed in 75:25 akermanite:PCL (70240±22501.80 - Figure 10g**)** and akermanite (59181.67±11948.23 - Figure 10m) which had DNA content significantly greater than CellCeramic^{TM} (41640±4484.65 - Figure 10s) and 60:40 β-TCP:HA (40665±7908.80 - Figure 10p) and the two akermanite:PCL (50:50, 28720±7229.06 - Figure 10d; 25:75, 27578.33±4708.83 - Figure 10a) scaffolds. After 7 days, the DNA content was the lowest in PCL scaffolds (7356.66±828.07 - Figure 10j). After 14 days, the DNA content in 60:40 β-TCP:HA (377700±5654.08 - Figure 10q) was the highest, followed by akermanite (293816.70±27296.70 - Figure 10n), CellCeramic^{TM} (215666.70±8920.15 - Figure 10t) and the akermanite:PCL scaffolds (25:75, 179123.30±51537.14 - Figure 10b; 50:50, 162813.30±33623.31 - Figure 10e; 75:25, 207240±53526.80 - Figure 10h) which had comparable DNA content. Within this time point, the lowest DNA content was observed in PCL scaffolds (87756.66±10172.56 - Figure 10k).

After 21 days in culture, increased DNA content was observed in both akermanite (436716.70±31693.88 - Figure 10o) and CellCeramic^{TM} (511316.70±44057 - Figure 10u) scaffolds which were significantly greater than the DNA contents observed in 60:40 β-TCP:HA (319066.70±2419.32 - Figure 10r), the 50:50 (213580±62017.20 - Figure 10f) and 75:25 (252968.30±73711.24 - Figure 10i) akermanite:PCL scaffolds and the 25:75 akermanite:PCL (120111.70±28936.16 - Figure 9c). At the end of the experiment, the lowest DNA content was observed in PCL scaffolds (36158.33±7866.60 - Figure 9l).

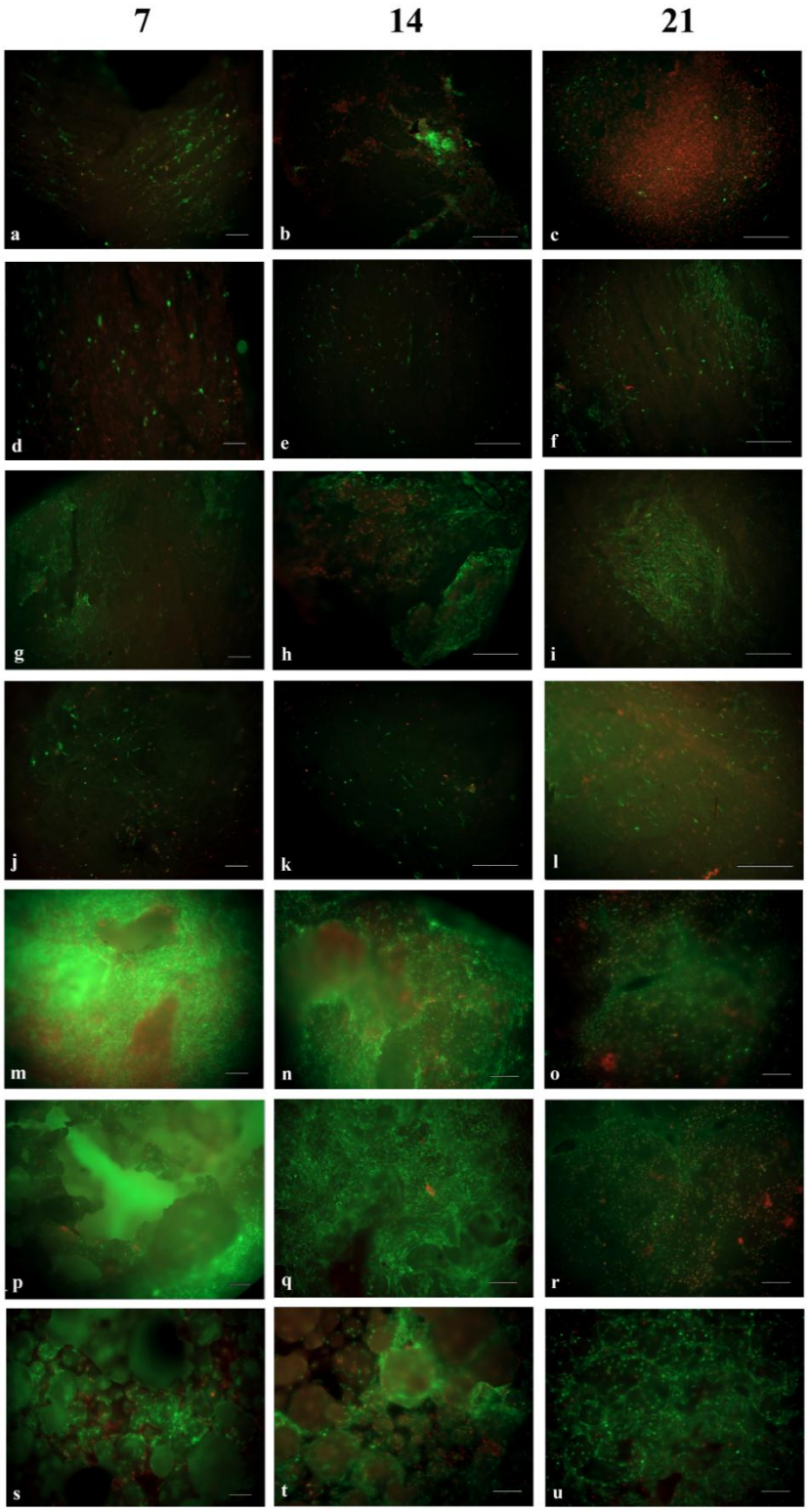

Figure 8. Live (green) and Dead (read) stain of the scaffolds loaded with hASC (n = 3 donors) after 7, 14 and 21 days of culture. Briefly, 25:75 akermanite:PCL (a-c), 50:50 akermanite:PCL (d-f), 75:25 akermanite:PCL (g-i), PCL (j-l), akermanite (m-o), 60:40 β-TCP:HA (p-r) and CellCeramic^{TM} (s-u). Scale bars 500 μm, 5X.

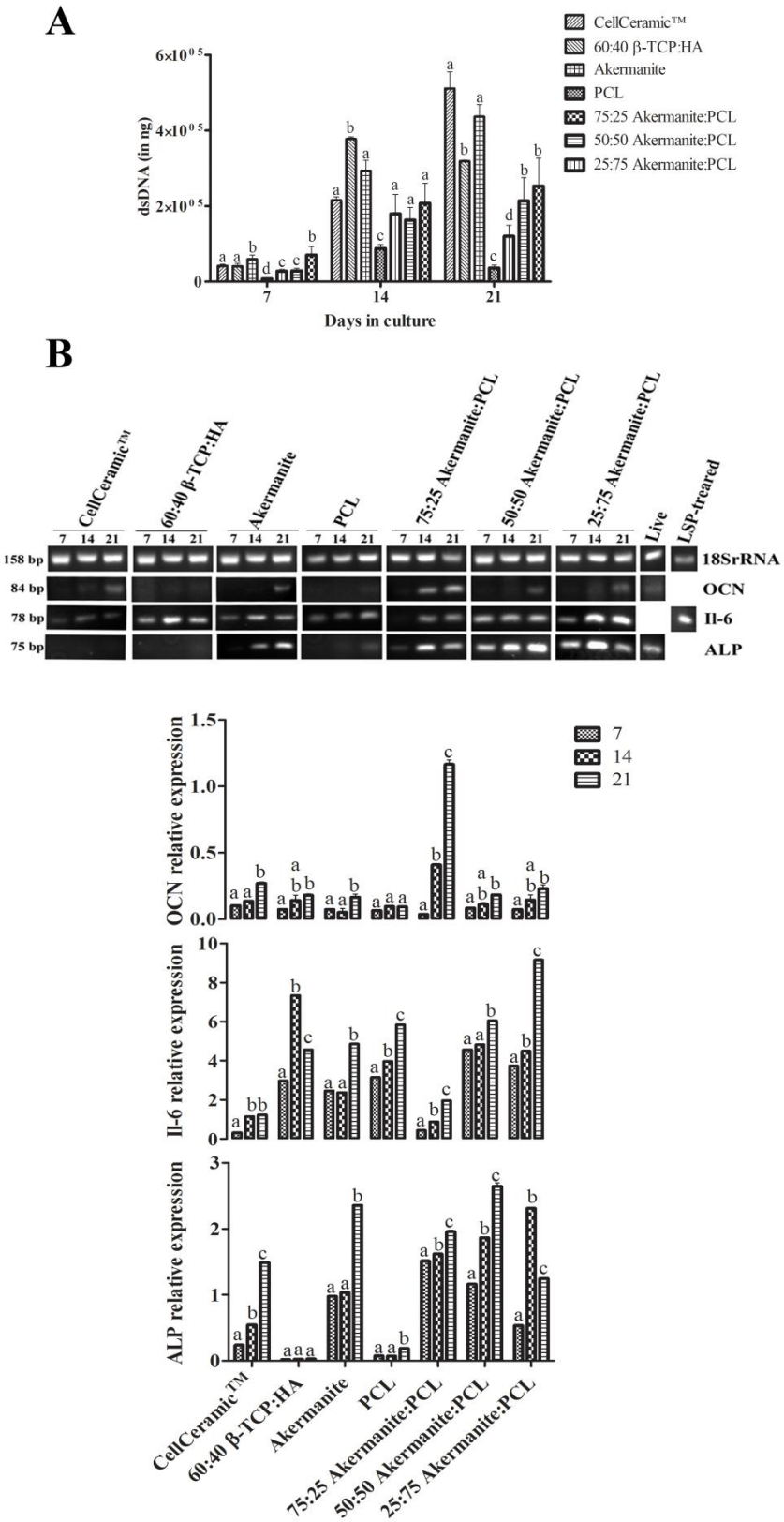

Figure 9. hASC proliferation, cytotoxicity and osteogenic differentiation in different scaffolds after 7, 14 and 21 days. In A, DNA quantification of hASC on different scaffolds, determinate by the Picogreen assay. In B, the gels and the semi-quantitative analysis of OCN, Il-6 and ALP relative expression are depicted after different culture periods. For A and B, significant differences over time in the DNA content and the relative expression of OCN, Il-6 and ALP within the same time scaffold type are represented by different lowcase letters.

2.3.9. Semi-Quantitative RT-PCR Analysis of hASC Loaded to Scaffolds Using a Spinner Flask

The relative expression of Il-6 mRNA in hASC cultured on scaffolds was observed within each time point (Figure 9B). After 7 days, the highest relative expression was observed in hASC loaded to 50:50 akermanite:PCL (4.56±0.01), followed by 25:75 akermanite:PCL (3.74±0.03) which was significantly greater than PCL (3.15±0.03), 60:40 b-TCP:HA (2.97±0.01) and akermanite (2.46±0.01). The lowest Il-6 expression within the first week was observed in hASC loaded to 75:25 akermanite:PCL (0.45±0.02) and CellCeramic^{TM} (0.32±0.01) scaffolds. After 14 days, hASC loaded to 60:40 b-TCP:HA had the highest relative Il-6 expression (7.34±0.02), followed by two of the akermanite:PCL scaffolds (50:50, 4.83±0.01; 25:75, 4.49±0.01) which did not differ between each other but were statistically greater than PCL (3.96±0.01) and akermanite (2.37±0.01). After 14 days the lowest Il-6 expression were observed in cells cultured on 75:25 akermanite:PCL (0.88±0.01) and CellCeramic^{TM} (1.14±0.01) scaffolds. At day 21, the Il-6 relative expression was the highest in hASC loaded to 25:75 akermanite:PCL scaffolds (9.15±0.02), followed by 50:50 akermanite:PCL (6.04±0.02) and PCL (5.84±0.02) which were statistically greater than in hASC loaded to akermanite (4.85±0.02), 60:40 b-TCP:HA (4.56±0.01) and 75:25 akermanite:PCL (1.96±0.03). After 21 days, hASC loaded to CellCeramic^{TM} (1.23±0.01) had the lowest Il-6 relative expression.

In addition to Il-6, the relative expression of early (ALP) and middle (OCN) stage osteogenic markers were also investigated within the same time points (Figure 9B). According to these results, after 7 days, the highest ALP relative expression was observed in hASC cultured on 75:25 akermanite:PCL (1.51±0.01), followed by 50:50 akermanite:PCL (1.16±0.01) and akermanite (0.98±0.01) which were all significantly greater than 25:75 akermanite:PCL

(0.53±0.01) and CellCeramic™ (0.24±0.01). Cells cultured on PCL (0.07±0.01) and 60:40 b-TCP:HA (0.02±0.01) had the lowest ALP relative expression after the first 7 days of culture. At day 14, hASC cultured on 25:75 akermanite:PCL (2.31±0.01) had the highest ALP relative expression, followed by 50:50 akermanite:PCL (1.86±0.015) which was significantly greater than 75:25 akermanite:PCL (1.62±0.01), akermanite (1.03±0.01) and CellCeramic™ (0.54±0.01). Within this time point, the lowest ALP relative expression was again observed in hASC cultured on either PCL (0.07±0.01) and 60:40 b-TCP:HA (0.02±0.01) scaffolds.

Cells loaded to 50:50 akermanite:PCL (2.64±0.05) and akermanite (2.35±0.01) had the highest ALP relative expression after 21 days of culture which was followed by 75:25 akermanite:PCL (1.95±0.02), CellCeramic™ (1.49±0.01), 25:75 akermanite:PCL (1.24±0.01) and PCL (0.18±0.01). At day 21, the lowest ALP relative expression was again observed in hASC cultured on to 60:40 b-TCP:HA (0.02±0.01) scaffolds.

Osteocalcin (OCN), a mid-stage marker of osteogenesis, after 7 days in culture, the OCN relative expression was constant among hASC cultured most of the scaffolds (Figure 9B) with the exception of hASC loaded to 75:25 akermanite:PCL (0.04±0.01) scaffolds which had a much lower expression. A reversal was seen at 14 days, where the relative OCN expression in hASC cultured on 75:25 akermanite:PCL (0.41±0.01) was the highest, with similar expression in cells on CellCeramic™ (0.13±0.01), 60:40 b-TCP:HA (0.14±0.03) and the other two akermanite:PCL scaffolds (25:75, 0.14±0.03; 50:50, 0.11±0.01) which were all significantly greater than PCL (0.09±0.01) and akermanite (0.05±0.03). After 21 days, the OCN relative expression was the highest in hASC loaded to 75:25 akermanite:PCL (1.16±0.03), followed by comparable OCN expression in hASC loaded to CellCeramic™ (0.27±0.01), 60:40 b-TCP:HA (0.18±0.01), akermantie (0.16±0.02) and the two other akermanite:PCL scaffolds (25:75, 0.231903±0.028443;

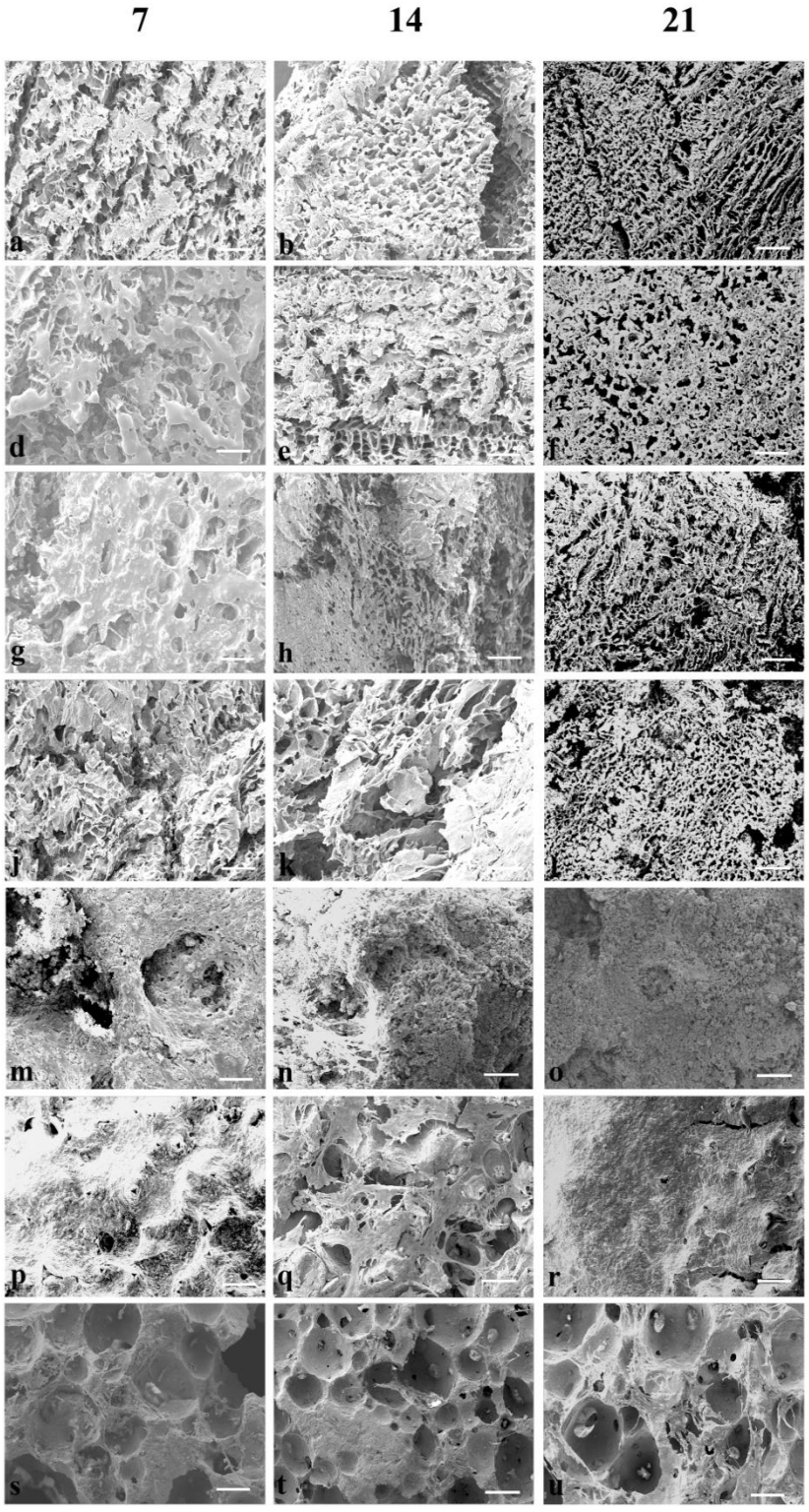

Figure 10. Scanning electron micrographs of hASC (n = 3 donors) loaded to different scaffolds at 7, 14 and 21 days of culture. Briefly, 25:75 akermanite:PCL (a-c), 50:50 akermanite:PCL (d-f), 75:25 akermanite:PCL (g-i), PCL (j-l), akermanite (m-o), 60:40 β-TCP:HA (p-r) and CellCeramic^{TM} (s-u). Scale bars 200 μm.

50:50, 0.18±0.01) which were significantly greater than the OCN relative expression in hASC loaded to PCL (0.09±0.01) scaffolds.

2.4. Discussion

The aim of this study was to characterize a moldable akermanite:PCL composite scaffold for hASC bone tissue applications in terms of scaffold properties (porosity, pore size, compressive strength and degradation) and hASC viability, attachment, proliferation and osteogenic differentiation. Three different akermanite:PCL blends were used to compare the referred parameters against PCL, akermanite, commercial CellCeramic^{TM} or custom-made 60:40 β-TCP:HA scaffolds. According to the results of this study, porous scaffolds composed of PCL and all three akermanite:PCL combinations had porosity greater than ceramic control scaffolds with the exception of CellCeramic^{TM} which had the greatest pore size. When examining the compression strength of the same specimens, it can be seen that scaffolds composed of 25:75 akermanite:PCL (% wt) were the strongest, followed by PCL while the other two akermanite:PCL composites (50:50 and 75:25) were statistically equal but significantly stronger than all ceramic scaffolds. These results were predictable based on previous results of PCL-based composites. Incubation of scaffolds in stromal medium at 37^{o}C in an orbital shaker resulted in a significant mass loss from all ceramic scaffolds and two akermanite:PCL combinations (50:50; 75:25) in stromal medium which significantly influenced the metabolic activity and the expression of the proinflammatory cytokine Il-6 in hASC exposed to the scaffolds media extracts. However, loading hASC onto the scaffolds using a spinner flask resulted in markedly different outcomes. After 21 days in stromal medium, hASC loaded to composites made of 50:50 and 75:25 akermanite:PCL scaffolds had DNA content comparable to hASC loaded to custom-made 60:40 β-TCP:HA scaffolds. Moreover, hASC cultured on 75:25

akermanite:PCL scaffolds had hASC similar viability after 21 days of culture, comparable to ceramic scaffolds. The highest expression of mature osteoblast marker (OCN) was also found in cells cultured on the 75:25 akermanite:PCL scaffolds. Together, the information provided in this study indicates that 75:25 akermanite:PCL composites are potential moldable scaffold candidates for future hASC bone tissue engineering applications.

In this study, pure akermanite made by solid-state synthetic methods was used to create porous scaffolds, both pure ceramic and composite for mechanical, biocompatibility and osteogenic evaluation. Custom synthesized 60:40 β-TCP:HA scaffolds and commercially available (CellCeramic^{TM}) were also prepared for comparisons. Multi-phase ceramics containing a mixture of akermanite, merwinite, and dicalcium silicate have been recently studied (Chen et al., 2008) as potential osteogenic materials. It should be noted that merwinite was demonstrated to promote osteogenesis and bone regeneration (Ou et al., 2008; Chen et al., 2010) and was carefully removed for the purpose of observing behavior of a pure akermanite phase. Further investigations should be conducted to investigate if the merwinite phase plays a role in the akermanite biocompatibility and osteogenic differentiation.

Porosity and pore size are critical for bone-substitute scaffolds because they facilitate cell migration and nutrient transport (Lawrence and Madihally, 2010). In this study, the scaffolds fabricated by blending akermanite and PCL at different concentrations were highly porous and had pore diameter similar to the observed in native bone (Reichert and Hutmacher, 2011). On the other hand, with the exception of CellCeramic^{TM}, the low porosity and pore size observed in the other two control ceramic scaffolds is likely the result of the morphology of the polyurethane template used to fabricate the scaffolds. The nature of this sacrificial template method results in pore-sizes dictated by the scale of the foam features. Nevertheless, scanning electron

micrographs taken at several time points revealed that hASC could adhere and proliferate in all scaffolds independent of the scaffold microarchitecture. Migration into the scaffold was not assessed and it is likely that pore size will influence cell penetration depth by either size exclusion or reduced diffusion of nutrient and waste.

Current scaffold-hASC bone engineering strategies assessed hASC osteogenesis under non-weight bearing conditions (Hattori et al., 2004; Leong et al., 2006; Scherberich et al., 2007; Dégano et al., 2008; Jeon et al., 2008; Ahn et al., 2009; Zhang et al., 2009; Levi et al., 2010; Muller and Mehrkens, 2010; Wang et al., 2010; Lee and Lee, 2011). However, future investigations assessing scaffold-hASC osteogenesis under compressive loads will rely, in part, on the mechanical properties of the scaffolds. Ceramic scaffolds have poor mechanical properties and behavior in compressive load. Issue which may in part be mitigated by the use of composite scaffolds due to their more robust and flexible mechanical properties (Reichert and Hutmacher, 2011). Currently, only composites made of HA:PLGA (Jeon et al., 2008; Levi et al., 2010) and β-TCP:gelatin (Weinand et al., 2011), β-TCP:PLA (Haimi and Suuriniemi, 2009; McCullen and Zhu, 2009) and β-TCP:PCL (Leong et al., 2006; Leong et al., 2008; , 2009; Zhang et al., 2009) have been proposed to support hASC osteogenesis. In this study, at maximum compression strain of 90%, novel akermanite:PCL scaffolds (25:75 wt%) displayed the highest strength. The presence of an inorganic phase significantly improved the PCL mechanical performance in the 25:75 akermanite:PCL scaffolds. Similar result has been described for PCL scaffolds blended with HA (Fabbri et al., 2010). However, at a higher akermanite wt% (50:50 and 75:25 akermanite:PCL scaffolds) no significant differences between the two composites and pure PCL were observed. The decreased PCL concentration in the blend might have influenced the stability of the composite scaffolds in a manner similar to that previously reported in

chitosan:PCL scaffolds by Sarasam et al. (2007). Nevertheless, the fact that PCL has a gel transition phase close to the body's temperature (Gaalen et al., 2008), makes a high akermanite weight content composite attractive for the development of moldable scaffolds. Further investigations will be needed to assess the mechanical properties of akermanite:PCL composites under physiological load.

Agitation significantly influenced the leaching of scaffold components into the media extracts. In the literature, β-TCP has been shown to degrade at rates greater than akermanite (Bouler et al., 2000; Liu et al., 2008) in physiological solutions, but in this study under the continuous agitation, significant weight losses were observed in both ceramic scaffolds. These results are similar to the increased weight loss associated with continuous agitation of akermanite scaffolds observed by Wu et al. (2006). Among the akermanite:PCL scaffolds, leaching was shown to be ceramic phase concentration-dependent, with increased weight losses in high akermanite scaffolds (50:50 and 75:25). It is well established that in aqueous environments, synthetic apatites degrade overtime through physiochemical dissolution and, possibly, phase transformation. Depending on the concentration of the biomaterial this may result in decreased biocompatibility (Bouler et al., 2000; Chen et al., 2008; Chen et al., 2010). The PCL phase of the composite is poorly water-soluble; has a melting temperature of 58 to 63^{o}C (Fabbri et al., 2010); and degrades by surface hydrolysis of ester linkages with release of caproic acid which, has also been demonstrated to be cytotoxic at high concentrations (Sarasam et al., 2007). For the hASC exposed to the media extracts of commercial and custom-made 60:40 β-TCP:HA scaffolds or PCL, the decreased metabolic activity and increased expression of proinflammatory cytokine observed in this study might had been the result of scaffolds phase transformation and cytotoxicity. However, for the akermanite and akermanite:PCL scaffolds, recent information

indicated that the decreased hASC proliferation during the osteogenic differentiation of the cells after exposure to akermanite media extracts seems to be the result of DNA synthesis and cell division suppression rather than cell death (Gu et al., 2011). This information might explain, in part, the decreased metabolic activity and the low expression of proinflammatory cytokine observed in hASC exposed to either scaffold type overtime, however, the fact that increased cell detachment was associated with high akermanite content in the akermantie:PCL scaffolds also indicated that the decreased hASC metabolic activity after exposure to the akermanite:PCL media extracts might had been the result of toxic changes in ion or caproic acid concentration in the media (Sarasam et al., 2007). As a conclusion, the Il-6 profile presented in this study after exposure to the scaffolds media extracts is interesting and led to the assumption that high PCL, HA, β-TCP or combination of both (HA and β-TCP) triggered inflammation. However, more studies are needed to address scaffold-hASC cytotoxicity in the molecular level. Nevertheless, scaffold agitation might have played a critical role in the increased expression of this marker.

Cell attachment to 3D scaffolds is crucial for clinical meaningful bone engineering. Therefore, a seeding technique resulting in a fast delivery is attractive to minimize the culture time in suspension for anchorage-dependent and shear-sensitive cells (Lawrence and Madihally, 2010). In this study, a custom-made spinner flask was used to load hASC to different scaffold types. In principal, the technique relies on fluid convection and collision with the immobilized scaffolds to improve cell attachment and distribution throughout the scaffolds (Griffon et al., 2010). Even though, the spinner flask used in this study yielded high cell adherence immediately after loading, the number of hASC loaded on PCL and akermanite:PCL composites was overtime lower than the observed in the control ceramic scaffolds as determined by live/dead staining and DNA content. Surface roughness is believed to influence cell adhesion and behavior (Yeo et al.,

2010ab; Lawrence and Madihally, 2010). Yeo et al. (2010ab) reported that β-TCP:PCL scaffolds with increased surface roughness displayed the highest cell growth and bone formation both *in vitro* and *in vivo*. While this remains to be tested in the PCL and akermanite:PCL scaffolds used in this study, the increased live cell staining and DNA content observed overtime in the ceramic scaffolds could be the result of the increased surface roughness of the scaffolds. For the akermanite:PCL scaffolds, viability seemed to be akermanite dose-dependent as was observed after 14 and 21 days in hASC cultured on 75:25 akermanite:PCL scaffolds. Recently, an increased number of studies had also indicated the increased viability of cells cultured on akermanite (Wu et al., 2006; Liu et al., 2008; Gu et al., 2011).

In addition to Live/Dead staining and DNA content, this study also assessed scaffold biocompatibility to hASC in terms of Il-6 gene expression using semi-quantitative analysis. According to the results, hASC loaded to CellCeramic^{TM} and 75:25 akermanite:PCL scaffolds displayed the lowest expression of pro-inflammatory cytokine during the course of this study. However, the degree to which the expression of this marker is critical for scaffold biocompatibility still remains to be investigated *in vivo*.

The ability to drive hASC osteogenesis is another key component of successful bone tissue engineering (Reichert and Hutmacher, 2011). In this study, ALP was used as early osteogenic differentiation marker. The highest ALP expression was observed after 7 days of culture on 75:25 akermanite:PCL scaffolds, followed by pure porous akermanite and the other two akermanite:PCL combinations. Compared to β-TCP, hASC cultured on akermanite also had a higher level of ALP activity after 10 days of culture (Liu et al., 2008). For this study, OCN was also used as a marker for differentiation of mature osteoblasts. The 75:25 akermanite:PCL scaffolds demonstrated the highest OCN expression after 14 and 21 days, indicating that the

75:25 akermanite:PCL composites may promote osteogenic differentiation of hASCs more effectively than the other tested scaffolds.

In summary, the combined mechanical, biological and osteogenic properties of 75:25 akermanite:PCL scaffolds are promising for bone repair applications when combined with hASC. Further studies are needed to investigate the hASC osteogenic potential and biocompatibility of akermanite:PCL scaffolds *in vivo*.

2.5. References

Ahn HH, Kim KS, Lee JH, et al., 2009; In vivo osteogenic differentiation of human adipose-derived stem cells in an injectable in situ-forming gel scaffold. *Tissue Eng Part A* **15:** 1821-1832.

Bouler JM, LeGeros RZ, Daculsi G., 2000; Biphasic calcium phosphates: influence of three synthesis parameters on the HA/β-TCP ratio. *J Biomed Mater Res* **51:** 680–4.

Bragg WL., 1920; Crystal structure. *Nature* **105:** 646-648.

Chen XC, Wei Y, Huang ZB, *et al.*, 2008; Synthesis and characterization of multiphase bioactive glass-ceramics in the CaO-MgO-SiO_2 system with B_2O_3 additive. *J Mater Res* **23:** 2873-2879.

Chen XC, Ou J, Wei Y, et al., 2010; Effect of MgO contents on the mechanical properties and biological performances of bioceramics in the MgO-CaO-SiO_2 system. *J Mater Sci Mater Med* **21:** 1463-1471.

De Girolamo L, Sartori MF, Arrigoni E, et al., 2008; Human adipose-derived stem cells as future tools in tissue regeneration: osteogenic differentiation and cell-scaffold interaction. *Int J Artif Organs* **31:** 467-479.

De Girolamo L, Lopa S, Arrigoni E, et al., 2009; Human adipose-derived stem cells isolated from young and elderly women: their differentiation potential and scaffold interaction during in vitro osteoblastic differentiation. *Cytotherapy* **11:** 793-803.

Dégano IR, Vilalta M, Bagó JR, et al., 2008; Bioluminescence imaging of calvarial bone repair using bone marrow and adipose tissue-derived mesenchymal stem cells. *Biomaterials* **29:** 427-437.

Gaalen S, Kruyt M, Meijer G, et al., 2008; Tissue Engineering of Bone. In: Clemens van Blitterswijk . *Tissue Engineering* 740.

Gastaldi G, Asti A, Scaffino MF, et al., 2010; Human adipose-derived stem cells (hASCs) proliferate and differentiate in osteoblast-like cells on trabecular titanium scaffolds. *J Biomed Mater Res A* **94:** 790-799.

Gerlach W. 1922; The lattice structure of alkali-earth oxides. *Z Phys* **9:** 184-192.

Gimble JM, Bunnell BA, Casteilla L, et al., 2010; Phases I-III Clinical Trials Using Adult Stem Cells. *Stem Cells Int* **2010:** 604713.

Gimble JM, Bunnell BA, Guilak F, et al., 2011; Isolation and Growth of Stem Cells. In: Pallua. *Tissue Engineering* 643.

Griffon D, Abulencia JP, Ragetly GR, et al., 2010; A comparative study of seeding techniques and three-dimensional matrices for mesenchymal cell attachment. *J Tissue Eng Regen Med* **5:** 169-179.

Gu H, Guo F, Zhou X, et al., 2011; The stimulation of osteogenic differentiation of human adipose-derived stem cells by ionic products from akermanite dissolution via activation of the ERK pathway. *Biomaterials* **32:** 7023-7033.

Fabbri P, Bondioli F, Messori M, et al., 2010; Porous scaffolds of polycaprolactone reinforced with in situ generated hydroxyapatite for bone tissue engineering. *J Mater Sci Mater Med* **21:** 343-351.

Frohlich M, Grayson W, Marolt D, et al., 2010; Bone grafts engineered from human adipose-derived stem cells in perfusion bioreactor culture. *Tissue Eng Part A* **16:** 179-189.

Haimi S, Gorianc G. 2009; Characterization of zinc-releasing three-dimensional bioactive glass scaffolds and their effect on human adipose stem cell proliferation and osteogenic differentiation. *Acta Biomater* **5:** 3122-3131.

Haimi S, Moimas L, Pirhonen E, et al., 2009; Calcium phosphate surface treatment of bioactive glass causes a delay in early osteogenic differentiation of adipose stem cells. *J Biomed Mater Res A* **91:** 540-547.

Haimi S, Suuriniemi N. 2009; Growth and osteogenic differentiation of adipose stem cells on PLA/bioactive glass and PLA/beta-TCP scaffolds. *Tissue Eng Part A* **15:** 1473-1480.

Hattori H, Sato M, Masuoka K, et al., 2004; Osteogenic potential of human adipose tissue-derived stromal cells as an alternative stem cell source. *Cells Tissues Organs* **178:** 2-12.

Jeon O, Rhie JW, Kwon Ik, et al., 2008; In vivo bone formation following transplantation of human adipose-derived stromal cells that are not differentiated osteogenically. *Tissue Eng Part A* **14:** 1285-1294.

Kneser U, Schaefer DJ, Polykandriotis E, et al. 2006; Tissue engineering of bone: the reconstructive surgeon's point of view. *J Cell Mol Med* **10:** 7-19.

Lawrence BJ, Madihally SV. 2008; Cell colonization in degradable 3D porous matrices. *Cell Adh Migr* **2:** 9-16.

Lee JS, Lee JM. 2011; Electroporation-mediated transfer of Runx2 and Osterix genes to enhance osteogenesis of adipose stem cells. *Biomaterials* **32:** 760-768.

Lendeckel S, Jodicke A, Christophis P, et al., 2004; Autologous stem cells (adipose) and fibrin glue used to treat widespread traumatic calvarial defects: case report. *J. Craniomaxillofac. Surg* **32:** 370–373.

Leong DT, Abraham MC, Rath SN, et al., 2006; Investigating the effects of preinduction on human adipose-derived precursor cells in an athymic rat model. *Differentiation* **74:** 519-529.

Levi B, James AW, Nelson ER, et al., 2010; Human adipose derived stromal cells heal critical size mouse calvarial defects. *PLoS One* **5:** e11177.

Liu Q, Cen L, Yin S, et al., 2008; A comparative study of proliferation and osteogenic differentiation of adipose-derived stem cells on akermanite and beta-TCP ceramics. *Biomaterials* **29:** 4792-4799.

Marino G, Rosso F, Cafiero G, et al., 2010; Beta-tricalcium phosphate 3D scaffold promote alone osteogenic differentiation of human adipose stem cells: in vitro study. *J Mater Sci Mater Med* **21:** 353-363.

McCullen SD, Zhu Y. 2009; Electrospun composite poly(L-lactic acid)/tricalcium phosphate scaffolds induce proliferation and osteogenic differentiation of human adipose-derived stem cells. *Biomed Mater* **4:** 035002.

Miranda P, Pajares A, Saiz E, et al., 2008; Mechanical properties of calcium phosphate scaffolds fabricated by robocasting. *J Biomed Mater Res A* **85:** 218–27.

Moore PB, Araki T. 1972; Atomic arrangement of merwinite, $Ca_3Mg(SiO_4)_2$, an unusual dense-packed structure of geophysical interest. *Am Miner* **57:** 1355-1374.

Muller AM, Mehrkens A. 2010; Towards an intraoperative engineering of osteogenic and vasculogenic grafts from the stromal vascular fraction of human adipose tissue. *Eur Cell Mater* **19:** 127-135.

Ou J, Kang YQ, Huang ZB, *et al.* 2008; Preparation and in vitro bioactivity of novel merwinite ceramic. *Biomed Mater* **3:** 015015.

Reichert JC, Hutmacher DW. 2011; Bone tissue engineering. In: Pallua. *Tissue Engineering* 643.

Sarasam AR, Samli AI, Hess L, et al., 2007; Blending chitosan with polycaprolactone: porous scaffolds and toxicity. *Macromol Biosci* **7:** 1160-1167.

Scherberich A, Galli R, Jacquiery C, et al., 2007; Three-dimensional perfusion culture of human adipose tissue-derived endothelial and osteoblastic progenitors generates osteogenic constructs with intrinsic vascularization capacity. *Stem Cells* **25:** 1823-1829.

Wang CZ, Chen SM, Chen CH, et al., 2010; The effect of the local delivery of alendronate on human adipose-derived stem cell-based bone regeneration. *Biomaterials* **31:** 8674-8683.

Warren BE. 1930; The structure of melilite (Ca, $Na)_2$(Mg, Al)(Si, $Al)_2O_7$. *Z Kristall* **74:** 131-138.

Weinand C, Nabili A, Khumar M, et al., 2011; Factors of osteogenesis influencing various human stem cells on third-generation gelatin/beta-tricalcium phosphate scaffold material. *Rejuvenation Res **32:*** 3166-3177.

Wu C, Chang J, Zhai W et a., 2006; Porous akermanite scaffolds for bone tissue engineering: preparation, characterization, and in vitro studies. *J Biomed Mater Res B Appl Biomater* **78:** 47-55.

Yeo A, Wong WJ, Teoh SH. 2010a; Surface modification of PCL-TCP scaffolds in rabbit calvaria defects: Evaluation of scaffold degradation profile, biomechanical properties and bone healing patterns. *J Biomed Mater Res A* **93:** 1358-1367.

Yeo A, Wong WJ, Teoh SH. 2010b; Surface modification of PCL-TCP scaffolds improve interfacial mechanical interlock and enhance early bone formation: An in vitro and in vivo characterization. *J Biomed Mater Res A* **92:** 311-321.

Zhang ZY, Teoh SH, Chong MS, et al., 2009; Superior osteogenic capacity for bone tissue engineering of fetal compared with perinatal and adult mesenchymal stem cells. *Stem Cells* **27:** 126-137.

Chapter 3. *In Vitro* Human Adipose-Derived Stem Cells Osteogenesis in Akermanite:Poly-E-Caprolactone Bone Scaffolds

3.1. Introduction

Bone tissue engineering presents an alternative approach to the repair and regeneration of damaged bone tissue (Gaalen et al., 2008; Reichert & Hutmacher, 2011). Bioceramics, especially calcium phosphate materials have been widely used for bone tissue repair due to their superior bioactivity (defined as biocompatibility, osteoconduction and osteoinduction) (Scherberich et al., 2007; Dégano et al., 2008; De Girolamo et al., 2008; Gaalen et al., 2008; Liu et al., 2008; De Girolamo et al., 2009; Haimi et al., 2009; Haimi & Suuriniemi, 2009; Haimi & Gorianc, 2009; Marino et al., 2010; Gastaldi et al., 2010; Muller & Mehrkens, 2010). Among the different types of bioactive ceramics, the utilization of silica-based glasses in bone tissue engineering strategies have recently received considerable attention; particularly, because of their mechanical properties and enhanced bioactivity (Agathopoulos et al., 2005; Wu et al., 2006a; Chen at al., 2010). Moreover, due to the ability to form apatite-like layers at a physiological fluid interface, porous bioactive glasses have been shown to enhance cell adhesion, proliferation osteogenic differentiation, and extracellular matrix mineralization (Sun et al., 2006; Liu et al., 2008; Gu et al., 2011).

As one kind of silica-based bioactive glass, akermanite ($Ca_2MgSi_2O_7$) has shown to to enhance cell adhesion, proliferation and osteogenesis with a controllable degradation rate and desirable mechanical properties (Sun et al., 2006; Wu et al., 2006ab; Wu et al., 2007; Huang et al., 2009; Gu et al., 2011). Akermanite is an end member of the melilite (sorosilicates); it has a high melting point (around 1450^{o}C); and exhibits increased stability, hardness, density and refractory properties (Zhuang et al., 1990; Yang et al., 1997; Wu et al.,2007). Moreover, the Ca, Mg and Si content of akermanite have been shown to increase the calcium deposition and

osteogenic differentiation of human adult stem cells and mature osteoblast (Sun et al., 2006; Wu et al., 2006ab; Liu et al., 2008). In human adipose-derived stem cells (hASC) the Ca, Mg, and Si ion extracts of akermanite scaffolds have been linked to hASC osteogenesis via up-regulation of extracellular signal-related kinase (ERK), a member of the mitogen-activated protein kinases (MAPKs) signaling pathway (Gu et al., 2011). Human adipose-derived stem cells represent a readily available, autogenous cell source with well-documented *in vivo* osteogenic potential (Gaalen et al., 2008; Gimble et al., 2011). Therefore, akermanite-based bone tissue engineering strategies resulting in enhanced hASC osteogenesis are appealing.

The brittleness of pure bioactive glass ceramics is the major factor limiting their use in bone repair and making the translation to clinical settings difficult (Kneser et al., 2006; Gaalen et al., 2008; Reichert & Hutmacher, 2011). Recent innovations address this limitation by combining bioactive ceramics with bioabsorbable polymeric fiber reinforcement in the same composite structure (De Girolamo et al., 2009; Haimi & Suuriniemi, 2009; Zhang et al., 2009; Reichert & Hutmacher, 2011). Of the many polymers compositions used in hASC bone tissue engineering applications, poly-e-caprolactone (PCL) is widely used as a resin for composite scaffolds (Leong et al., 2006; Gaalen et al., 2008; Reichert & Hutmacher, 2011). PCL is a poorly water-soluble aliphatic polyester that has a slow *in vivo* degradation rate(Fabbri et al., 2010). With a melting point close to the body temperature, current bone tissue engineering paradigms seek to utilize PCL as a moldable scaffolding material (Leong et al., 2006; Gaalen et al., 2008; Zhang et al., 2009; Fabbri et al., 2010). As both akermanite and PCL appear to have unique qualities suitable for bone tissue repair, we recently developed a novel composite scaffold (akermanite:PCL) to combine the desirable properties of both biomaterials. In our previous study, we demonstrated that novel 75:25 (wt. %) akermanite:PCL composite scaffolds had compressive strength greater

than and bioactivity comparable to control ceramic scaffolds. However, as part of the characterization of this new composite for bone tissue engineering applications, studies comparing the *in vitro* osteogenic potential of hASC loaded to akermanite:PCL in growth (control) and osteogenic media still remain to be conducted.

Therefore in this study we compared the metabolic activity, calcium deposition and morphogical changes as well as the expression of markers associated with early and later osteogenic differentiation in hASC loaded to akermanite:PCL and cultured in growth or osteogenic media for up to 21 days. The hypothesis of this study was that, compared to scaffolds cultured in control medium, osteogenesis, measured by decreased metabolic activity and increased calcium deposition and expression of osteogenic markers, would be greater in scaffolds cultured in osteogenic medium.

3.2. Materials and Methods

3.2.1. Synthesis of Akermanite

Akermanite, $Ca_2MgSi_2O_7$, was synthesized by ceramic methods with calcium carbonate (1.237 g, 12.4 mmol), magnesium carbonate (0.521 g, 6.2 mmol), and silicon dioxide (0.742 g, 12.4 mmol) as the starting materials. These materials were mixed and ground thoroughly using an agate mortar and pestle. The 2.5 g white powder mixture was then pressed into a pellet with hydraulic press (approximately 1 metric ton of applied pressure) and then heated multiple times in an open to air boat-shaped alumina crucible using a programmable box furnace to achieve the following net reaction:

$$2\ CaCO_3 + MgCO_3 + 2\ SiO_2 \rightarrow Ca_2MgSi_2O_7 + 3\ CO_2\ (g)$$

The initial heat treatment was carried out at 950°C (after increasing the furnace chamber temperature from room temperature at rate of 100°C/h) for 48 hours. This intermediate reaction,

which involves the conversion of the carbonate starting materials to oxides, was then allowed to cool to room temperature by heat loss through the top exhaust port of the furnace. The pellet was then weighed to confirm the mass loss of approximately 0.8 g (or 18.5 mmol) of carbon dioxide. Subsequent heat treatments involved additional grinding, pellet pressing, and heating the crude product at the dwell temperature of 1300°C (after ramping up the temperature from room temperature at rate of 100°C/h) for 48 hours. Each 48 hour heat treatment was followed by cooling back to room temperature by furnace exhaust. The number of heat treatments at 1300°C required was dictated by proof of desired product purity (as judged by powder X-ray diffraction) and typically varied with each batch from 2 to 3 times.

3.2.2. Synthesis of Ceramic Scaffolds

Akermanite and β-tricalcium phosphate (β-TCP) powders (3 g) were suspended in polyvinyl alcohol aqueous solution (10 wt %) and stirred in a glass beaker to obtain a well-dispersed slurry (Liu et al., 2008). Polyurethane foam templates were cut into the desired shape and sizes (5mmX4mm) to replicate a porous scaffold. Then, the prepared templates were immersed in a glass beaker containing akermanite or β-TCP slurry and compressed with glass stick to force the slurry to migrate into the pores of the foams which were then incubated at 60°C for 1 day. After drying, the scaffolded materials (either akermanite or β-TCP) were placed in an open to air boat-shaped alumina crucible and heated up in a programmable box furnace from room temperature (at rate of 50°C/h) to 500°C and allowed to dwell this temperature for 5 hours in order to burn off the polyurethane foam. After allowing the furnace to cool down to room temperature by furnace exhaust, the scaffolds were then heat treated at 1300°C (increasing the furnace chamber temperature from room temperature at rate of 60°C/h) for 3 hours and cooled back down by furnace exhaust.

3.2.3. Fabrication of PCL and Akermanite:PCL Scaffolds

Composites (akermanite:PCL) and pure PCL solutions were frozen overnight at -80°C (5mmX4mm discs). A 10% PCL solution in 8 ml of 1-4, dioxane was prepared and akermanite was added at weight (g) ratio of 0,0:0,8 (PCL) and 0.6:0.2 (75:25 akermanite:PCL wt.%) in a glass bottle. The mixtures were molded into 5mmX4mm polydimethylsiloxane (PDMS) templates and immediately incubated in a freeze-drier for 48 hours.

3.2.4. Adult Stem Cells Isolation and Culture

Liposuction aspirates from subcutaneous adipose tissue were obtained from male (n = 1) and females (n = 2) subjects undergoing elective procedures. All tissues were obtained with informed consent under a clinical protocol reviewed and approved by the Institutional Review Board at the Pennington Biomedical Research Center. Isolation of hASC was performed as described elsewhere (Gimble et al., 2011). Briefly, tissues was washed 3–4 times with phosphate buffered saline and suspended in an equal volume of PBS supplemented with 1% bovine serum and 0.1% collagenase type I. The tissues were placed in a shaking water bath at 37°C with continuous agitation for 60 min and centrifuged for 5 min at 300–500 g at room temperature. The supernatant, containing mature adipocytes was then aspirated. The cell pellet, referred to as the stromal vascular fraction (SVF), was suspended and plated immediately in T125 flasks in stromal medium at density of 0.156 ml of tissue digest/cm^2 of surface area for expansion and culture. The initial passage was referred to as ‘‘Passage 0’’ (p0). The cells were passaged after trypsinization and plated at a density of 5,000 cells/cm^2 (‘‘Passage 1’’) for expansion on T125 flasks until 80% of confluence was reached. Passage 2 of each individual was used for *in vitro* hASC osteogenesis alone or in different scaffold types. In both cases, hASC were cultured in

either growth (control) or osteogenic media for up to 21 days with media maintenance performed three times a week.

3.2.5. hASC Loading on Scaffolds and Culture

Passage 2 of each donor (n = 3) were pooled and directly loaded on the top of each scaffold type at loading density of $5.0X10^4$ cells/5μL. After 30 min of incubation at 37°C and 5% CO_2 an additional $5.0X10^4$ cells/5μL was directly loaded on the opposite side of each scaffold. Experimental groups included: 75:25 (% wt/v) akermanite:PCL, akermanite, PCL and β-TCP. Immediatelly after, scaffolds loaded with hASC were transferred to 48-well plates and cultured in control or osteogenic media (DMEM, 10% FBS, 0.1 μM dexamethasone, 50 μM ascorbate-2-phosphate, 10 mM β-glycerophosphate, and 1% triple antibiotic solution) for 21 days with weekly sample collection to assess cell viability with Alamar blue stain; and osteogenic differentiation with alizarin red stain as well as mRNA expression of ALP and OCN.

3.2.6. *In vitro* hASC Viability on Scaffolds with Alamar Blue Stain

The viability of cells within the scaffolds at 7, 14 and 21 days in control and osteogenic media was determined using an Alamar Blue™ metabolic activity assay. The scaffolds were removed from culture, washed three times in PBS, and incubated with 10% Alamar Blue™ in Hank's balanced salt solution (HBSS) without phenol red (pH 7) for 90 min. Aliquots (100 μL) of Alamar Blue™/HBSS were placed in a 96-well plate in triplicate, and the fluorescence was measured at an excitation wavelength of 530 nm and an emission wavelength of 595 nm using a fluorescence plate reader.

3.2.7. *In Vitro* Calcium Deposition

hASC osteogenesis (cells alone and cells-scaffolds) was assessed after 7, 14 and 21 days of culture in control and osteogenic medium using alizarin red stain. Briefly, cells and scaffolds

were washed with 0.9% NaCl a total of four times (1 ml/well) and fixed with 70% ethanol (1 ml/well). Subsequently, the fixative was removed by aspiration and plates were stained with 2% alizarin red for 10 min and washed with H_2O six times. The samples were destained by the addition of 400 ml of 10% cetylpyridinium chloride monohydrate to each well followed by shaking for 10 min at room temperature. The calcium deposition expressed by the optical density of the aliquots was then measured at 540 nm with a plate reader.

3.2.8. Quantification of DNA on Scaffolds *In Vitro*

Total DNA content was used to determine the number of cells on each scaffold as previously described (Liu et al., 2008). Briefly, scaffolds were crushed and then incubated with 0.5 mL proteinase K (0.5 mg/mL) at 56ºC overnight. The mixture was centrifuged at 108 g for 5 minutes and then 50 µl aliquots was mixed with 50 µl Picogreen dye solution (0.1 g/mL, Invitrogen) in 96-well plates. Samples were excited at 480 nm and total DNA concentration was compared to a standard curve generated from serial dilutions of hASC. Scaffold without cells were used to subtract the background fluorescence emission from all readings.

3.2.9. Quantitative Real Time Polymerase Chain Reaction (QPCR)

Total RNA was extracted from cell-scaffolds using the Trizol reagent (Sigma). QPCR was performed using 2X iTaq SYBR green with ROX (Biored) and alkaline phosphatase (ALP) forward (5'- AATATGCCCTGGAGCTTCAGAA -3') and reverse (5'- CCATCCCATCTCCCAGGAA -3') and osteocalcin (OCN) forward (5'- GCCCAGCGGTGCAGAGT -3') and reverse (5'- TAGCGCCTGGGTCTCTTCAC -3') to assess the osteogenic differentiation of hASC loaded to scaffolds at 7, 14 and 21 days in scaffolds culture in either growth and osteogenic media. Reactions were performed with a MJ Mini Thermal Cycler (BioRad). Water (negative) and hASC culture in osteogenic medium for

14 days were used as controls. Samples were normalized (ΔCt) against the house keeping gene 18SrRNA and the fold change expression of ALP and OCN in scaffolds cultured in osteogenic and control media was calculated using the ΔΔCt method (Liu et al., 2008).

3.2.10. Statistical Analysis

All results were expressed as mean ± SEM. Normality of the data was confirmed using the Shapiro-Wilk test ($P < 0.001$). Data was analyzed with one-way analysis of variance (ANOVA), followed by Tukey's minimum significant difference (MSD) post hoc test for pairwise comparisons of main effects. For all comparisons, a *P*-value of 0.05 was considered significant.

3.3. Results

3.3.1. Calcium Deposition in hASC Cultured in Control and Osteogenic Media

Confirmation of the osteogenic potential of hASC isolated from three donors was assessed by staining hASC cultured in growth (control) and osteogenic media with alizarin red stain (Figure 11). In general, hASC cultured in osteogenic medium had calcium deposition significantly greater than control samples ($P < 0.05$). Moreover, significant increase in the calcium deposition between different time points was also observed in hASC cultured in osteogenic medium.

3.3.2. hASC Viability on Scaffolds Cultured in Control and Osteogenic Media

hASC loaded on different scaffold types and cultured in both control and osteogenic media displayed significant changes in the metabolic activity during the course of this study. The changes in the color of the scaffolds after alamar blue staining are represented in Figure 12A.

After 7 days significant differences in the metabolic activity were observed for hASC cultured in control and osteogenic media in all scaffold types with the exception of hASC loaded to akermanite scaffolds, (Figure 12B). In general, the metabolic activity of hASC loaded to scaffolds cultured in control medium were significantly greater than scaffolds cultured in

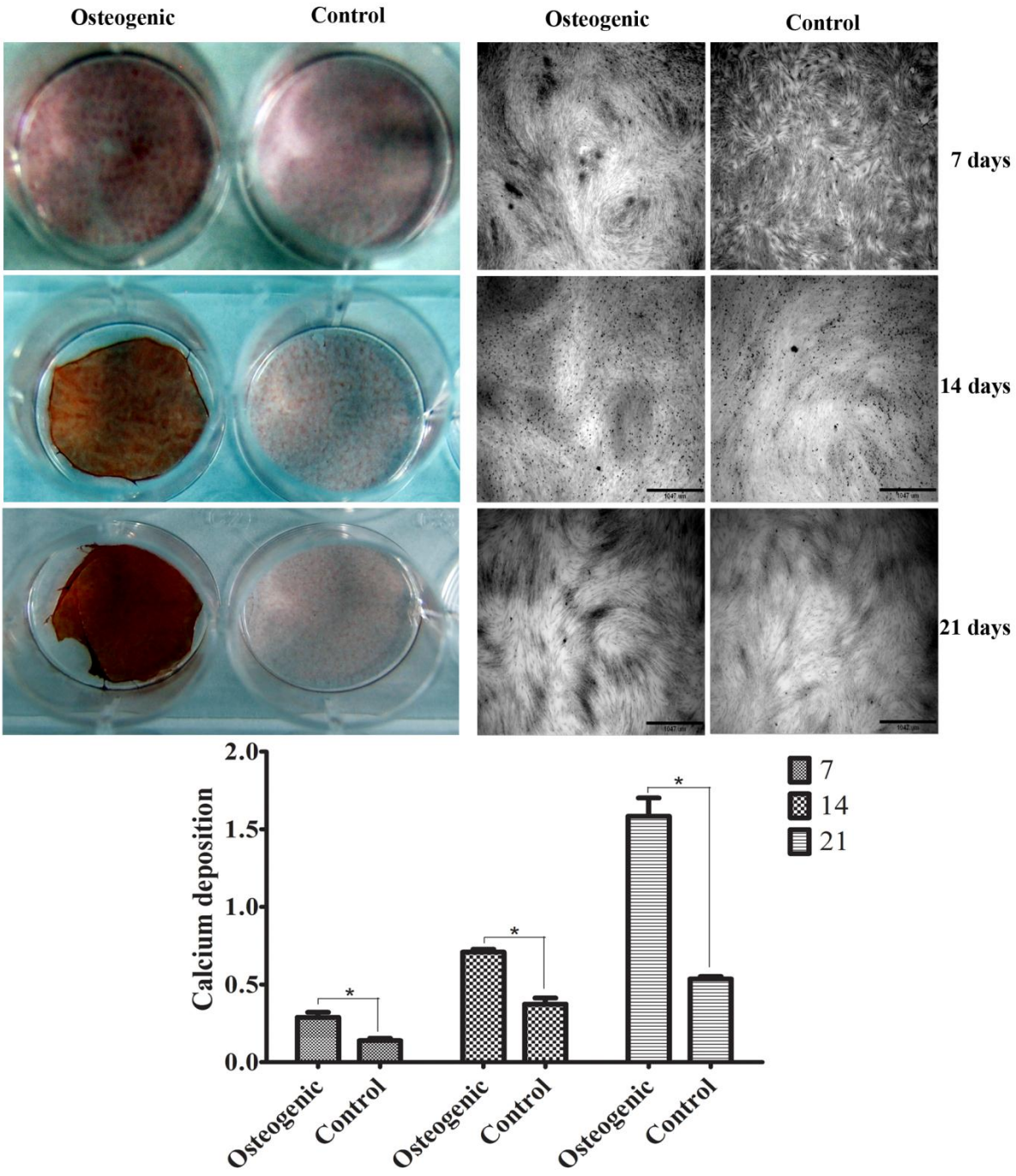

Figure 11. Alizarin red stain of hASC (Passage 2) cultured in growth (control) and osteogenic media for a 21 days period. *Represent significant differences between the calcium deposition in hASC culture in control and osteogenic media with the same time point (Anova, $P < 0.05$).

osteogenic medium. Within the different scaffold types, after 7 days of culture in control medium, increased metabolic activity was observed in hASC loaded to akermanite:PCL scaffolds (232161.50±70531.34), with comparable levels in hASC loaded to PCL and β-TCP (176503.80±42308.36; 158579.70±15143.07, respectively, $P > 0.05$) and akermanite (74974.16±8632.26).

After 14 days of culture, significant differences in the metabolic activity of hASC cultured in control and osteogenic media were observed only in hASC loaded to akermanite and PCL scaffolds (Figure 12B). Compared to scaffolds cultured in osteogenic medium (174529.70±23776.19), the hASC metabolic activity in PCL scaffolds cultured in control medium was significantly higher after 14 days (359494.30±22494.01). However, hASC loaded to akermanite scaffolds cultured in osteogenic medium (143524.20±2841.45) had metabolic acitivity significantly higher than the observed in control scaffolds (92600.16±1089.52). After 14 days of culture in control medium, comparable metabolic activity was observed in hASC loaded to akermanite:PCL (551391.80±199465.40) and PCL (359494.30±22494.01) scaffolds, which were significantly higher than comparable levels in β-TCP (105708.7±7404.53) and akermanite (92600.16±1089.52) scaffolds.

Finally, after 21 days of culture, scaffolds cultured in both media conditions displayed comparable hASC metabolic activity with significant differences observed only between scaffold types (Figure 12B). In general, after 21 days, hASC loaded to β-TCP scaffolds cultured in either control (320338.00±49213.05) or osteogenic (489036.00±51962.24) media had metabolic activity significantly higher than akermanite (control – 101356±1170.472; osteogenic – 104408.00±1445.43) or akermanite:PCL (control – 98067.16±6166.95; osteogenic – 118553.20±10272.57) scaffolds, and PCL (control – 69221.34±8387.938; osteogenic –

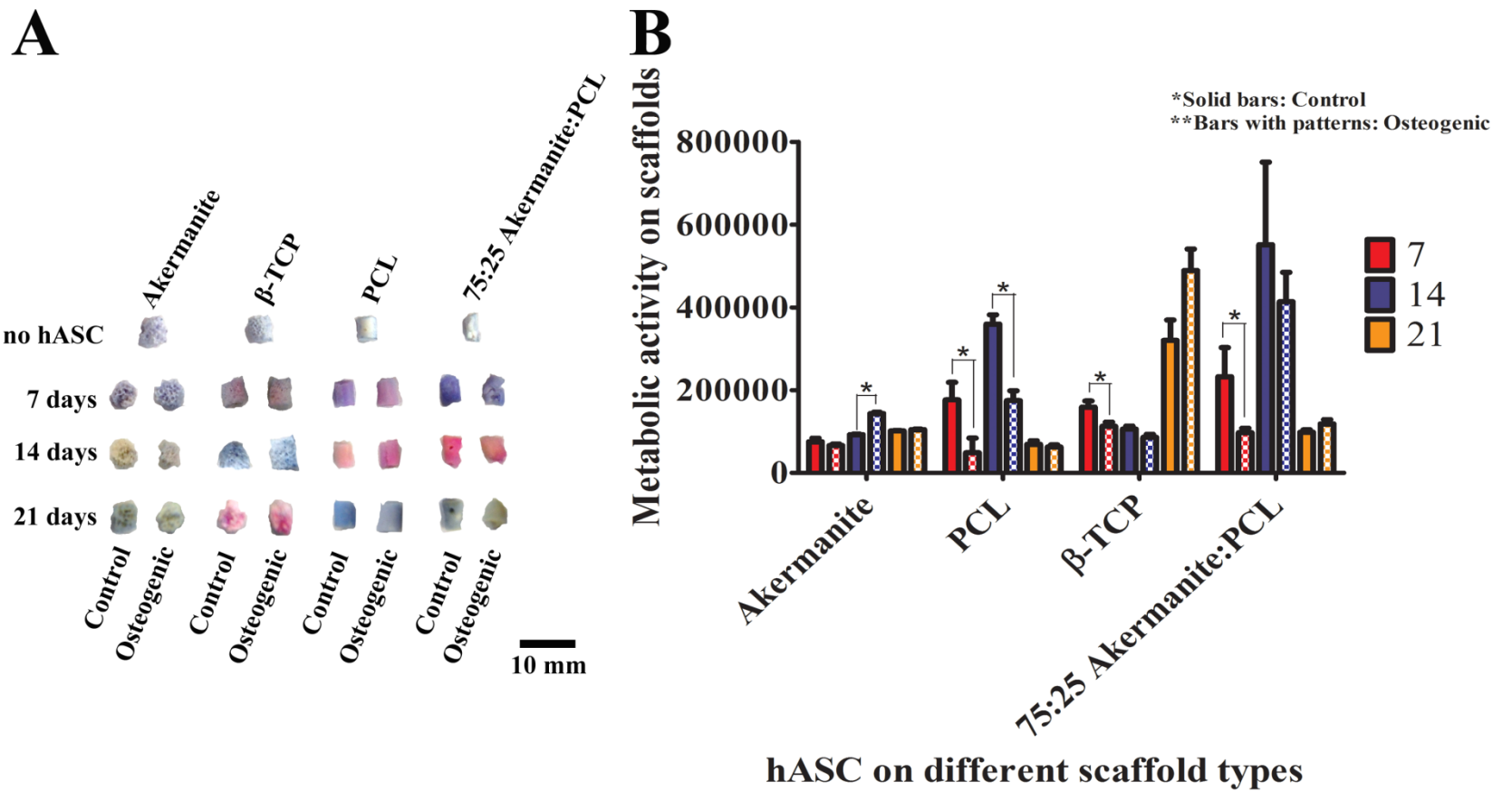

Figure 12. Metabolic activity as a function of Alamar blue stain on different scaffold types and time points. In (A), different staining patterns within each time point can be observed in scaffolds loaded with hASC and culture in control and osteogenic media. In (B), the metabolic activity of hASC loaded to the scaffolds is represented within each time point and culture condition. *Represent significant differences in the metabolic activity of hASC loaded to different scaffolds within the same time point (Anova, $P < 0.05$).

62675.00±5042.52).

3.3.3. *In Vitro* hASC Calcium Deposition on Scaffolds

Calcium deposition, as measured by alizarin red, on scaffolds loaded with hASC and cultured in both growth (control) and osteogenic media for 21 days is depicted in Figure 13. In general, scaffolds had different accumulation of calcium after 21 days of culture in both media conditions (Figure 13A). During the first 7 days of this study, significant changes in the calcium deposition on scaffolds cultured in growth (control) and osteogenic media were observed only in hASC loaded to β-TCP scaffolds (control – 0.211±0.067; osteogenic – 0.710±0.133, $P < 0.05$) (Figure 13B). However, between scaffold types, calcium accumulation in akermanite scaffolds cultured in either media conditions (control – 3.61±0.50; osteogenic – 3.58±0.05, $P > 0.05$) was, significantly higher than in akermanite:PCL scaffolds (control – 1.72±0.22; osteogenic – 2.52±0.71, $P > 0.05$), β-TCP and PCL (control – 0.028±0.01; osteogenic – 0.12±0.03, $P < 0.05$) scaffolds.

After 14 days of culture, significant differences in the calcium deposition were observed between growth (control) and osteogenic media only on akermanite scaffolds (control – 2.47±0.13; osteogenic – 3.55±0.12, $P < 0.05$) (Figure 13B). However, when analyzed for differences between scaffold types, akermanite scaffolds cultured in osteogenic medium had the highest calcium deposition, followed by comparable levels in akermanite scaffolds cultured in control medium and akermanite:PCL scaffolds cultured in either media conditions (control – 1.92±0.39; osteogenic – 1.90±0.48, $P > 0.05$). Both akermanite containing scaffolds had significantly higher values for calcium deposition than β-TCP (control – 0.37±0.10; osteogenic – 0.62±0.16, $P > 0.05$) and PCL (control – 0.17±0.06; osteogenic – 0.11±0.03, $P > 0.05$) scaffolds.

After 21 days, significant differences in the calcium deposition were observed in scaffolds

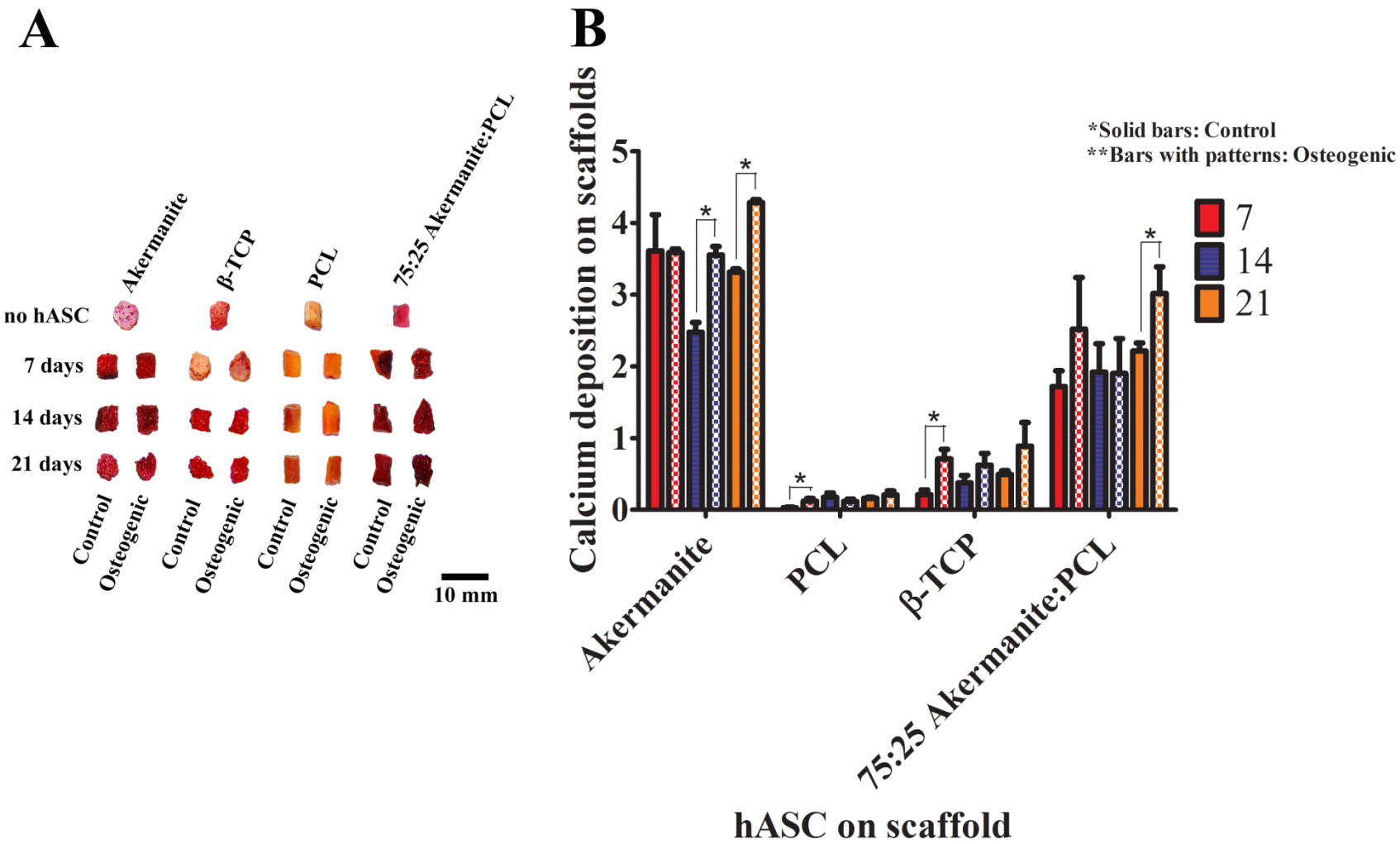

Figure 13. Calcium deposition as a function of the Alizarin red stain on different scaffold types and time points. In (A), different staining patterns within each time point can be observed in scaffolds loaded with hASC and culture in control and osteogenic media. In (B), the calcim deposition in scaffolds loaded with hASC is represented within each time point and culture condition. *Represent significant differences in the calcium deposition in hASC loaded to different scaffolds within the same time point (Anova, $P < 0.05$).

cultured in growth (control) and osteogenic media only akermanite (control – 3.31±0.04; osteogenic – 4.28±0.04, $P < 0.05$) and akermanite:PCL (control – 2.21±0.11; osteogenic – 3.02±0.37, $P < 0.05$) scaffolds (Figure 13B). When interscaffold differences are compared, akermanite scaffolds cultured in osteogenic medium had the highest calcium deposition, followed closely by comparable levels in akermanite scaffolds cultured in control medium and akermanite:PCL scaffolds cultured in osteogenic medium. These values were significantly higher than akermanite:PCL scaffolds cutured in control medium, β-TCP (control – 0.49±0.05; osteogenic – 0.89±0.72, $P > 0.05$) and PCL (control – 0.16±0.01; osteogenic – 0.21±0.05, $P > 0.05$) scaffolds.

3.3.4. *In Vitro* hASC Proliferation on Scaffolds Cultured in Control and Osteogenic Media

Figure 14 depicts the total DNA content (cell proliferation) in scaffolds loaded with hASC and cultured under different media conditions for 21 days. Significant differences in the cell proliferation was observed in scaffolds cultured in growth (control) and osteogenic media at 7 days only in hASC loaded to β-TCP (control – 148152.00±44331.24; osteogenic – 64021.33±1471.26, $P < 0.05$) and PCL (control – 188922.76±10699.14; osteogenic – 46380.67±9538.36, $P < 0.05$) scaffolds. When compared between scaffold types, cell proliferation was the highest in akermanite:PCL scaffolds cultured in both media conditions (control – 442218.70±169825.50; osteogenic –334082.00±95255.57, $P > 0.05$), followed by PCL and β-TCP scaffolds (both cultured in control medium), which were significantly higher than either akermanite (control – 38913.33±9004.578; osteogenic – 47062.33±8730.08, $P > 0.05$), PCL and β-TCP scaffolds cultured in osteogenic medium.

At 14 days, significant differences in the cell proliferation in scaffolds cultured in growth (control) and osteogenic media were observed only in β-TCP (control – 107493.30±3977.34;

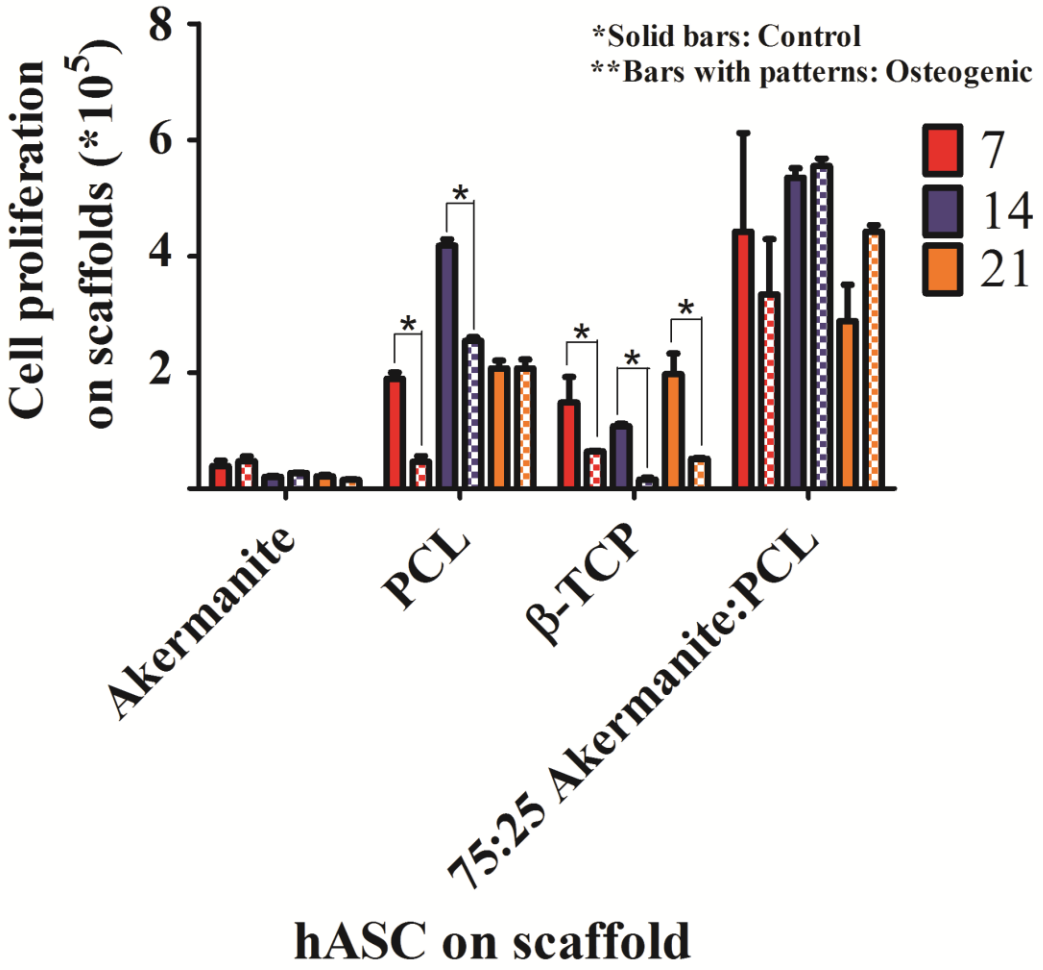

Figure 14. Cell proliferation on different scaffold types and time points. *Represent significant differences in the total DNA content in hASC loaded to different scaffolds within the same time point (Anova, $P < 0.05$).

osteogenic – 15499.33±3524.02, $P < 0.05$) and PCL (control – 417911.33±10953.73; osteogenic – 254046.70±6564.63, $P < 0.05$) scaffolds. Between scaffold types, cell proliferation was the highest in akermanite:PCL scaffolds cultured in both media conditions (control – 535119.30±16157.50; osteogenic – 555045.30±12661.80, $P > 0.05$), followed, respectively, by PCL scaffolds cultured in control medium, PCL scaffolds cultured in osteogenic medium and β-TCP scaffolds cultured in control medium. At 14 days, the lowest cell proliferation was observed in akermanite (control – 20431.33±1731.71; osteogenic – 26918.67±988.60, $P > 0.05$) and β-TCP scaffolds cultured in osteogenic medium.

At 21 days, significant differences in the cell proliferation in scaffolds cultured in growth (control) and osteogenic media were observed only in hASC loaded to β-TCP (control – 196960.30±35467.99; osteogenic – 51252.67±1510.23, $P < 0.05$) scaffolds. Between scaffold types, cell proliferation was the highest in akermanite:PCL scaffolds cultured in both media conditions (control – 287820.30±62987.16; osteogenic – 442140.30±11247.61, $P > 0.05$), followed by comparable levels in β-TCP scaffolds cultured in control medium and PCL (control – 207037.33±13518.60; osteogenic – 206693.37±15442.30, $P > 0.05$) which were significantly higher than β-TCP scaffolds cultured in osteogenic medium. After 21 days, the lowest cell proliferation was again observed in akermanite scaffolds (control – 21174.67±2487.99; osteogenic – 15243.33±1475.49, $P > 0.05$).

3.3.5. Quantitative Real-Time Polymerase Chain Reaction (QPCR)

The differences in the expression of ALP (A) and OCN (B) in hASC loaded to different scaffolds and cultured in control and osteogenic media are represented in Figure 15. In general, the ALP fold change significantly decresead overtime in all scaffold tested, with the exception of PCL which had comparable ALP fold change at 7 (16.38±4.98) and 14 (12.00±2.39) days of

culture. At 7 days, the highest ALP fold change was observed in hASC loaded to akermanite scaffolds (83.61±4.97) which was followed by comparable ALP fold change in PCL, akermanite:PCL (15.29±0.85) and β-TCP (10.57±0.67) scaffolds. After 14 days, the ALP fold change was the highest in akermanite (19.48±5.69), followed by PCL which was significantly higher than the ALP fold change observed in β-TCP (3.27±0.35) and akermanite:PCL (2.90±3.24) scaffolds. At 21 days, the highest ALP fold change was observed in hASC loaded to akermanite scaffolds (8.81±4.40), followed by PCL (0.75±0.09) and β-TCP (0.68±0.48) scaffolds which were significantly higher the ALP fold change observed in akermanite:PCL (0.02±0.01) scaffolds.

The OCN fold change in hASC loaded to different scaffolds and cultured in control and osteogenic media significantly increased overtime in all scaffold tested, with the exception of PCL which had comparable OCN fold change at 7 (2.69±0.88) and 14 (3.28± 0.10) days of culture. At 7 days, the highest OCN fold change was observed in hASC loaded to akermanite scaffolds (11.67±1.93) which was significantly higher than comparable OCN fold change in akermanite:PCL (3.05±0.33), PCLand β-TCP (1.53±0.43) scaffolds. After 14 days, the OCN fold change was the highest in akermanite (20.94±1.79) and akermanite:PCL (16.33±8.47) scaffolds, followed by β-TCP (9.19±2.73) which was significantly higher than the OCN fold change in PCL scaffolds. At 21 days, the highest OCN fold change was observed in hASC PCL which had comparable OCN fold change at 7 (2.69±0.88) and 14 (3.28± 0.10) days of loaded to akermanite scaffolds (372.32±33.78), followed by akermanite:PCL (100.90±0.77) which was significantly higher than the OCN fold change observed in β-TCP (15.22±3.41) scaffolds. After 21 days, the lowest OCN fold change was observed in hASC loaded to PCL (5.61±1.95) scaffolds.

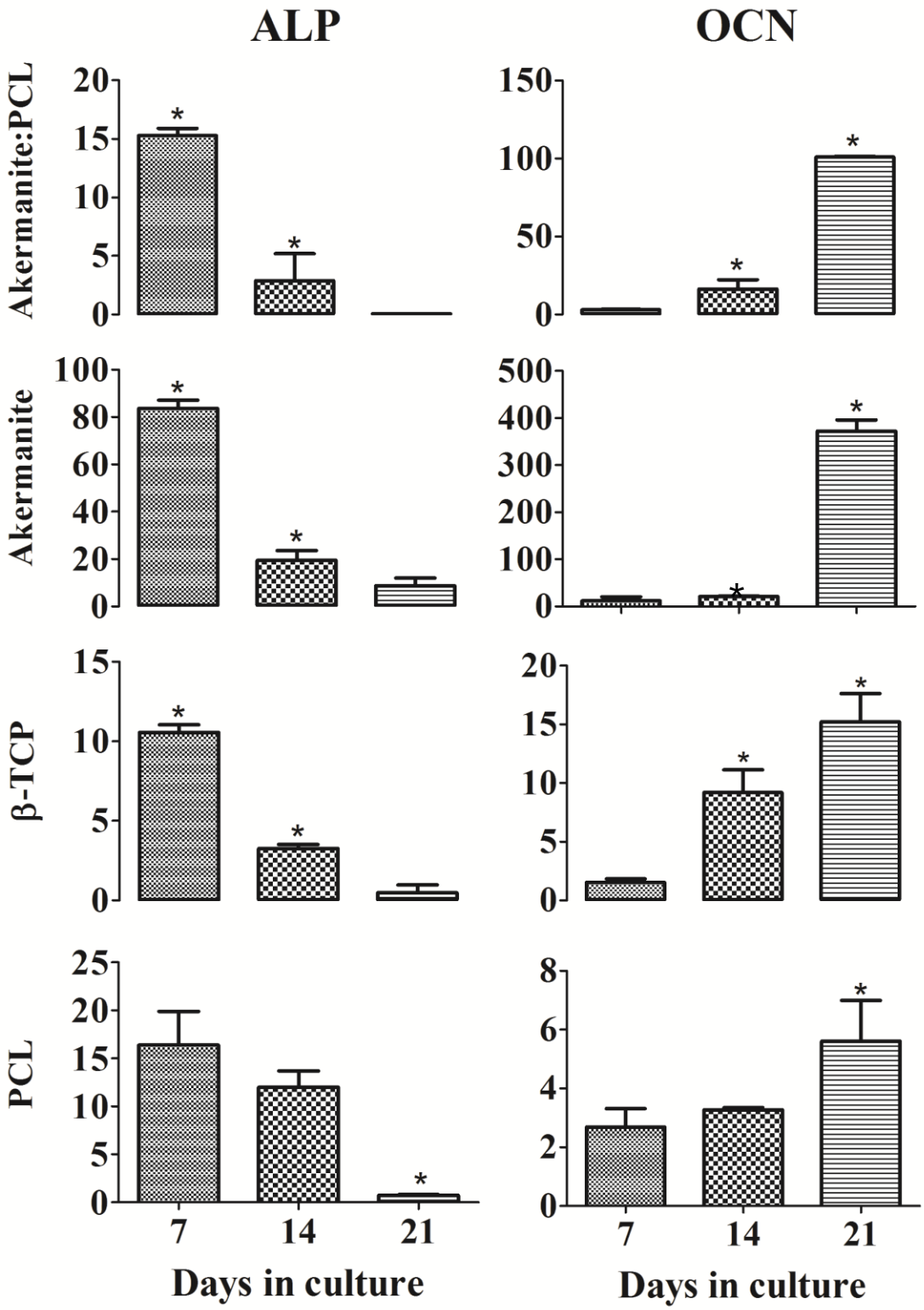

Figure 15. Fold change of ALP (alkaline phosphatase) and OCN (osteocalcin) in hASC loaded to different scaffold types and cultured conditions (control and osteogenic) for a 21 days period. *Represent significant between scaffolds type and targeted osteogenic gene (Anova, $P < 0.05$).

3.4. Discussion

A suitable scaffold for bone regeneration must allow for high density cell attachment, proliferation, and ultimately support *in vivo* bone regeneration with degradation rate largely matched to the rate of cell ingrowth and mineralization(Gaalen et al., 2008). Additionally, current paradigms also describe some other desirable properties, such as the easy-of-use of bone scaffolds during surgical implantation and the scaffolds mechanical properties (Reichert & Hutmacher, 2011). Among the bioactive glass-ceramics, akermanite ($Ca_2MgSi_2O_7$) can enhance cell adhesion, proliferation and osteogenesis while providing predictable and controllable degradation rate (Sun et al., 2006; Wu et al., 2006ab; Wu et al., 2007; Huang et al., 2009; Gu et al., 2011). However due to the brittle behavior of akermanite, pure scaffolds are difficult to use, adding complexity to the clinical translation of this technology(Kneser et al., 2006; Gaalen et al., 2008; Reichert & Hutmacher, 2011). In our previous study, we developed a novel akermanite:PCL composite as a potential moldable scaffold for future bone tissue engineering applications. As part of the *in vitro* characterization of this material, we now report the osteogenic potential of hASC loaded to akermanite:PCL scaffolds and cultured in growth (control) or osteogenic media for 21 days. In summary, after 21 days of culture in both media conditions, the hASC metabolic activity and proliferation in akermanite:PCL scaffolds were similarly decreased but inversally proportional to the calcium deposition and expression of mature osteogenic marker (OCN) observed in akermanite:PCL scaffolds cultured in osteogenic medium.

The ideal scaffolds materials for bone tissue engineering should be bioactive. The bioactivity of the bone tissue engineering scaffolds contributes to their capability for forming an apatite-like layer when they are in contact with physiological fluids (Sun et al., 2006; Liu et al., 2008; Gu et

al., 2011). Previous, the Ca, Mg and Si ions extracted from akermanite were demonstrated to facilitate the osteogenic differentiation of hASCs via an ERK pathway, and suppress the metabolic acitivity and proliferation of hASCs without significant cytotoxicity (Gu et al., 2011). In this study, the decreased metabolic activity and proliferation observed in hASC loaded to pure akermanite scaffolds might also be the result of the cell proliferation suppression phenomenon demonstrated by Gu et al. (2011). Compared to pure akermanite scaffolds, hASC loaded on akermanite:PCL scaffolds and cultured in different media conditions had higher metabolic activity and cell proliferation. The media treatments used in this study influenced the metabolic activity of hASC loaded to akermanite:PCL scaffolds without significant changes in cell proliferation only within the first 7 days of culture. After 14 days, hASC metabolic activity and proliferation were increased in akermanite:PCL scaffolds but no differences between the media conditions were observed. At 21 days, the metabolic activity and proliferation of hASC in akermanite:PCL scaffolds were equally decreased in scaffolds cultured in both media conditions.

Part of the changes observed in the metabolic activity and proliferation of hASC loaded to akermanite:PCL scaffolds described in this study might be due to the concentration of akermanite in the composite scaffolds. According to the findings observed in pure akermanite scaffolds (Gu et al, 2011), suppression of DNA synthesis and cell division might had been initially delayed in hASC loaded to the akermanite:PCL scaffolds because, in this study, significant reductions in the hASC metabolic activity and proliferation were reported only after 21 days. Alternatively, it is well established that in aqueous environments, synthetic apatites degrade overtime through physiochemical dissolution and, possibly, phase transformation. Depending on the concentration of the biomaterial this may result in decreased biocompatibility (Bouler et al., 2000; Chen et al., 2008; Chen et al., 2010). Additionally, PCL is also known to

release caproic acid, which at high concentration can produce cytotoxic effects (Sarasam et al., 2007). Therefore, the changes observed after 21 days in the metabolic activity and proliferation of hASC loaded to akermanite:PCL scaffolds could had also been the result of increase phase transformation and release of caproic acid. However, even though hASC loaded to β-TCP scaffolds had higher metabolic activity than the observed in akermanite:PCL scaffolds after 21 days, cell proliferation in akermanite:PCL scaffolds was significantly higher than in β-TCP scaffolds. Moreover, after 21 days, both parameters were significantly higher in hASC loaded to akermanite:PCL scaffolds than in PCL scaffolds. As a result, the changes observed in this study in the metabolic activity and proliferation of hASC loaded to akermanite:PCL scaffolds seems to be related to the akermanite concentration rather than scaffold phase transformation or polymer breakdown. Further investigations are needed to characterize the influence of bioactive scaffolds on the hASC metabolic activity and proliferation.

Progression of *in vitro* osteogenesis is characterized by decreased cellular proliferation followed by increased amounts of calcium deposition over time (Hirano & Urist, 1981; Bauer & Muschler, 2000; Milat & Wah, 2009). In this study, decreased metabolic activity and cell proliferation were inversally proportional to the increased calcium deposition and expression of osteogenic markers. Moreover, calcium deposition was significanlty higher in akermanite and akermanite:PCL scaffolds cultured in both media conditions than in β-TCP and PCL scaffolds. Osteogenesis is known to be regulated by bone morphogenic proteins (BMPs) which have been reported to stimulate the transcription factor core binding factor alpha1 (Cbfa1) by activating osteoblast-specific genes such as ALP and OCN through the binding to the osteoblast-specific cis-acting element 2 (OSE2) in the promoter region of these genes (Liu et al., 2008; Milat & Wah, 2009). In this study, the ALP fold change between scaffolds cultured in control and

osteogenic media significantly decreased overtime. Alkaline phosphatase is an early stage marker for osteogenic differentiation (Gaalen et al., 2008; Gu et al., 2011) and, together with OCN it is part of rapid and robust osteogenic differentiation (Liu et al., 2008; Milat & Wah, 2009; Gu et al., 2011). Therefore, the results presented in this study, indicated that hASC loaded to akermanite or akermanite:PCL scaffolds or cultured in osteogenic medium had increased osteogenic differentiation and osteoblast maturation during the course of this study. Further investigations are needed to demonstrate the expression of proteins associated with these or other osteogenic markers.

In summary, this study demonstrated that hASC loaded to akermanite:PCL scaffolds have calcium deposition greater than β-TCP and PCL control scaffolds. Moreover, the expression of the mature osteoblast maker (OCN) in hASC loaded to akermanite:PCL scaffolds cultured in osteogenic medium was signifincantly higher than the observed in β-TCP and PCL scaffolds after 21 days. Further investigations are needed to investigate if cryopreservation of hASC loaded to akermanite:PCL scaffolds influence the *in vitro* viability and osteogenic differentiation potential of the hASC.

3.5. References

Reichert JC, Hutmacher DW. 2011; Bone tissue engineering. In: Pallua. *Tissue Engineering* 643.

Gaalen S, Kruyt M, Meijer G, et al., 2008; Tissue Engineering of Bone. In: Clemens van Blitterswijk . *Tissue Engineering* 740.

Scherberich A, Galli R, Jacquiery C, et al., 2007; Three-dimensional perfusion culture of human adipose tissue-derived endothelial and osteoblastic progenitors generates osteogenic constructs with intrinsic vascularization capacity. *Stem Cells* **25:** 1823-1829.

Dégano IR, Vilalta M, Bagó JR, et al., 2008; Bioluminescence imaging of calvarial bone repair using bone marrow and adipose tissue-derived mesenchymal stem cells. *Biomaterials* **29:** 427-437.

De Girolamo L, Sartori MF, Arrigoni E, et al., 2008; Human adipose-derived stem cells as future tools in tissue regeneration: osteogenic differentiation and cell-scaffold interaction. *Int J Artif Organs* **31:** 467-479.

Liu Q, Cen L, Yin S, et al., 2008; A comparative study of proliferation and osteogenic differentiation of adipose-derived stem cells on akermanite and beta-TCP ceramics. *Biomaterials* **29:** 4792-4799.

De Girolamo L, Lopa S, Arrigoni E, et al., 2009; Human adipose-derived stem cells isolated from young and elderly women: their differentiation potential and scaffold interaction during in vitro osteoblastic differentiation. *Cytotherapy* **11:** 793-803.

Haimi S, Gorianc G. 2009; Characterization of zinc-releasing three-dimensional bioactive glass scaffolds and their effect on human adipose stem cell proliferation and osteogenic differentiation. *Acta Biomater* **5:** 3122-3131.

Haimi S, Moimas L, Pirhonen E, et al., 2009; Calcium phosphate surface treatment of bioactive glass causes a delay in early osteogenic differentiation of adipose stem cells. *J Biomed Mater Res A* **91:** 540-547.

Haimi S, Suuriniemi N. 2009; Growth and osteogenic differentiation of adipose stem cells on PLA/bioactive glass and PLA/beta-TCP scaffolds. *Tissue Eng Part A* **15:** 1473-1480.

Marino G, Rosso F, Cafiero G, et al., 2010; Beta-tricalcium phosphate 3D scaffold promote alone osteogenic differentiation of human adipose stem cells: in vitro study. *J Mater Sci Mater Med* **21:** 353-363.

Gastaldi G, Asti A, Scaffino MF, et al., 2010; Human adipose-derived stem cells (hASCs) proliferate and differentiate in osteoblast-like cells on trabecular titanium scaffolds. *J Biomed Mater Res A* **94:** 790-799.

Muller AM, Mehrkens A. 2010; Towards an intraoperative engineering of osteogenic and vasculogenic grafts from the stromal vascular fraction of human adipose tissue. *Eur Cell Mater* **19:** 127-135.

Agathopoulos S, Tulyaganov DU, Valerio P, et al., 2005; A new model formulation of the SiO2-Al2O3-B2O3-MgO-CaO-Na2O-F glass-ceramics. *Biomaterials* **26:** 2255-2264.

Wu C, Chang J, Ni S, et al., 2006a; In vitro bioactivity of akermanite ceramics. *J Biomed Mater Res A* **76:** 73-80.

Chen X, Liao X, Huang Z, et al., 2010; Synthesis and characterization of novel multiphase bioactive glass-ceramics in the CaO-MgO-SiO(2) system. *J Biomed Mater Res B Appl Biomater* **93:** 194-202.

Sun H, Wu C, Dai K, et al., 2006; Proliferation and osteoblastic differentiation of human bone marrow-derived stromal cells on akermanite-bioactive ceramics. *Biomaterials* **27:** 5651-5657.

Gu H, Guo F, Zhou X, et al., 2011; The stimulation of osteogenic differentiation of human adipose-derived stem cells by ionic products from akermanite dissolution via activation of the ERK pathway. *Biomaterials* **32:** 7023-7033.

Wu C, Chang J, Zhai W, et al., 2006b; Porous akermanite scaffolds for bone tissue engineering: preparation, characterization, and in vitro studies. *J Biomed Mater Res B Appl Biomater* **78:** 47-55.

Wu C, Chang J, 2007; Degradation, bioactivity, and cytocompatibility of diopside, akermanite, and bredigite ceramics. *J Biomed Mater Res B Appl Biomater* **83:** 153-160.

Huang Y, Jin X, Zhang X, et al., 2009; In vitro and in vivo evaluation of akermanite bioceramics for bone regeneration. *Biomaterials* **30:** 5041-5048.

Zhuang L, Sai-Kit C, Subrata G, 1990; Elastic Properties of the Incommensurate Phase of Akermanite, Ca2MgSi207. *Phys Chem Minerals* **17:**462-466.

Yang H, Hazen RM, Downs RT, 1997; Structural change associated with the incommensurate-normal phase transition in akermanite, Ca2MgSi2O7 , at high pressure. *Phys Chem Minerals* 24: 510–519.

Kneser U, Schaefer DJ, Polykandriotis E, et al. 2006; Tissue engineering of bone: the reconstructive surgeon's point of view. *J Cell Mol Med* **10:** 7-19.

Zhang ZY, Teoh SH, Chong MS, Schantz JT, Fisk NM, Choolani MA, Chan J. Superior osteogenic capacity for bone tissue engineering of fetal compared with perinatal and adult mesenchymal stem cells. Stem Cells 2009;27:126-137.

Fabbri P, Bondioli F, Messori M, et al., 2010; Porous scaffolds of polycaprolactone reinforced with in situ generated hydroxyapatite for bone tissue engineering. *J Mater Sci Mater Med* **21:** 343-351.

Leong DT, Abraham MC, Rath SN, et al., 2006; Investigating the effects of preinduction on human adipose-derived precursor cells in an athymic rat model. *Differentiation* **74:** 519-529.

Ahn HH, Kim KS, Lee JH, et al., 2009; In vivo osteogenic differentiation of human adipose-derived stem cells in an injectable in situ-forming gel scaffold. *Tissue Eng Part A* **15:** 1821-1832.

Bouler JM, LeGeros RZ, Daculsi G., 2000; Biphasic calcium phosphates: influence of three synthesis parameters on the HA/β-TCP ratio. *J Biomed Mater Res* **51:** 680–4.

Bragg WL., 1920; Crystal structure. *Nature* **105:** 646-648.

Chen XC, Wei Y, Huang ZB, *et al.*, 2008; Synthesis and characterization of multiphase bioactive glass-ceramics in the CaO-MgO-SiO_2 system with B_2O_3 additive. *J Mater Res* **23:** 2873-2879.

Chen XC, Ou J, Wei Y, et al., 2010; Effect of MgO contents on the mechanical properties and biological performances of bioceramics in the MgO-CaO-SiO_2 system. *J Mater Sci Mater Med* **21:** 1463-1471.

Gerlach W. 1922; The lattice structure of alkali-earth oxides. *Z Phys* **9:** 184-192.

Gimble JM, Bunnell BA, Casteilla L, et al., 2010; Phases I-III Clinical Trials Using Adult Stem Cells. *Stem Cells Int* **2010:** 604713.

Gimble JM, Bunnell BA, Guilak F, et al., 2011; Isolation and Growth of Stem Cells. In: Pallua. *Tissue Engineering* 643.

Griffon D, Abulencia JP, Ragetly GR, et al., 2010; A comparative study of seeding techniques and three-dimensional matrices for mesenchymal cell attachment. *J Tissue Eng Regen Med* **5:** 169-179.

Frohlich M, Grayson W, Marolt D, et al., 2010; Bone grafts engineered from human adipose-derived stem cells in perfusion bioreactor culture. *Tissue Eng Part A* **16:** 179-189.

Hattori H, Sato M, Masuoka K, et al., 2004; Osteogenic potential of human adipose tissue-derived stromal cells as an alternative stem cell source. *Cells Tissues Organs* **178:** 2-12.

Jeon O, Rhie JW, Kwon Ik, et al., 2008; In vivo bone formation following transplantation of human adipose-derived stromal cells that are not differentiated osteogenically. *Tissue Eng Part A* **14:** 1285-1294.

Gimble JM, Bunnell BA, Guilak F, et al., 2011; Isolation and Growth of Stem Cells. In: Pallua. *Tissue Engineering* 643.

Bouler JM, LeGeros RZ, Daculsi G., 2000; Biphasic calcium phosphates: influence of three synthesis parameters on the HA/β-TCP ratio. *J Biomed Mater Res* **51:** 680–4.

Chen XC, Wei Y, Huang ZB, *et al.*, 2008; Synthesis and characterization of multiphase bioactive glass-ceramics in the CaO-MgO-SiO_2 system with B_2O_3 additive. *J Mater Res* **23:** 2873-2879.

Chen XC, Ou J, Wei Y, et al., 2010; Effect of MgO contents on the mechanical properties and biological performances of bioceramics in the MgO-CaO-SiO_2 system. *J Mater Sci Mater Med* **21:** 1463-1471.

Sarasam AR, Samli AI, Hess L, et al., 2007; Blending chitosan with polycaprolactone: porous scaffolds and toxicity. *Macromol Biosci* **7:** 1160-1167.

Bauer TW, Muschler GF. 2000; Bone graft materials. An overview of the basic science. *Clin Orthop Rel Res* **371:**10-27.

Hirano H, Urist MR. 1981; Bone-forming and bone-resorbing cell lines derived from bone marrow in tissue culture. *Clin Orthop Rel Res* **154:**234-248.

Milat F, Wah Ng. 2009; Is Wnt signalling the final common pathway leading to bone formation? *Mol Cell Endocrinol* **310:**52–62.

Chapter 4. Freezing Response and Optimal Cooling Rates of Human Adipose-Derived Stem Cells Loaded to Akermanite:Poly-E-Caprolactone Bone Scaffolds

4.1. Introduction

Tissue engineering scaffolds have recently emerged as potent substitutes to autologous and allogenous grafts in bone fracture repair strategies (Reichert & Hutmacher 2011). In part this success is due to the fact that bone scaffolds composed of different biomaterials have been demonstrated to promote bone growth by supporting cell migration, proliferation and differentiation in the fracture site (De Girolamo et al., 2008; Jeon et al., 2008; Ahn et al., 2009). Additionally, the utilization of donor adult stem cells in combination with bone scaffold materials has emerged as a potential therapeutic modality for musculoskeletal repair (Gimble et al., 2010). Among the adult stem cells sources used in current bone scaffold tissue engineering strategies, human adipose-derived stem cells (hASC) represent a readily available, autogenous cell source with well-documented *in vivo* osteogenic potential (Gaalen et al., 2008; Gimble et al., 2011). One of the foreseeable challenges to the clinical application of combination hASC-scaffold therapies is the lack of a predictable shelf life for cell/scaffold combinations (Gaalen et al., 2008; Reichert & Hutmacher 2011). With the growing interest in this therapeutic modality, methods of cryopreservation for stem cells on scaffolds that maintain the cell's differentiation potential and scaffolds may become an urgent need. Therefore, understanding the freezing and post-thaw characteristics of scaffold materials loaded with hASC could be essential.

The goal of any cryopreservation protocol is to minimize ultrastructural damage related to sudden intracellular or extracellular ice crystal formation (Thirumala et al., 2005; Goh et al., 2007). One advantage of the development of cryopreservation methods for synthetic scaffold-cell combinations compared to living tissue is that, depending on the scaffolding material, cryopreservation is unlikely to interfere with the morphological structure and architecture of the

construct, both vital for the post-thaw mechanical support and the biological function of the loaded cells (Kuleshova & Hutmacher 2008). Of the current cryoprotectants used in combination with hASC, polyvinylpyrrolidone (PVP) is a Food and Drug Administration (FDA) approved high molecular weight cryoprotectant agent that has been shown to enhance hASC viability and differentiation *in vitro* (Guha & Devireddy 2010; Thirumala et al., 2010a; Devireddy & Thirumala 2011). While PVP activity is not entirely understood, it is believed that PVP favorably influence the ice crystal formation in hASC by altering the physical properties of the solution during the freezing cycle (Thirumala et al., 2010a). Moreover, raised awareness of the potential for zoonotic disease transmission through bovine serum supplementation has resulted in an alternative PVP serum-free medium protocol for hASC cryopreservation (Thirumala et al., 2010b). Based on this information, PVP-based cryopreservation in serum-free medium might also be beneficial for cryopreservation of donor hASC on scaffolds. However, many fundamental questions related to the hASC-scaffold response to different cooling rates still remain to be investigated before an optimal scaffold freezing protocol can be developed.

Therefore the objective of this study was to compare cell viability, proliferation and osteogenic differentiation of hASC loaded to a bone scaffold composites made of akermanite:poly-e-caprolactone (PCL) under different cooling rates. The hypothesis of this study was that compared to unfrozen scaffolds (controls), cell-scaffold combinations frozen at optimal cooling rate would display similar or improved metabolic activity, cell proliferation and osteogenesis post-thawing and after 10 days of culture in stromal medium.

4.2. Materials and Methods

4.2.1. Synthesis of Akermanite

Akermanite, $Ca_2MgSi_2O_7$, was synthesized by ceramic methods with calcium carbonate (1.237 g, 12.4 mmol), magnesium carbonate (0.521 g, 6.2 mmol), and silicon dioxide (0.742 g, 12.4 mmol) as the starting materials. These materials were mixed and ground up thoroughly using an agate mortar and pestle. The 2.5 g white powder mixture was then pressed into a pellet with hydraulic press (with approximately 1 metric ton of applied pressure) and then heated up multiple times in an open to air boat-shaped alumina crucible using a programmable box furnace to achieve the following net reaction:

$$2\ CaCO_3 + MgCO_3 + 2\ SiO_2 \rightarrow Ca_2MgSi_2O_7 + 3\ CO_2\ (g)$$

The initial heat treatment was carried out at 950°C (after increasing the furnace chamber temperature from room temperature at rate of 100°C/h) for 48 hours. This intermediate reaction, which involves the conversion of the carbonate starting materials to oxides, was then allowed to cool down back to room temperature by heat loss through the top exhaust port of the furnace. The pellet was then weighed to confirm the mass loss of approximately 0.8 g (or 18.5 mmol) of carbon dioxide. Subsequent heat treatments involved additional grinding, pellet pressing, and heating the crude product at the dwell temperature of 1300°C (after ramping up the temperature from room temperature at rate of 100°C/h) for 48 hours. Each 48 hour heat treatment was followed by cooling back to room temperature by furnace exhaust. The number of heat treatments at 1300°C required was dictated by proof of desired product purity (as judged by powder X-ray diffraction) and typically varied with each batch from 2 to 3 times.

4.2.2. Fabrication of Akermanite:PCL Scaffolds

A 10% PCL solution in 8 ml of 1-4, dioxane was prepared and akermanite was added at weight (g) ratio of 0.6:0.2 (akermanite:PCL) in a glass bottle. The mixtures were molded into 10mmX4mm polydimethylsiloxane (PDMS) templates, frozen at -80^{o}C overnight and immediately incubated in a freeze-drier for 48 hours. Dried akermanite:PCL scaffolds were prepared for viability and osteogenic studies.

4.2.3. Isolation of hASC and Culture

Liposuction aspirates from subcutaneous adipose tissue were obtained from male (n = 1) and females (n = 2) subjects undergoing elective procedures. All tissues were obtained with informed consent under a clinical protocol reviewed and approved by the Institutional Review Board at the Pennington Biomedical Research Center. Isolation of hASC was performed as described elsewhere (Gimble et al., 2011). The initial passage of the primary cell culture was referred to as ‘‘Passage 0’’ (p0). The cells were passaged after trypsinization and plated at a density of 5,000 cells/cm^2 (‘‘Passage 1’’) for expansion on T125 flasks until 80% of confluence was reached. Passage 2 of each individual was used for all analysis.

4.2.4. hASC Loading on Scaffolds and Culture

Passage 2 of each donor (n = 3) was loaded to each scaffold using a custom-made spinner flask bioreactor at loading density of 2,500 cells/mL for 2 hours. Immediately after, 6 scaffolds were transferred into 6-well plates (1 scaffold/well) and maintained in DMEM + 10% PVP for 20 min and immediately collected for analysis or cultured in stromal medium for 10 days with weekly data collection (controls). The remaining scaffolds (n = 34) were frozen at cooling rates of 1^{o}C/min, 2^{o}C/min, 5^{o}C/min, 10^{o}C/min and 40^{o}C/min. Immediately after, the scaffolds were

thawed in a water bath incubated at 37°C and collected for analysis (time point 0) or cultured in stromal medium for 10 days.

4.2.5. Detection of Cell Viability with Alamar Blue Staining

The metabolic activity of cells within the scaffolds immediately after thawing (time point 0) and at 10 days in stromal medium was determined with the Alamar Blue™ assay. The scaffolds were removed from culture, washed three times in PBS, and incubated with 10% Alamar Blue™ in Hank's balanced salt solution (HBSS) without phenol red (pH 7) for 90 min. Aliquots (100 µL) of Alamar Blue™/HBSS were placed in a 96-well plate in triplicate, and the fluorescence was measured at an excitation wavelength of 530 nm and an emission wavelength of 595 nm using a fluorescence plate reader.

4.2.6. Alizarin Red Staining

hASC osteogenesis at time point 0 and after 10 days of culture was assessed with alizarin red. Briefly, scaffolds were washed with 0.9% NaCl (1 ml/well) and fixed with 70% ethanol (1 ml/well). Subsequently, the fixative was removed by aspiration and plates were stained with 2% alizarin red for 10 min and washed with deionized water. The scaffolds were destained by the addition of 2 ml of 10% cetylpyridinium chloride monohydrate to each well followed by shaking for 10 min at room temperature. The calcium deposition expressed by the optical density of the aliquots was then measured at 540 nm with a plate reader.

4.2.7. Quantification of DNA on Scaffolds

Total DNA content was used to determine the number of cells on each scaffold as previously described (Liu et al., 2008). Briefly, scaffolds were crushed and then incubated with 0.5 mL proteinase K (0.5 mg/mL) at 56ºC overnight. The mixture was centrifuged at 108g for 5 minutes and then 50 µl aliquots were mixed with 50 µl Picogreen dye solution (0.1 g/mL, Invitrogen) in

96-well plates. Samples were excited at 480 nm and total DNA concentration was compared to a standard curve generated from serial dilutions of hASC. Scaffold without cells were used to subtract the background fluorescence emission from all readings.

4.2.8. Quantitative Real-Time Polymerase Chain Reaction (QPCR)

Total RNA was extracted from cells and cell-scaffolds using the Trizol reagent (Sigma). QPCR was performed using 2X iTaq SYBR green with ROX (Biorad) and alkaline phosphatase (ALP) forward (5'- AATATGCCCTGGAGCTTCAGAA -3') and reverse (5'- CCATCCCATCTCCCAGGAA -3') and osteocalcin (OCN) forward (5'- GCCCAGCGGTGCAGAGT -3') and reverse (5'- TAGCGCCTGGGTCTCTTCAC -3') to assess the osteogenic differentiation of hASC loaded to scaffolds immediately after thawing and at 10 days of culture. Reactions were performed with a MJ Mini Thermal Cycler (BioRad). Water (negative) and hASC culture in osteogenic medium for 14 days were used as controls. Samples were normalized (ΔCt) against the house keeping gene 18SrRNA.

4.2.9. Micro-Computer Tomography (µ-CT) at Optimal Freezing Rate

Samples were aligned along their axial direction and stabilized with wet gauze in a 1.5 mL centrifuge tube. The tubes were clamped in the specimen holder of a SkiscanCT1074 system (Skiscan, Belgium). The pixel value in two-dimensional images were used to calculate the deposition of bone on the scaffolds after 10 days.

4.2.10. Statistical Analysis

All results were expressed as mean±SEM. Normality of the data was confirmed using the Shapiro-Wilk test ($P < 0.001$). Data was analyzed with one or two-way analysis of variance (ANOVA), followed by Tukey's minimum significant difference (MSD) post hoc test for

pairwise comparisons of main effects. For all comparisons, a *P*-value < 0.05 was considered significant.

4.3. Results

4.3.1. Cell Viability

The metabolic activity of hASC loaded to akermanite:PCL scaffolds significantly differed between fresh and frozen samples as shown in Figure 16A. At time point 0, comparable metabolic activity expressed by the Alamar blue stain was observed in scaffolds frozen at 1 and 5 ^{o}C/min (16469.92±174.42 and 15450.88±85.08, respectively), which were significantly greater than the metabolic activity in scaffolds frozen at 2 and 10^{o}C/min (14656.20±120.87 and 14809.21±39.73, respectively). Within this time point, the lowest metabolic activity of hASC loaded to akermanite:PCL scaffolds was observed in unfrozen scaffolds (control) 13386.30± 595.13) and scaffolds frozen at 40^{o}C/min (13242.81±36.17). However, after 10 days in stromal medium, hASC loaded to scaffolds frozen at 40 ^{o}C/min had the highest metabolic activity (32752.86±126.43) which was followed by scaffolds frozen at 5^{o}C/min (21146.90±172.33, 1 ^{o}C/min (14331.37±165.29), 10^{o}C/min (12545.92±54.30) and 2^{o}C/min (11505.14±69.43), respectively, as depicted in Figure 16A. At this time point, hASC loaded to control scaffolds (unfrozen) displayed the lowest metabolic activity (10145.12±72.47).

4.3.2. Calcium Deposition

Figure 16B depicts calcium deposition in fresh and frozen akermanite:PCL scaffolds loaded with hASC. At time point 0, increased deposition of calcium measured by the alizarin red stain was observed in unfrozen (control) scaffolds (0.506±0.006) which was significantly greater than scaffolds frozen at 2^{o}C/min (0.4237±0.001), 1 and 40^{o}C/min (0.295± 0.017; 0.329±0.011, respectively). At this time point, the lowest calcium deposition was observed in scaffolds frozen

at 5 and 10°C/min (0.245±0.003; 0.235±0.015, respectively). Following 10 days of culture in stromal medium, increased calcium deposition was observed in scaffolds frozen at 40°C/min (3.611±0.018), with reduced calcium deposition being found in scaffolds frozen at 1°C/min (2.017±0.009), 2°C/min (1.488±0.013), control and 10°C/min (1.353±0.003; 1.335±0.007). At this time point, hASC loaded to scaffolds frozen at 5°C/min displayed the lowest calcium deposition (1.044±0.009).

4.3.3. Quantification of DNA on Scaffolds

The loading efficiency of the scaffolds after 2 hours of incubation in the spinner flask averaged 60% (60.23±0.03). Total DNA content on fresh and frozen scaffolds significantly differed as represented in Figure 17. At time point 0, total DNA was the highest in scaffolds frozen at 1 or 5°C/min (39248.00±5616.81; 32000.00±355.67, respectively), followed by comparable values in control scaffolds (24057.33±1116.15) and scaffolds frozen at 2 and 40°C/min (22213.33±244.50; 21662.670± 2022.79, respectively). Within this time point, total DNA was the lowest in scaffolds frozen at 10°C/min (2500±538.65). After 10 days, total DNA was the highest in control scaffolds (79954.66±3167.46), followed by comparable values in scaffolds frozen at 10 and 40°C/min (49572.00±899.07; 56248.00± 2911.30, respectively) which were significantly greater than scaffolds frozen at 1 or 2°C/min (38833.33± 3574.86; 40798.67±1257.84) and 5°C/min (3904.00± 367.746).

4.3.4. Quantitative Real-Time Polymerase Chain Reaction (QPCR)

Quantitative data indicated that freezing significantly influenced the ALP expression at time point 0 (Figure 18A). With the exception of fresh scaffolds (control), ALP expression was upregulated in all scaffolds. Increased ALP mRNA expression immediately after scaffolds thawing was observed in scaffolds frozen at 5, 10 or 40°C/min (5.46±7.47; 9.71±1.90;

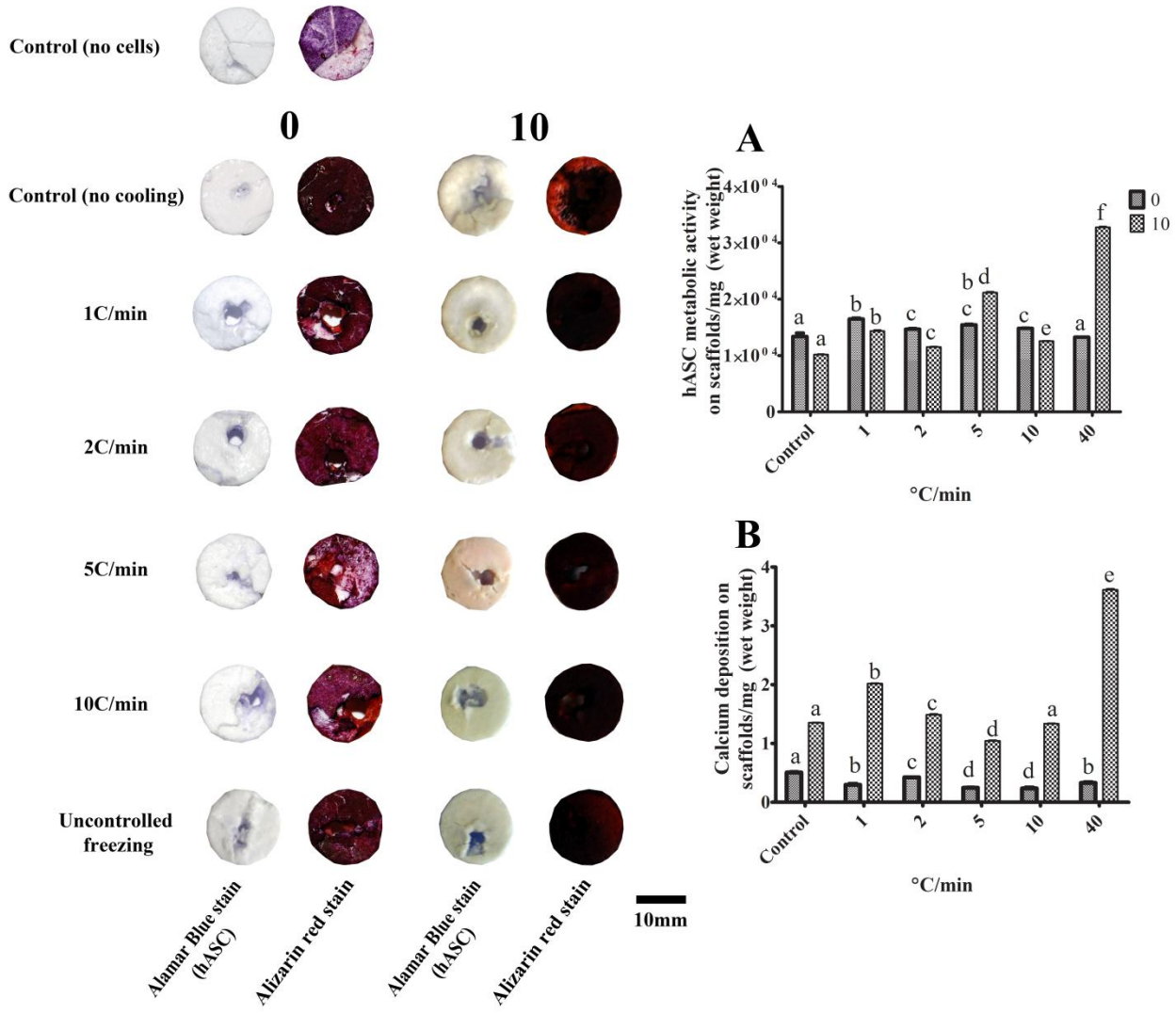

Figure 16. Metabolic activity (A) and calcium deposition (B) in fresh and frozen akermanite:PCL scaffolds loaded with hASC. Lowercase letters indicate significant differences between the cooling rates within each time point (Tukey's test, $P < 0.05$).

13.09± 5.20, respectively) which were significantly greater than the ALP expression observed in scaffolds frozen at 1 or 2°C/min (1.95±0.34; 2.57±1.64, respectively). After 10 days, ALP expression was comparable in scaffolds frozen at 1, 2 or 40°C/min (16.43±3.27; 19.24±3.76; 15.69±1.97, respectively) which were significantly greater than scaffolds frozen at 5 or 10°C/min (2.24± 0.80; 2.03±0.83, respectively).

Upregulation of the mature osteoblast marker OCN was observed only after 10 days of culture in scaffolds frozen at different cooling rates (Figure 18B). Increased OCN mRNA expression was significantly greater in scaffolds frozen at 2, 5 or 10°C/min (9.28±0.77; 13.06±5.14; 11.38±3.25, respectively) than scaffolds frozen at 1 or 40°C/min (4.68±1.99; 2.45±1.56, respectively).

4.3.5. Live/Dead staining at Optimal Freezing Rate

hASC loaded to akermanite:PCL scaffolds and frozen at 2 and 40°C/min were stained with Live/Dead stain after 10 days of culture to compare the number of viable cells post-culture to the observed in control (uncooled) scaffolds. Figure 19 indicates that after 10 days of culture, scaffolds frozen at 40°C/min had number of viable hASC similar to control scaffolds. Live hASC were also observed in scaffolds frozen at 2°C/min but compared to control or scaffolds frozen at 40°C/min that number was much lower.

4.3.6. Bone Deposition at Optimal Freezing Rate

The radiodensity of control and scaffolds frozen at 2 and 40°C/min changed after 10 days of culture (Figure 20). In general, the highest bone deposition was observed in control (68026±35853) and scaffolds frozen at 40°C/min (66478±6754) which were comparable but significantly higher than the observed in scaffolds frozen at 2°C/min (38131±816.5).

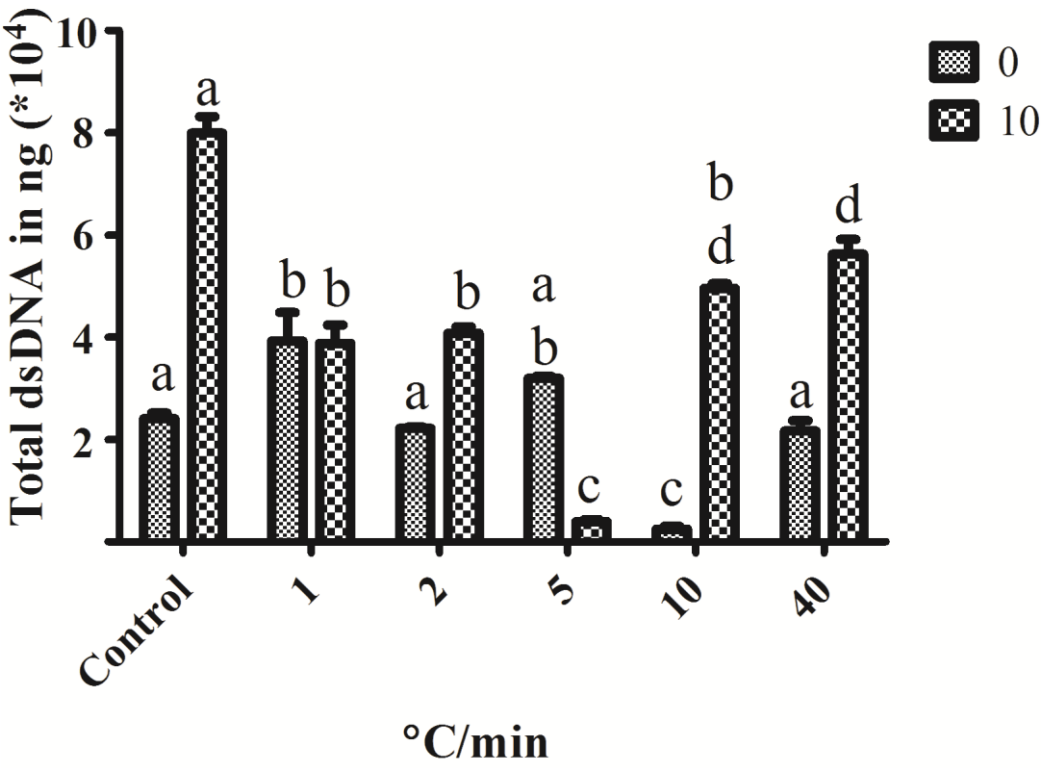

Figure 17. Total DNA quantification on scaffolds. Lowercase letters indicate significant differences between the cooling rates within each time point (Tukey's test, $P < 0.05$).

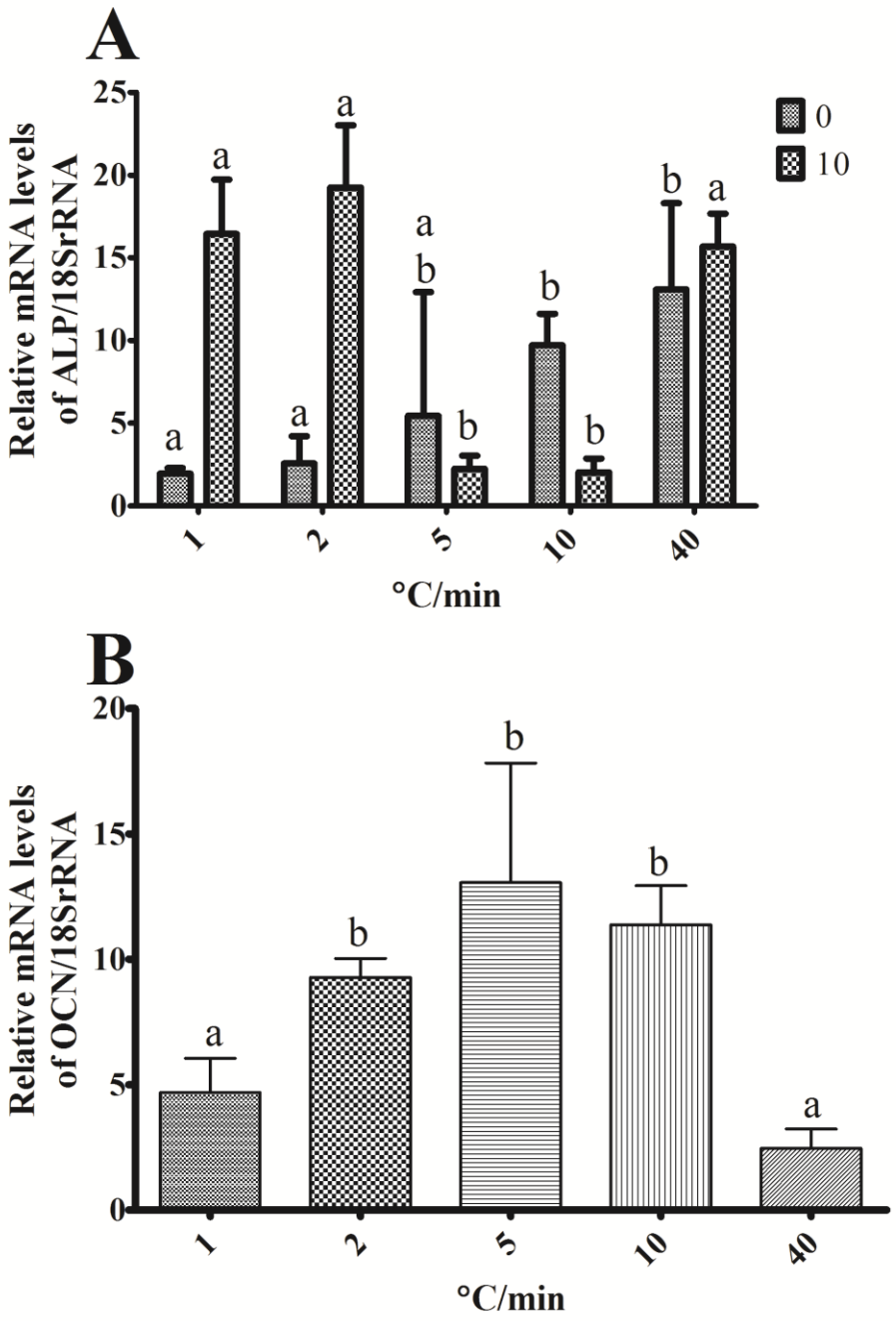

Figure 18. Relative mRNA expression of ALP (A – 0 and 10 days) and OCN (B – 10 days only) in scaffolds frozen at different cooling rates. Lowercase letters indicate significant differences between the cooling rates within each time point (Tukey's test, $P < 0.05$).

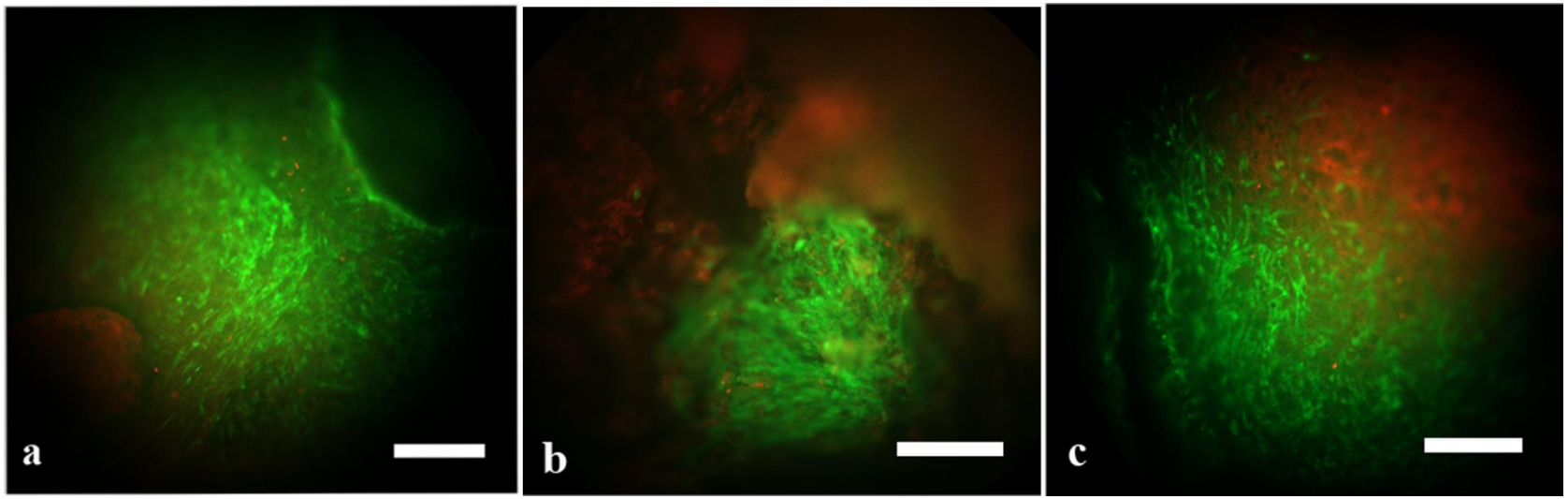

Figure 19. Live/Dead staining of uncooled scaffolds (a - control) and scaffolds frozen at 2°C/min (b) and 40°C/min (c). The images are showing increased number of live hASC (green) in control scaffolds and scaffolds frozen at 40°C/min compared to scaffolds frozen at 2°C/min. Scale bar 100μm.

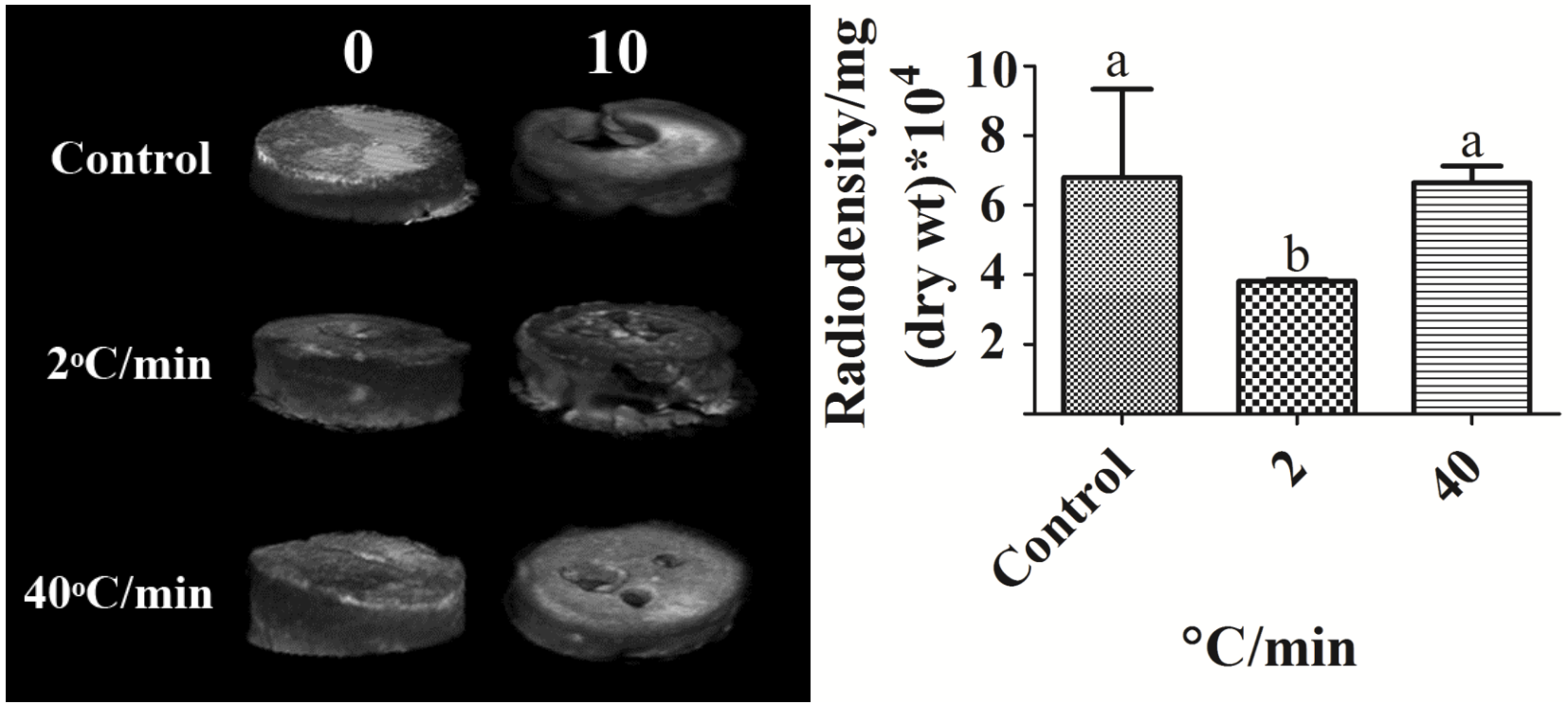

Figure 20. Micro-computer tomography (μ-CT) images of uncooled scaffolds (control) and scaffolds frozen at 2 and 40°C/min at time point 0 and after 10 days of culture; and the scaffold radiodensity differences after 10 days of culture. Lowercase letters indicate significant differences in the radiodensity of the scaffolds between the cooling rates (T-test, $P < 0.05$).

4.4. Discussion

Adult stem cells cultured on composite scaffolds are emerging as the alternative method to regenerate bone in the 21st century. As freshly collected adult stem cells are not always readily available, there will be a need for improved cryopreservation methods to reproducibly maintain viability and osteogenesis of stem cells loaded to the scaffolds during long-term storage. The objective of this work was to assess the effect of freezing on the metabolic activity and osteogenesis of hASC loaded to akermanite:PCL scaffolds and frozen in 10% PVP at different cooling rates in the absence of serum and other cryoprotective agents. According to the results, the metabolic activity and DNA content of hASC in post-thaw scaffolds were the highest in scaffolds frozen at 1 and 5°C/min, however significant differences in hASC osteogenesis were observed across the treatment groups. While increased calcium deposition was observed in post-thawed control (uncooled) scaffolds, the expression of an early marker for osteogenesis (ALP) was the highest in scaffold frozen at 5, 10 and 40°C/min. Moreover, after 10 days of culture in stromal medium, the metabolic activity and osteogenic differentiation of hASC-scaffolds frozen at different cooling rates were greater than in control (uncooled) scaffolds. In summary, this study demonstrated that DMEM+PVP can be used to cryopreserve hASC loaded to akermanite:PCL bone scaffolds. The data also suggested that freezing contributed to the hASC differentiation on the scaffolds.

As cell attachment to scaffolds is a critical aspect of cell-assisted bone tissue engineering cryopreservation of scaffolds loaded with adult stem cells is dependant on the seeding technique applied (Lawrence and Madihally 2010; Reichert & Hutmacher 2011). Therefore, an easy to use high throughput method that allows a fast and homogeneous cell delivery before scaffold freezing will be preferred in future research or clinical strategies (Lawrence and Madihally,

2010). In this study, a custom-made spinner flask was used to load hASC to akermanite:PCL scaffolds. In principal, the technique relies on fluid convection and collision with the immobilized scaffolds to improve cell attachment and distribution throughout the scaffolds (Griffon et al., 2010). Even though, the spinner flask used in this study yielded high cellular adherence in both control and post-thawed scaffolds, significant differences in the DNA content across both groups and time points were observed. Such differences might be the result of differences in initial loading efficiency between scaffolds within the same spinner flask, the post-freezing effect in scaffolds cultured for 10 days or losses associated with the DNA extraction protocol used in this study. Nevertheless, Live/Dead (control; and scaffolds frozen at 2^{o}C/min and 40^{o}C/min) staining revealed an increased number of cells on the surface of the scaffolds after 10 days of culture, indicating that with prolonged culture time (i.e., 8 weeks post-implantation) an increased number of viable cells, and therefore, bone growth, would be observed in the scaffolds. While this assumption remains to be tested *in vivo*, nearer term *in vitro* studies are needed to optimize the concentration of cells on scaffolds before cryopreservation.

Bone scaffolds should mimic, as closely as possible, the natural bone architecture to ensure cell attachment and migration within the porous materials. More important, they should degrade or be integrated with the surrounding tissue and eventually be replaced by new or existing host tissue overtime (Gaalen et al., 2008). Therefore, the bioactivity and slow degradation is highly desirable in scaffold-assisted bone healing. In this study, hASC were loaded to akermanite:PCL scaffolds before cryopreservation. Akermanite (Ca2MgSi2O7), is a bioactive glass ceramic with controllable degradation rate and desirable mechanical and biological properties previously shown to enhance hASC biocompatibility and osteogenesis *in vitro* (Liu et al., 2008; Gu et al., 2011). Poly-e-caprolactone (PCL) is an aliphatic polyester, poorly water-soluble that has a slow

degradation *in vivo* (Fabbri et al., 2010). Due to the PCL melting temperature close to physiologic body temperature, current bone tissue engineering paradigms seek the utilization of PCL as a moldable scaffolding material (Leong et al., 2008; Fabbri et al., 2010). As both Akermanite and PCL have well described biocompatibility and osteogenic qualities we sought to develop a novel composite scaffold (akermantie:PCL) combining the desirable properties of both biomaterials.

Several studies investigated akermanite biocompatibility and osteogenesis with adult stem cells (Sun et al., 2006; Liu et al., 2008; Gu et al., 2011). In general, akermanite has been shown to be highly biocompatible when combined with adult stem cells. Moreover, hBMSC (human bone marrow-derived stem cells) and hASC proliferation on the surface of akermanite scaffolds has been reported to improve overtime (Sun et al., 2006; Liu et al., 208). However, these previous studies assessed hASC osteogenesis and metabolic activity (biocompatibility) in the absence of a cryopreservation and thaw cycle. In this study, Alamar blue stain was used to quantitate the metabolic activity of hASC loaded akermanite:PCL scaffolds frozen at different cooling rates. The data indicates that, compared to control (uncooled) scaffolds, increased metabolic activity was observed in post-thawed scaffolds frozen at 1 and 5^{o}C/min. But after 10 days of culture in stromal medium, scaffolds frozen at 40^{o}C/min displayed remarkably greater hASC metabolic activity. On the other hand, significant differences in hASC osteogenesis were observed across the group treatments. While increased calcium deposition was observed in post-thawed control (uncooled) scaffolds, the ALP expression was the highest in scaffold frozen at 5, 10 and 40^{o}C/min. Moreover, after 10 days of culture, scaffolds frozen at 40^{o}C/min had the highest calcium deposition and up-regulation of ALP and OCN (marker for mature osteoblasts). Even though, OCN expression in scaffolds frozen at 40^{o}C/min was significantly lower than in

scaffolds frozen at 2, 5 or 10°C/min, μ-CT comparisons between scaffolds frozen at 40°C/min and 2°C/min and cultured for 10 days in stromal medium revealed significant increases in mineralization in scaffolds frozen at 40°C/min. Polyvinylpyrrolidone (PVP) might have influenced, in part, the hASC metabolic activity and osteogenesis in both control and post-thawed scaffolds (Guha & Devireddy 2010; Devireddy & Thirumala 2011). However, after 10 days of culture, increased metabolic activity and osteogenesis was observed in scaffolds frozen using the most rapid cryopreservation protocol (40°C/min). While interesting, the mechanism underlying these results remain to be investigated. The authors hypothesize that the combined akermanite bioactivity (Sun et al., 2006; Liu et al., 2008; Gu et al., 2011) and the favorable PVP influence in the nucleation process during the freezing cycle (Thirumala et al., 2010a) might play a role in the increased metabolic activity of scaffolds frozen at 40°C/min. Mechanical damage related to the scaffold from thermal expansion may result in higher concentrations of calcium, magnesium and silicon ions being released from the scaffold into the cell's local microenviroment contributing to osteogenic potential. Alternatively, mechanical stresses imposed by the scaffold on the cells during freezing and thawing may modulate differentation. Future investigations will further assess these assumptions, partiularly, in hASC loaded to other bioactive scaffold materials.

As a conclusion, this study demonstrated that akermanite:PCL scaffolds loaded with hASC can be cryopreserved with 10% PVP in serum-free medium. Moreover, after 10 days of culture, optimal hASC metabolic activity and osteogenesis were observed in scaffolds initially frozen at 40°C/min. However, before this protocol can be adapted for the preservation and preparation of cell-scaffold therapies further investigations are needed to elucidate the mechanisms of scaffold modulated osteogenic upregulation and PVP cryopreservation.

4.5. References

Reichert JC, Hutmacher DW. 2011; Bone tissue engineering. In: Pallua. *Tissue Eng* 643.

Ahn HH, Kim KS, Lee JH, et al., 2009; In vivo osteogenic differentiation of human adipose-derived stem cells in an injectable in situ-forming gel scaffold. *Tissue Eng Part A* **15:** 1821-1832.

De Girolamo L, Sartori MF, Arrigoni E, et al., 2008; Human adipose-derived stem cells as future tools in tissue regeneration: osteogenic differentiation and cell-scaffold interaction. *Int J Artif Organs* **31:** 467-479.

Jeon O, Rhie JW, Kwon Ik, et al., 2008; In vivo bone formation following transplantation of human adipose-derived stromal cells that are not differentiated osteogenically. *Tissue Eng Part A* **14:** 1285-1294.

Gimble JM, Bunnell BA, Casteilla L, et al., 2010; Phases I-III Clinical Trials Using Adult Stem Cells. *Stem Cells Int* **2010:** 604713.

Gimble JM, Bunnell BA, Guilak F, et al., 2011; Isolation and Growth of Stem Cells. In: Pallua. *Tissue Engineering* 643.

Gaalen S, Kruyt M, Meijer G, et al., 2008; Tissue Engineering of Bone. In: Clemens van Blitterswijk . *Tissue Engineering* 740.

Thirumala S, Zvonic S, Floyd E, et al., 2005; Effect of various freezing parameters on the immediate post-thaw membrane integrity of adipose tissue derived adult stem cells. *Biotechnol Prog* **21**:1511-1524.

Goh BC, Thirumala S, Kilroy G, et al., 2007; Cryopreservation characteristics of adipose-derived stem cells: maintenance of differentiation potential and viability. *J Tissue Eng Regenerat Medicine* **1**:322-324.

Kuleshova L, Hutmacher D. 2008. Cryobiology. In: Clemens van Blitterswijk . *Tissue Eng* 740.

Guha A, Devireddy R. 2010; Polyvinylpyrrolidone (PVP) mitigates the damaging effects of intracellular ice formation in adult stem cells. *Annals of Biomed Eng* **38**:1826-1835.

Thirumala S, Wu X, Gimble JM, et al., 2010a; Evaluation of polyvinylpyrrolidone as a cryoprotectant for adipose tissue-derived adult stem cells. *Tissue Eng Part C, Methods* **16**:783-792.

Devireddy R, Thirumala S. 2011; Preservation protocols for human adipose tissue-derived adult stem cells. *Methods in Mol Biol* **702**:369-394.

Thirumala S, Gimble JM, Devireddy RV, 2010b; Cryopreservation of stromal vascular fraction of adipose tissue in a serum-free freezing medium. *J Tissue Eng Regenerat Medicine* **4:**224-232.

Liu Q, Cen L, Yin S, et al., 2008; A comparative study of proliferation and osteogenic differentiation of adipose-derived stem cells on akermanite and beta-TCP ceramics. *Biomaterials* **29:** 4792-4799.

Lawrence BJ, Madihally SV, 2008. Cell colonization in degradable 3D porous matrices. *Cell Adh Migr* **2:**9-16.

Sun H, Wu C, Dai K, et al., 2006; Proliferation and osteoblastic differentiation of human bone marrow-derived stromal cells on akermanite-bioactive ceramics. *Biomaterials* **27:**5651e7.

Griffon D, Abulencia JP, Ragetly GR, et al., 2010; A comparative study of seeding techniques and three-dimensional matrices for mesenchymal cell attachment. *J Tissue Eng Regen Med* **5:** 169-179.

Gu H, Guo F, Zhou X, et al., 2011; The stimulation of osteogenic differentiation of human adipose-derived stem cells by ionic products from akermanite dissolution via activation of the ERK pathway. *Biomaterials* **32:** 7023-7033.

Fabbri P, Bondioli F, Messori M, et al., 2010; Porous scaffolds of polycaprolactone reinforced with in situ generated hydroxyapatite for bone tissue engineering. *J Mater Sci Mater Med* **21:** 343-351.

Leong DT, Nah WK, Gupta A, Hutmacher DW, Woodruff MA. The osteogenic differentiation of adipose tissue-derived precursor cells in a 3D scaffold/matrix environment. Curr Drug Discov Technol 2008;5:319-327.

Chapter 5. *In Vivo* Evaluation of Five Bone Substitute Scaffolds for Human Adult Mesenchymal Stem Cell Osteogenesis

5.1. Introduction

The engineering of osteogenic bone substitute grafts based on scaffolds loaded with human adult mesenchymal stem cells offers an attractive opportunity for the replacement of posttraumatic bone loss, treatment of delayed or non healing fractures or fusion of degenerated joints (Gaalen et al., 2008; Reichert & Hutmacher, 2011). The concept has the potential to overcome the main limits associated with autologous and allogeneic bones, currently the golden standard bone grafts, namely donor site morbidity (Arrington et al., 1996; Ahlmann et al., 2002) and reduced availability (Boden, 2000) as well as time consuming bone banking procedures (Bauer & Muschler, 2000) and the risk for disease transmission (Reichert & Hutmacher, 2011). Among the biomaterials currently used in bone scaffold strategies, bioactive ceramics and highly purified polymers are the most common (Hattori et al., 2004; Scherberich et al., 2007; Dégano et al., 2008; De Girolamo et al., 2008; Liu et al., 2008; De Girolamo et al., 2009; Haimi et al., 2009; Haimi and Suuriniemi, 2009; Haimi and Gorianc, 2009; Gastaldi et al., 2010; Marino et al., 2010; Muller and Mehrkens, 2010; Wang et al., 2010; Lee and Lee, 2011). Particularly, because of their predictable manufacturing procedures which make both biomaterials easily processed for a variety of clinical/research bone tissue engineering applications (Gaalen et al., 2008). However, an ideal scaffolding material for *in vivo* cell-assisted bone formation independent of the donor stem cell source still remains to be identified.

Several studies have indicated that the presence of a mineral biomimetic phase, such as hydroxyapatite (HA) or β-tricalcium phosphates (β-TCP), is important for the success of a scaffold promoting bone regeneration (De Girolamo et al., 2008; Marino et al., 2010; Muller and Mehrkens, 2010). HA is more stable, exhibiting much lower dissolution rates (De Girolamo et

al., 2008; Gaalen et al., 2008; Muller and Mehrkens, 2010), whereas β-TCP is more soluble and its degradation products, calcium and phosphate, are released into the surrounding environment, potentially inducing bioactivity (Bouler et al., 2000; Gaalen et al., 2008; Liu et al., 2008; Marino et al., 2010). More recently, silica-based glass ceramics, such as akermanite, has been also observed to promote bone growth (Sun et al., 2006; Wu et al., 2006ab; Wu et al., 2007; Huang et al., 2009; Gu et al., 2011). Compared to HA and β-TCP, porous akermanite scaffolds have enhanced mechanical and bioactivity properties (Agathopoulos et al., 2005; Wu et al., 2006a; Chen at al., 2010). Moreover, due to the ability to form apatite-like layers at a physiological fluid interface, akermanite scaffolds have been shown to enhance cell adhesion, proliferation, osteogenic differentiation, and extracellular matrix mineralization *in vitro* (Sun et al., 2006; Liu et al., 2008; Gu et al., 2011). However, independent of the bioceramic used, the native brittleness of current ceramic scaffolds make translation to clinical setting difficult (Kneser et al., 2006; Reichert & Hutmacher, 2011).

In contrast, many synthetic biodegradable polymers are proposed in various tissue engineering applications, including bone tissue repair, based on their flexibility of material properties and the ability to support cell growth (Hattori et al., 2004; Dégano et al., 2008; Wang et al., 2010; Lee and Lee, 2011). Poly-e-caprolactone (PCL) is one of the most versatile synthetic polymers used today (Leong et al., 2006; Leong et al., 2008; Zhang et al., 2009). Due to its biocompatibility, poor water solubility, melting point close to physiologic body temperature and slow *in vivo* degradation, PCL has been proposed as a composite moldable scaffolding material in many bone scaffold applications (Leong et al., 2006; Gaalen et al., 2008; Zhang et al., 2009; Fabbri et al., 2010). However, *in vivo* osteogenic comparisons of pure PCL

to others commonly used bioceramic materials in the presence or absence of human adult mesenchymal stem cells isolated from different tissue sources remain to be investigated.

Identification of a scaffolding material that display similar *in vivo* bone growth independent of the human adult mesenchymal stem cells source is appealing because it could facilitate comparisons between current *in vivo* protocols. Due to the PCL recognized biological and mechanical properties, in this study, we compared the *in vivo* ectopic bone formation of pure porous PCL scaffolds to β-TCP and β-TCP:HA (CellCeramic^{TM}) ceramic scaffolds in the presence or absence of human adipose-derived mesenchymal stem cells (hASC) and bone marrow-derived mesenchymal stem cells (hBMSC) 8 weeks post-implantation. Additionally, we reported an acute phosphorous depletion toxicity associated with subcutaneous implantation of akermanite and akermanite:PCL scaffolds in immunodeficient mice.

5.2. Materials and Methods

5.2.1. Synthesis of Akermanite

Akermanite, $Ca_2MgSi_2O_7$, was synthesized by ceramic methods with calcium carbonate (1.237 g, 12.4 mmol), magnesium carbonate (0.521 g, 6.2 mmol), and silicon dioxide (0.742 g, 12.4 mmol) as the starting materials. These materials were mixed and ground up thoroughly using an agate mortar and pestle. The 2.5 g white powder mixture was then pressed into a pellet with hydraulic press (with approximately 1 metric ton of applied pressure) and then heated up multiple times in an open to air boat-shaped alumina crucible using a programmable box furnace to achieve the following net reaction:

$$2\ CaCO_3 + MgCO_3 + 2\ SiO_2 \rightarrow Ca_2MgSi_2O_7 + 3\ CO_2\ (g)$$

The initial heat treatment was carried out at 950 °C (after increasing the furnace chamber temperature from room temperature at rate of 100 °C/h) for 48 hours. This intermediate reaction,

which involves the conversion of the carbonate starting materials to oxides, was then allowed to cool down back to room temperature by heat loss through the top exhaust port of the furnace. The pellet was then weighed to confirm the mass loss of approximately 0.8 g (or 18.5 mmol) of carbon dioxide. Subsequent heat treatments involved additional grinding, pellet pressing, and heating the crude product at the dwell temperature of 1300°C (after ramping up the temperature from room temperature at rate of 100°C/h) for 48 hours. Each 48 hour heat treatment was followed by cooling back to room temperature by furnace exhaust. The number of heat treatments at 1300°C required was dictated by proof of desired product purity (as judged by powder X-ray diffraction) and typically varied with each batch from 2 to 3 times.

5.2.2. Synthesis of Ceramic Scaffolds

Akermanite and β-tricalcium phosphate (β-TCP) powders (3 g) were suspended in polyvinyl alcohol aqueous solution (10 wt %) and stirred in a glass beaker to obtain a well-dispersed slurry (Liu et al., 2008). Polyurethane foam templates were cut into the desired shape and sizes (5mmX4mm) to replicate a porous scaffold. Then, the prepared templates were immersed in a glass beaker containing akermanite or β-TCP slurry and compressed with glass stick to force the slurry to migrate into the pores of the foams which were then incubated at 60°C for 1 day. After drying, the scaffolded materials (either akermanite or β-TCP) were placed in an open to air boat-shaped alumina crucible and heated up in a programmable box furnace from room temperature (at rate of 50°C/h) to 500°C and allowed to dwell this temperature for 5 hours in order to burn off the polyurethane foam. After allowing the furnace to cool down to room temperature by furnace exhaust, the scaffolds were then heat treated at 1300°C (increasing the furnace chamber temperature from room temperature at rate of 60°C/h) for 3 hours and cooled back down by furnace exhaust.

5.2.3. Fabrication of PCL and Akermanite:PCL Scaffolds

Composites (akermanite:PCL) and pure PCL solutions were frozen at -80°C overnight. A 10% PCL solution in 8 ml of 1-4, dioxane was prepared and akermanite was added at weight (g) ratio of 0,0:0,8 (PCL) and 0.6:0.2 (75:25 akermanite:PCL wt.%) in a glass bottle. The mixtures were molded into 5mmX4mm polydimethylsiloxane (PDMS) templates and immediately incubated in a freeze-drier for 48 hours.

5.2.4. Adult Stem Cells Isolation and Culture

Liposuction aspirates from subcutaneous adipose tissue were obtained from male (n = 1) and females (n = 2) subjects undergoing elective procedures. All tissues were obtained with informed consent under a clinical protocol reviewed and approved by the Institutional Review Board at the Pennington Biomedical Research Center. Isolation of hASC was performed as described elsewhere (Gimble et al., 2011). Briefly, tissues was washed 3–4 times with phosphate buffered saline and suspended in an equal volume of PBS supplemented with 1% bovine serum and 0.1% collagenase type I. The tissues were placed in a shaking water bath at 37°C with continuous agitation for 60min and centrifuged for 5min at 300–500g at room temperature. The supernatant, containing mature adipocytes was then aspirated. The cell pellet, referred to as the stromal vascular fraction (SVF), was suspended and plated immediately in T125 flasks in stromal medium at density of 0.156ml of tissue digest/cm^2 of surface area for expansion and culture. Human bone marrow-derived stem cells (hBMSC) were isolated from the bone marrow of three females at Tulane University School of Medicine. The initial passage of each adult stem cell type was referred to as ‘‘Passage 0’’ (p0). The cells were passaged after trypsinization and plated at a density of 5,000 cells/cm^2 (‘‘Passage 1’’) for expansion on T125 flasks until 80% of

confluence was reached. Passage 2 of each individual and cell type was used for *in vivo* ectopic bone formation studies.

5.2.5. hASC Loading on Scaffolds and Culture

Passage 2 of each donor (n = 3) and adult stem cell type were pooled together and directly loaded on the top of each scaffold type at loading density of $5.0X10^4$ cells/5μL. After 30 min of incubation at 37°C and 5% CO_2, the same process was repeated on the opposite top of each scaffold. Experimental groups included: akermanite:PCL, akermanite, PCL, β-TCP and CellCeramic™. After overnight incubation at 37°C and 5% CO_2, scaffolds with or without each adult stem cells type were subcutaneously implanted in adult male immunodeficient (nude) mice [1 scaffold type (with and without cells)/mouse] with sample collection performed 8 weeks post-implantation to assess ectopic bone formation (Figure 21).

5.2.6. *In* vivo Implantation in Nude Mice

Five adult male immunodeficient mice were divided in five groups (akermanite:PCL, akermanite, PCL, β-TCP and CellCeramic™) for each stem cell type. Animals were anesthetized with isofluorane. Three incisions were made just dorsal to the midline of each animal and the subcutaneous pockets were made parallel to each side. Scaffolds were implanted in the pockets (6 pockets per animal) and the skin incisions were apposed using stainless steel Michel clips. Each mouse had one scaffold type (with and without cells) implanted into subcutaneous pockets (Figure 21). Eight weeks post-implantation, PCL, β-TCP and CellCeramic™ scaffolds were harvested immediately post-mortem following humane euthanasia and divided for expression of mature osteogenic marker, histological analysis and bone deposition.

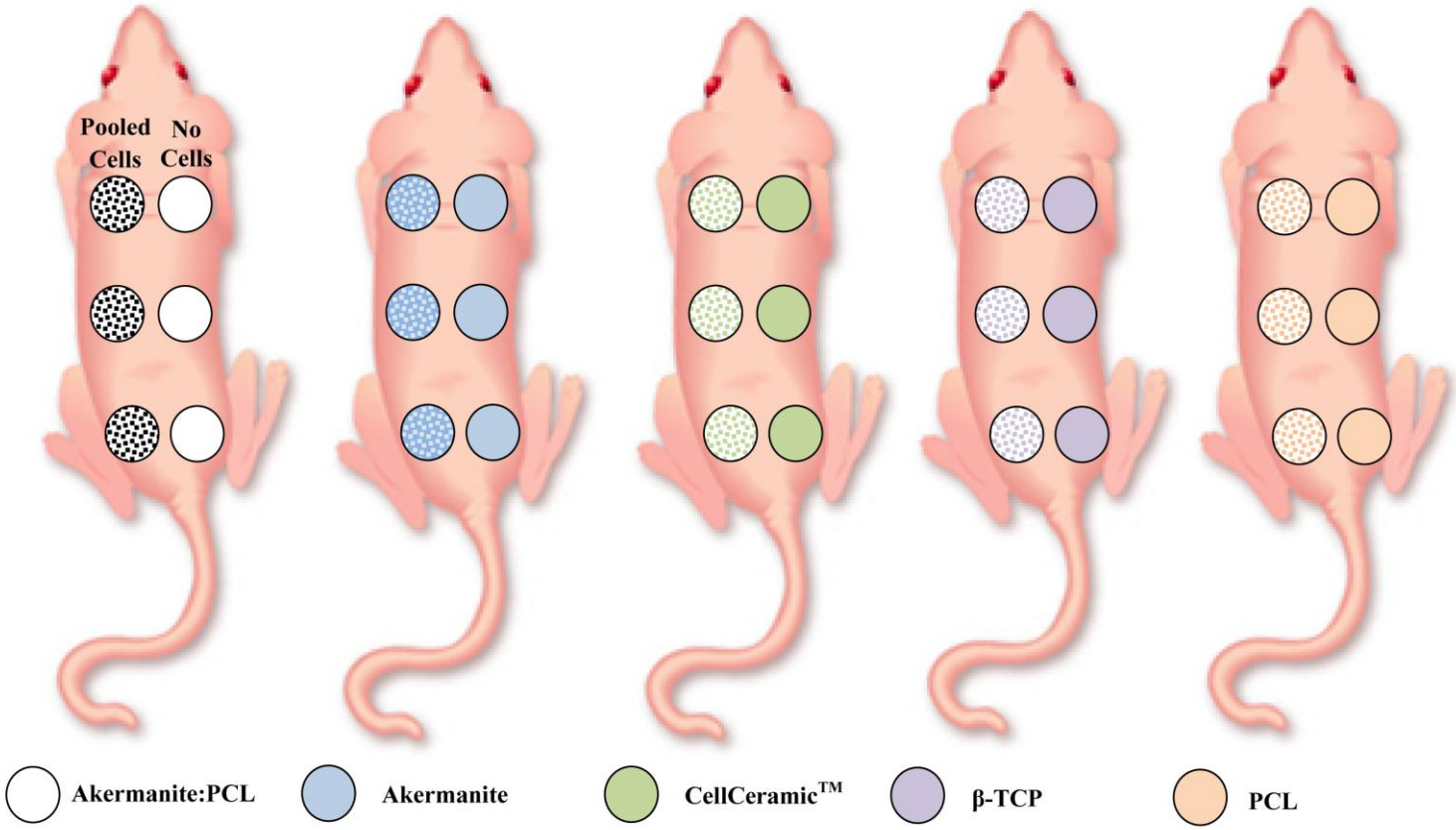

Figure 21. Experimental design for *in vivo* evaluation of 5 bone substitute scaffolds. Briefly, three scaffolds (with and without adult stem cells pooled from 3 individuals) were subcutaneously implanted in opposite sides as shown (one mouse/scaffold type/stem cell type). Ectopic bone formation of PCL, β-TCP and CellCeramic™ scaffolds loaded with hASC and hBMSC were compared 8 weeks post-implantation.

5.2.7. Effect of Ionic Dissolution of Akermanite and Akermanite:PCL Scaffolds

The dissolution of akermanite and akermanite:PCL scaffolds 48 hours post-implantation was prepared by overnight nitric acid digestion. The ratio of the akermanite and akermanite:PCL weight and the medium volume was 200 mg/mL. The ionic concentration of calcium, magnesium, silicon and phosphorous on the akermanite and akermanite:PCL digests was measured by inductively coupled plasma spectroscopy (ICP-OES) as previously described (Wu et al., 2006b).

5.2.8. Characterization of the Ionic Composition on the Surface of Akermanite and Akermanite:PCL Scaffolds

The percentage of calcium, magnesium, silicon and phosphorous on the surface of akermanite and akermanite:PCL scaffolds 48 hours post-implantation was assessed with X-ray Photoelectron Spectroscopy (XPS) in a Kratos Axis-165 XPS/AES instrument (Kratos).

5.2.9. Quantitative Real Time Polymerase Chain Reaction (QPCR)

Total RNA was extracted from cell-scaffolds (PCL, β-TCP and CellCeramic^{TM}) using the Trizol reagent (Sigma). QPCR was performed using 2X iTaq SYBR green with ROX (Biored) and osteocalcin (OCN) forward (5'- GCCCAGCGGTGCAGAGT -3') and reverse (5'-TAGCGCCTGGGTCTCTTCAC -3') to assess expression of mature osteogenic marker in hASC loaded to scaffolds 8 weeks post-implantation. Reactions were performed with a MJ Mini Thermal Cycler (BioRad). Water (negative) and hASC culture in osteogenic medium for 21 days were used as controls. Samples were normalized (ΔCt) against the house keeping gene 18SrRNA and the fold change expression of OCN in scaffolds preloaded with adult stem cells was compared to scaffolds implanted without cells using the ΔΔCt method (Liu et al., 2008).

5.2.10. Histological Analysis

The constructs were washed in PBS and fixed in 10% formalin for 1 day, decalcified with immunocal solution (Decal Chemical) for 3 hours, dehydrated with graded ethanol washes, embedded in paraffin, sectioned to 9 μm, stained with hematoxilin & eosin (H&E) and mounted on glass slides.

5.2.11. Micro-computed Tomography (μ-CT)

Samples were aligned along their axial direction and stabilized with wet gauze in a 1.5 mL centrifuge tube. The tubes were clamped in the specimen holder of a vivaCT 40 system (SCANCO Medical AG, Basserdorf, Switzerland). The 4 mm length of the scaffold was scanned at 21 mm isotropic resolution. The radiodensity of the scaffolds (PCL, β-TCP and CellCeramic^{TM}) 8 weeks post-implantation (bone formation) was normalized to pre-implanted scaffolds.

5.2.12. Statistical Analysis

All results were expressed as mean ± SEM. Normality of the data was confirmed using the Shapiro-Wilk test ($P < 0.001$). Data was analyzed with one-way analysis of variance (ANOVA), followed by Tukey's minimum significant difference (MSD) post hoc test for pairwise comparisons of main effects. For all comparisons, a *P*-value of 0.05 was considered significant.

5.3. Results

5.3.1. *In Vivo* Akermanite and Akermanite:PCL Scaffolds Acute Toxicity

Within the first 36 hours post-implantation, sudden death was observed in animals implanted with akermanite scaffolds loaded with hASC and akermanite:PCL scaffolds (both stem cell types). At 48 hours post-implantation, severe hypothermia and weakness were observed in the mouse implanted with akermanite scaffolds loaded with hBMSC (Figure 22).

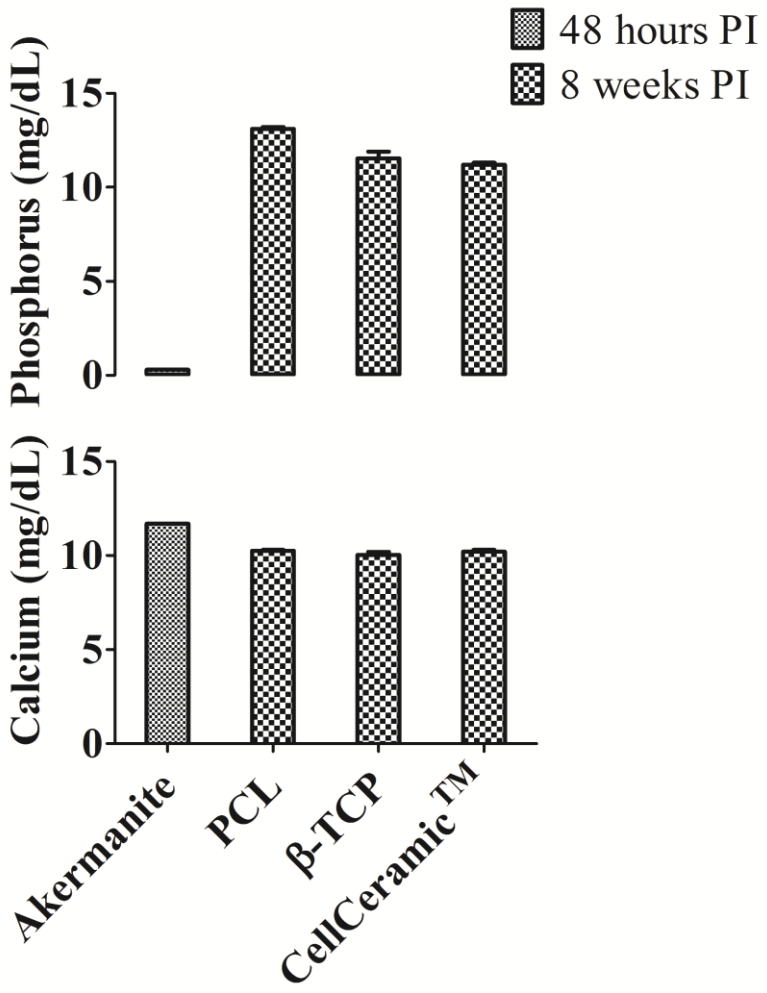

Figure 22. Calcium and phosphorus blood content 48 hours post-implantation (PI) in a mouse implanted with akermanite scaffolds loaded with hBMSC and mice implanted with PCL, β-TCP and CellCeramic™ scaffolds 8 weeks post-implantation.

Cardiac puncture after human euthanasia revealed hemolysis and chemistry analysis of the hemolyzed blood revealed severe hypophosphatemia (< 0.3 mg/dL - Figure 22). Based on this information, the sudden death and clinical signs observed within the first 48 hours post-implantation in mice implanted with akermanite and akermanite:PCL scaffolds were initially attributed to severe phosphorous deficiency. Animals implanted with PCL, β-TCP and CellCeramic^{TM} scaffolds (both stem cell types) displayed normal blood phosphorous values 8 weeks post-implantation (11.95±1.01 – Figure 22).

5.3.2. ICP-OES Analysis of Akermanite and Akermanite:PCL Scaffolds

The calcium (17.82±2.17), magnesium (2.91±0.31) and silicon (2.03±0.67) contents in akermanite scaffolds 48 hours post-implantation were significantly higher than in akermanite:PCL scaffolds (4.77±1.62; 0.75±0.27; 0.10±0.01, respectively), however no significant differences in phosphorus (akermanite – 0.73±0.10; akermanite:PCL – 0.56±0.05) were observed between both scaffold types (Figure 23).

5.3.3. XPS Analysis of Akermanite and Akermanite:PCL Scaffolds

Figure 24 represents the percentages of calcium, magnesium, silicon and phosphorous on the akermanite and akermanite:PCL scaffolds surface within the first 48 hours of this study. In general, no significant differences on the ionic percentage of these elements were observed on the surface of both scaffold types.

5.3.4. Macroscopic Changes in PCL, β-TCP and CellCeramic^{TM} Scaffolds 8 Weeks Post-Implantation

Scaffolds harvested from nude mice 8 weeks post-implantation had grossly different color patterns (Figure 25A). PCL and CellCeramic^{TM} scaffolds preloaded with hASC had a marked

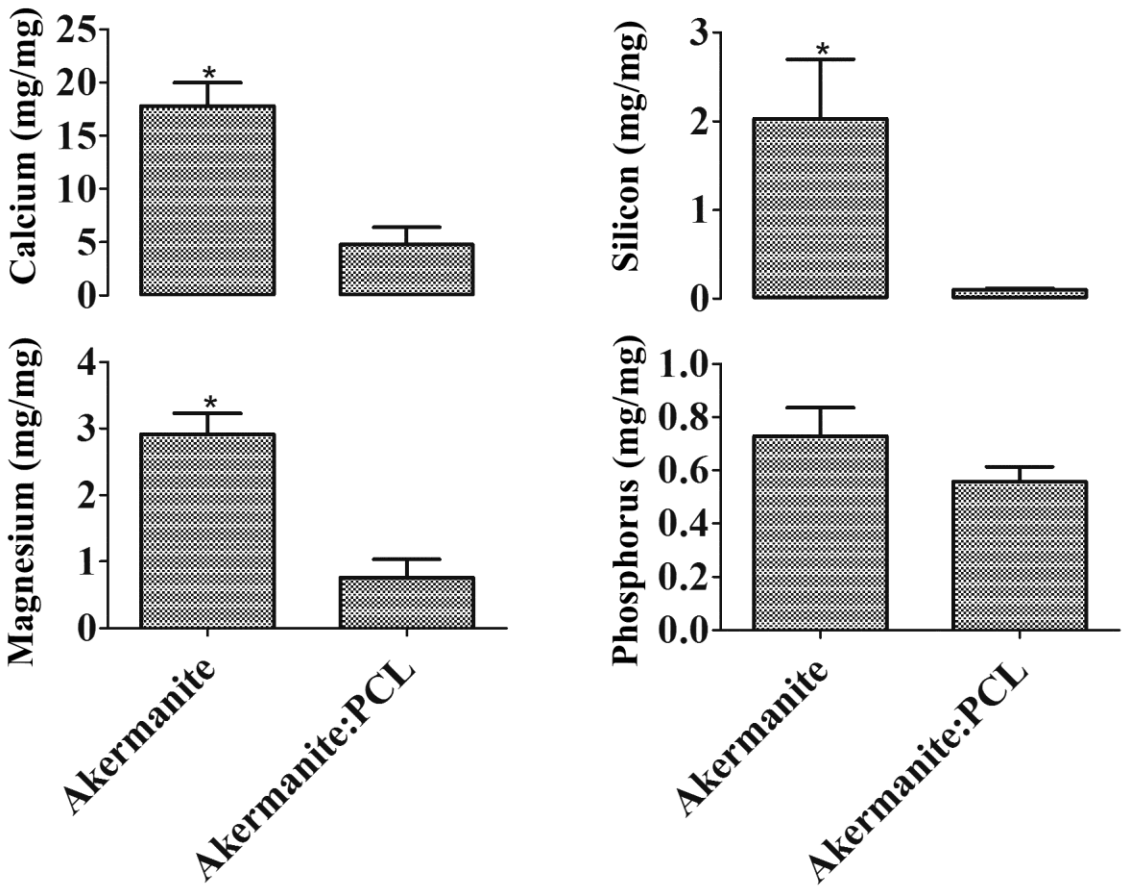

Figure 23. Ionic content in akermanite and akermanite:PCL scaffolds 48 hours post-implantation. *Represent significant differences between scaffold types (Tukey's test, $P < 0.05$).

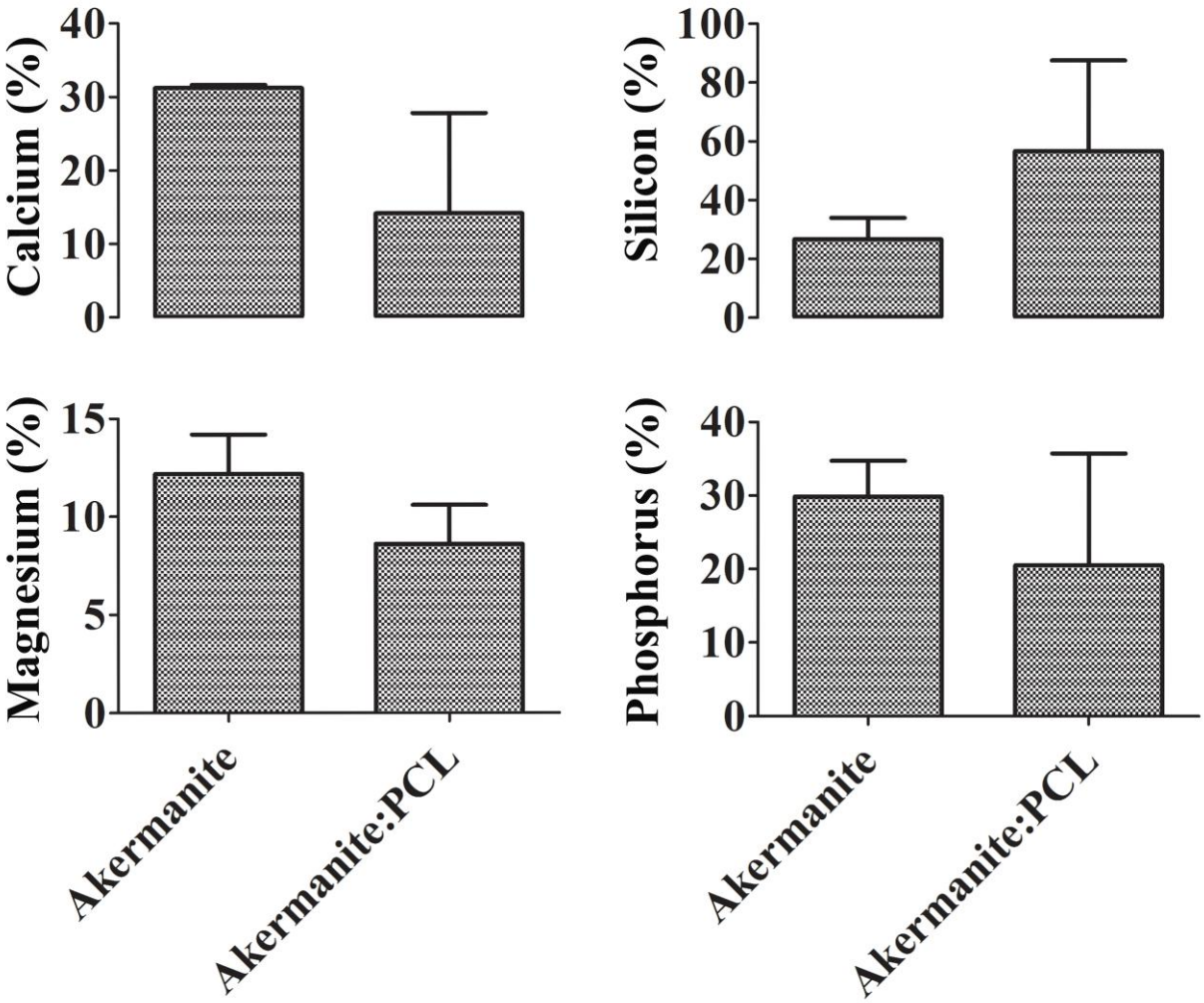

Figure 24. Percentage of calcium, magnesium, silicon and phosphorus on the surface of akermanite and akermanite:PCL scaffolds 48 hours post-implantation (Tukey's test, $P > 0.05$).

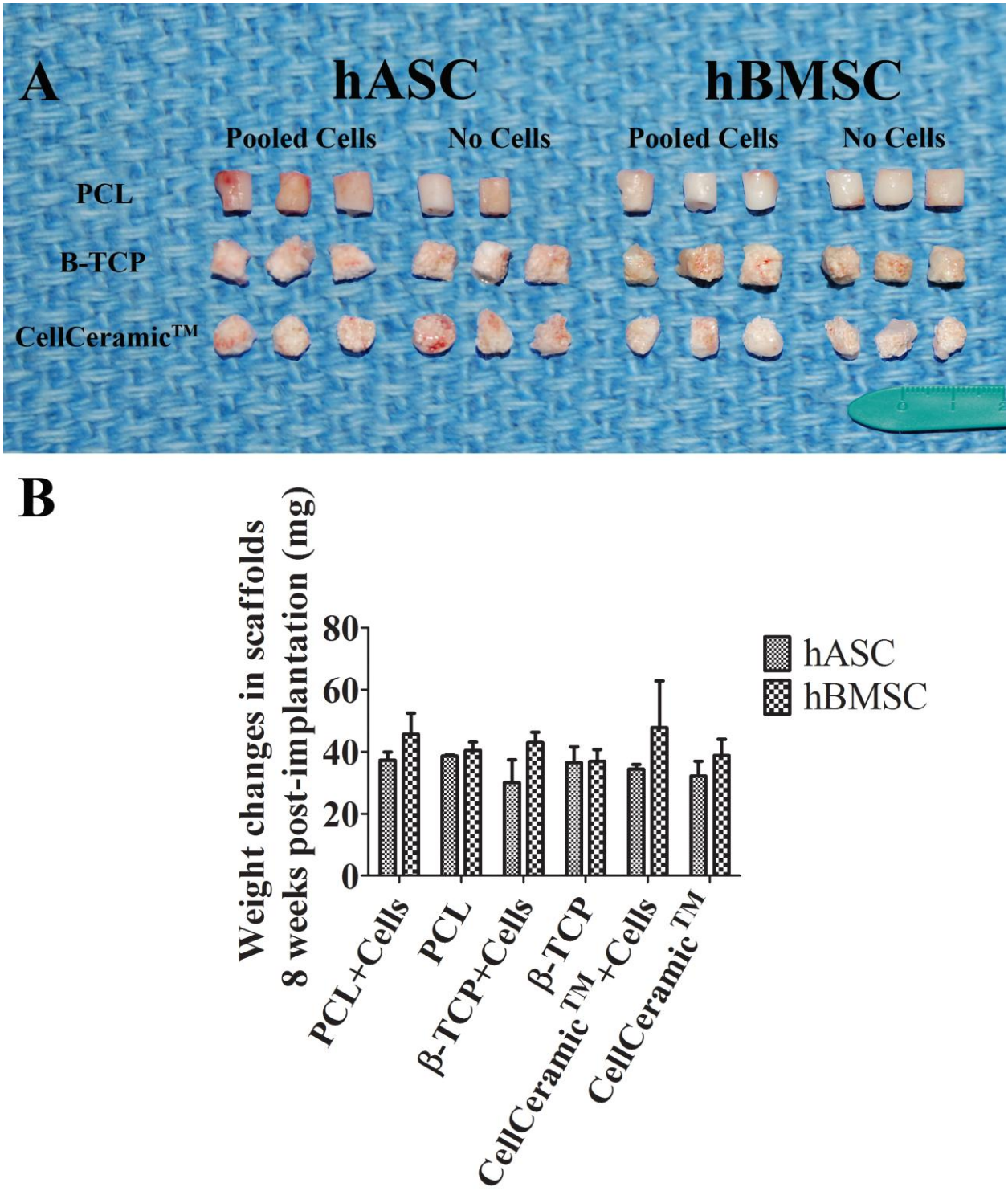

Figure 25. Qualitative analysis of PCL, β-TCP and CellCeramic™ scaffolds 8 weeks post-implantation (A). In B, weight gain (in mg) of the scaffolds 8 weeks post-implantation (Tukey's test, $P > 0.05$).

reddish coloration compared to scaffolds preloaded with hBMSC or scaffolds implanted without hBMSC. Color changes were also observed in β-TCP scaffolds preloaded with hASC and hBMSC or β-TCP scaffolds implanted without adult stem cells, but no noticeable differences between them.

Figure 25 also depicts the weight gain of PCL, β-TCP and CellCeramic^{TM} scaffolds 8 weeks post-implantation (B). In general, the scaffolds gained in average 38.47±5.2 mg in weight 8 weeks post-implantation but no significant differences between scaffolds or adult stem cell types were observed.

5.3.5. Quantitative Real-Time Polymerase Chain Reaction (QPCR)

The OCN fold change between scaffolds preloaded with adult stem cells and scaffolds implanted without cells is represented in Figure 26. According to the results, significant differences in the OCN expression were observed within each scaffold and adult stem cell types, with the exception of PCL (23.42±2.531) and CellCeramic^{TM} (32.24±2.935) preloaded with hASC, which were not significant different.

Within scaffolds preloaded with hBMSC, the OCN fold change 8 weeks post-implantation was the highest in β-TCP (842.89±60.08) scaffolds, which was significantly higher than the OCN fold change observed in CellCeramic^{TM} (78.54±9.59) and PCL (5.39±2/88). In scaffolds preloaded with hASC, the OCN fold change 8 weeks post-implantation was the highest in β-TCP (59.16±1.66) scaffolds which was significantly higher than the OCN fold change observed in PCL and CellCeramics^{TM} scaffolds. Moreover, comparisons between the OCN fold change in scaffolds preloaded with hASC and hBMSC, indicated that after 8 weeks, hASC-scaffolds had OCN expression significantly higher than hBMSC-scaffolds only in hASC preloaded to PCL scaffolds.

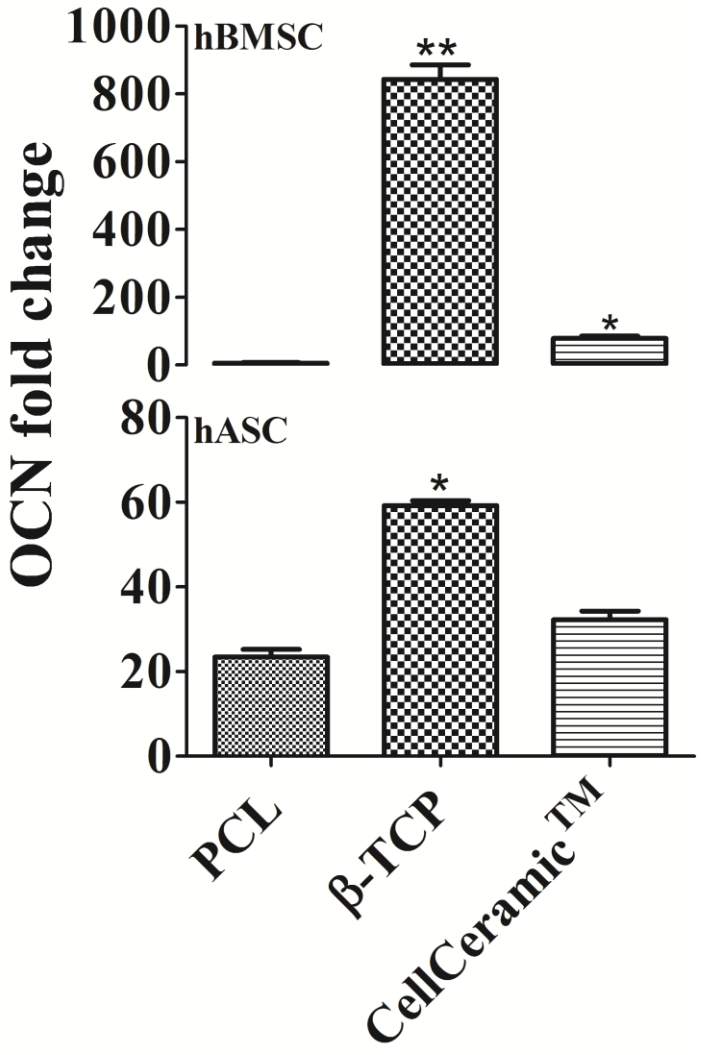

Figure 26. Fold change expression of OCN in PCL, β-TCP and CellCeramic™ scaffolds preloaded with hASC and hBMSC compared to scaffolds implanted without adult stem cells. *Represent significant differences between scaffold types loaded with the same adult stem cell source (Tukey's test, $P < 0.05$).

5.3.6. Morphological Analysis of Implanted Scaffolds

Routine H&E staining of PCL (a-d), β-TCP (e-h) and CellCeramic^{TM} (i-l) scaffolds 8 weeks post-implantation indicated high cell proliferation and a very dense collagenous matrix in all scaffolds tested independent of the presence or absence of hASC or hBMSC in pre-implanted scaffolds (Figure 26). In general, this extracellular matrix (ECM) resembled the osteoid tissue formed prior to the maturation of bone tissue and its mineralization. However, no frank bone, with its typical histological morphology, was observed in any of the scaffolds.

Within the scaffolds preloaded with human adult stem cells, ECM deposition 8 weeks post-implantation was higher in hASC-scaffolds (a, e and i) than in hBMSC-scaffolds (c, g and k). Additionally, between scaffold types, similar ECM deposition was observed in hASC-scaffolds (a, e and i), however, in hBMSC-scaffolds ECM deposition was higher in β-TCP (g) and CellCeramic^{TM} (k) than in PCL (c) scaffolds.

Signs of neovascularization were observed in β-TCP scaffolds preloaded with hASC (e – arrowhead) and hBMSC (g – arrowhead). One of these blood vessels contained erythrocytes inside (g – arrowhead), indicating that they were functionally connected to the vasculature of the host. Erythrocytes were also observed in PCL scaffold preloaded with hBMSC (c – arrowhead) and in PCL scaffolds implanted without hASC (b – arrowhead), also suggesting migration of host cells through the newly formed vessels in all tested scaffolds.

5.3.7. *In Vivo* Bone Density Formation

Compared to μ-CT images taken in pre-implanted scaffolds (time point 0); noticeable differences in the scaffolds bone deposition 8 weeks post-implantation were observed only in PCL scaffolds (Figure 28). In general, after 8 weeks, no significant differences in the

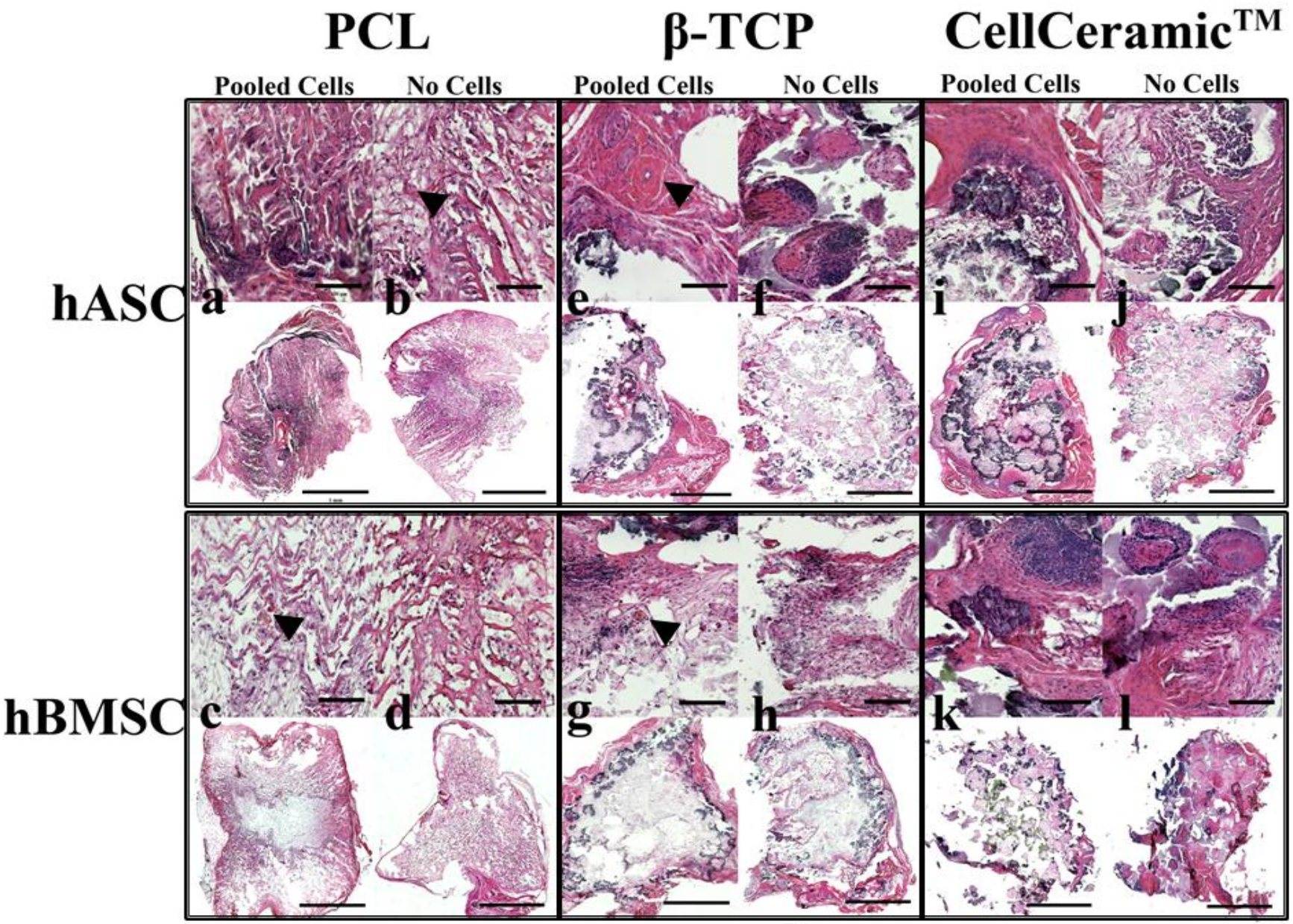

Figure 27. Morphological changes in PCL (a-d), β-TCP (e-h) and CellCeramic™ (i-l) scaffolds 8 weeks post-implantation in nude mice. Increased cell proliferation and extracellular matrix deposition can be observed at high magnifications (20x – scale bar 100 μm) in all scaffold tested independent of the presence or the type of adult stem cells preloaded to the scaffolds. Moreover, erythrocytes (b and c) and neovascularization (e and g) can be observed, respectively, in PCL and β-TCP scaffolds (arrowhead). Panoramic view of each scaffold type can be observed at low magnifications (2.5x – scale bar 1 mm).

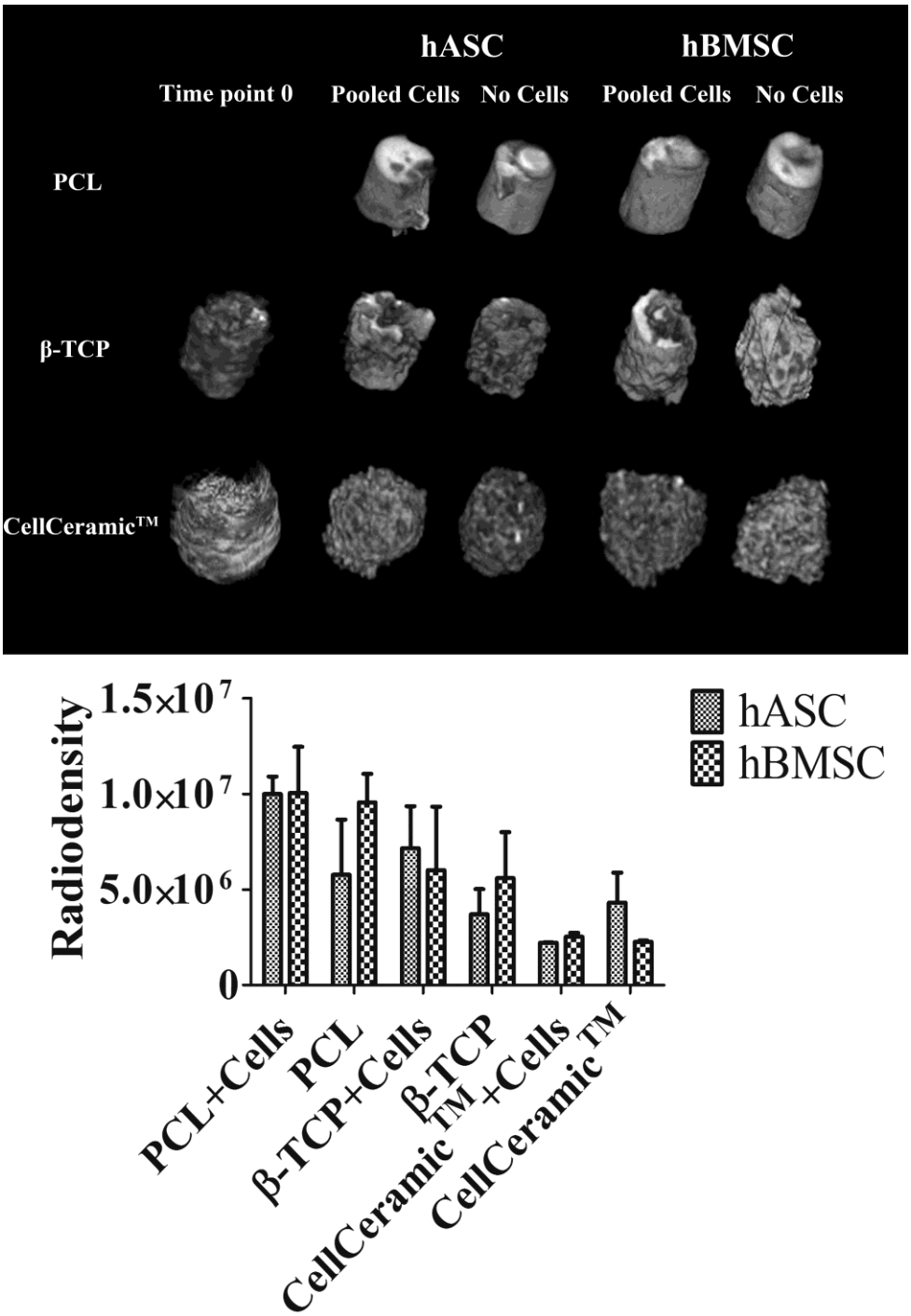

Figure 28. Microcomputer tomography analysis pre-implantation (time point 0) and 8 weeks post-implantation in PCL, β-TCP and CellCeramic^{TM} scaffolds. Note that at time point 0, PCL scaffolds were not radiodense. Moreover, quantitative analysis indicated no significant differences between the radiodensity of same scaffold types 8 weeks post-implantation independent of the presence of hASC or hBMSC (Tukey's test, $P > 0.05$).

radiodensity of scaffolds preloaded with adult stem cells and scaffolds implanted without cells were observed within each scaffold type. The average radiodensities of PCL, β-TCP and CellCeramic^{TM} scaffolds 8 weeks post-implantation were, respectively, 8844738.75±2061543.79, 5616419.54±1435693.65 and 2833596.75±1001725.68 ($P > 0.05$).

Significant differences in the radiodensity of different scaffolds 8 weeks post-implantation were observed only between PCL scaffolds preloaded with hASC or hBMSC (average 10023553±36397.61) or PCL scaffold implanted without hBMSC (10049286.43±4174207.85) which had radiodensity significantly higher than β-TCP scaffolds implanted without hASC (3707187.66±2276128.72) and CellCeramic^{TM} scaffolds preloaded with hASC and hBMSC or implanted without hBMSC (average 2337684.55±234983.60).

5.4. Discussion

Identification of scaffolding materials that display consistent *in vivo* osteogenesis independent of the human adult mesenchymal stem cells source is highly desirable in many bone tissue engineering applications (Reichert & Hutmacher, 2011). In an experimental point of view, the utilization of biomaterials with similar properties under human adult mesenchymal stem cells stimulation could also facilitate comparisons between current *in vivo* protocols (Gimble et al., 2011). In this study, we evaluated five different biomaterials with recognized bone formation potential in nude mice. However, within the initial 48 hours of this study, acute phosphorous depletion toxicity was associated with subcutaneous implantation of two of those bone substitute scaffolds (akermanite and akermanite:PCL). *In vivo* comparisons of ectopic bone formation were carried out 8 weeks post-implantation in pure porous PCL, β-TCP and CellCeramic^{TM} scaffolds preloaded with hASC and hBMSC. Due to the PCL slow *in vivo* degradation and neovascularization potential, this study indicated that PCL scaffolds preloaded with hASC and

hBMSC displayed similar radiodensity to PCL scaffolds implanted without cells or ceramic scaffolds 8 weeks post-implantation. However, even though the expression of mature osteogenic marker was higher in hASC-PCL than in hBMSC-PCL scaffolds, after 8 weeks, the highest OCN expression was observe in β-TCP scaffolds preloaded with hBMSC.

In this study, we observed an unexpected acute dose-dependent toxicity in animals assigned to the akermanite and akermanite:PCL scaffolds 48 hours post-implantation. Over the past years, accumulative evidences have suggested that akermanite is biocompatible and can enhance adhesion, proliferation and osteogenic phenotype maintenance of mature osteoblasts, hBMSC and hASC (Agathopoulos et al., 2005; Sun et al., 2006; Wu et al., 2006ab; Wu et al., 2007; Chen at al., 2010; Gu et al., 2011). However, we could not foresee the deleterious effects of akermanite overexposure in the animal model selected for this study, because a femur defect model had been successfully proposed to study akermaninte osteogenesis in rabbits (Huang et al., 2009).

Within the first 48 hours of this study, we initially suspected that the signs of phosphorus deficiency observed in all animals implanted with akermanite and akermanite:PCL scaffolds was associated with disturbance of the magnesium and phosphorous homeostasis (DiBartole DiBartola & Willard, 2011), because *in vitro* leaching of magnesium ions from akermanite scaffolds had been previously reported (Wu et al., 2006ab ; Gu et al., 2011) and it seems to be related in part, to the enhanced osteogenic potential of hASC exposed to akermanite media extracts (Gu et al., 2011). However, ICP-OES and XPS analysis indicated comparable phosphorous content in the akermanite and akermanite:PCL scaffolds harvested 48 hours post-implantation, which confirmed the acute phosphorous depletion observed in the murine serum. Phosphorus plays an essential role in cellular structure and function (DiBartola & Willard, 2011).

As a constituent of structural phospholipids in cell membranes and hydroxyapatite in bone, phosphorus also is an integral component of nucleic acids and phosphoproteins involved in mitochondrial oxidative phosphorylation. Consequently, severe hypophosphatemia can cause many detrimental effects (DiBartola & Willard, 2011). As observed in this study, hypophosphatemia associated with akermanite depletion of phosphorous, lead to hemolysis due to the increased erythrocyte fragility associated with the decreased concentration of ATP in the blood (DiBartola & Willard, 2011). Moreover, the neuromuscular signs observed 48 hours post-implantation were also associated with the akermanite scaffolds, because decreased phosphate can impair central nervous system glucose use and ATP production, leading to metabolic encephalopathy, which can be fatal (DiBartola & Willard, 2011). Therefore, the increased ability that akermanite has to form apatite-like layers at a physiological fluid interface (Sun et al., 2006; Liu et al., 2008; Gu et al., 2011) seems to have played a role in the acute toxicity associated with the akermanite scaffolds used in this study. Further studies are needed to address the akermanite dose-dependent toxicity in murine models for akermanite-assisted bone regeneration.

Evaluation of the *in vivo* ectopic bone formation of PCL, β-TCP and CellCeramic™ scaffolds revealed remarkable similarities between the bone substitute scaffolds independent of the presence of hASC or hBMSC 8 weeks post-implantation. According to the results, all scaffolds tested displayed similar weight gains after 8 weeks; however μ-CT images revealed increased bone formation in PCL and β-TCP scaffolds. Further morphologic analysis, revealed a very dense collagenous matrix resembling osteoid tissue in all scaffolds independent of the presence of hASC and hBMSC, however, no bone-like tissue, with its typical histological morphology, was observed in any of the scaffolds.

Osteogenesis is known to be regulated by bone morphogenic proteins (BMPs) which have been reported to stimulate the transcription factor core binding factor alpha1 (Cbfa1) by activating osteoblast-specific genes such as OCN through the binding to the osteoblast-specific cis-acting element 2 (OSE2) in the promoter region of these genes (Liu et al., 2008; Gu et al., 2011). In this study, OCN was also used to asses mature osteogenic differentiation of the scaffolds preloaded with hASC and hBMSC. Even though the OCN expression was higher in hASC-PCL than in hBMSC-PCL scaffolds, after 8 weeks, the highest OCN expression was observe in β-TCP scaffolds preloaded with hBMSC. β-TCP is known to stimulate adult stem cells osteogenesis (Sun et al., 2006; Liu et al., 2008; Huang et al., 2009). Therefore, the results presented in this study can be also used to support the osteoinductive potential of β-TCP in bone tissue engineering applications.

The similarities observed in this study between PCL and other two bone substitute scaffolds, in terms of weight gain and radiodensity, might had been associated with the fast *in vivo* degradation potential of β-TCP and CellCeramic^{TM} scaffolds (Bouler et al., 2000; Gaalen et al., 2008; Liu et al., 2008; Marino et al., 2010). Synthetic apatites degrade overtime through physiochemical dissolution and phagocytosis (Bouler et al., 2000; Gaalen et al., 2008; Chen et al., 2010). PCL has slow degradation *in vivo* (Leong et al., 2006; Gaalen et al., 2008; Zhang et al., 2009; Fabbri et al., 2010), therefore, the comparable weight gains and the calcified ECM deposition observed between the scaffolds after 8 weeks could have been the result the stability of the PCL scaffolds.

In this study, scaffolds implanted without hASC and hBMSC had weight gains, radiodensities and morphological features similar the observed in scaffolds preloaded with either adult stem cell type. As observed in the histological sections, neovascularization could had

offered an avenue for host cell migration, adhesion and proliferation in the implanted scaffolds. Further investigations to assess the presence of human sex chromosomes in scaffolds implanted without cells would be beneficial to determine the origin of the cells adhered to the scaffolds 8 weeks post-implantation, as previously described (Levi et al., 2010).

As a conclusion, we observed in this study that PCL scaffolds had weight gain, radiodensity and morphological features similar to the observed in β-TCP and CellCeramic^{TM}, independent of the presence or the source of the adult stem cells. However, increased OCN expression was observed in β-TCP scaffolds preloaded to hBMSC. Host cell migration might had played a role in the high cell proliferation and matrix deposition observed in scaffolds implanted without cells, but further investigations are needed to identify the origin of those cells. Finally, the sudden death observed in nude mice implanted with akermanite and akermanite:PCl within the first 48 hours of this study was associated to acute phosphorous depletion from the blood. Further investigations are also needed to determine an optimal akermanite dose for murine models.

5.5. References

Gaalen S, Kruyt M, Meijer G, et al., 2008; Tissue Engineering of Bone. In: Clemens van Blitterswijk . *Tissue Engineering* 740.

Reichert JC, Hutmacher DW. 2011; Bone tissue engineering. In: Pallua. *Tissue Eng* 643.

Arrington ED, Smith WJ, Chambers HG, et al., 1996; Complications of iliac crest bone graft harvesting. *Clin Orthop Relat Res* **329**: 300-309.

Ahlmann E, Patzakis M, Roidis N, et al., 2002; Comparison of anterior and posterior iliac crest bone grafts in terms of harvest-site morbidity and functional outcomes. *J Bone Joint Surg Am* **84**: 716-720.

Boden SD. 2000; Biology of lumbar spine fusion and use of bone graft substitutes: present, future, and next generation. *Tissue Eng* **6**: 383-399.

Bauer TW, Muschler GF: Bone graft materials. An overview of the basic science. *Clin Orthop Rel Res* 2000;371:10-27.

Hattori H, Sato M, Masuoka K, et al., 2004; Osteogenic potential of human adipose tissue-derived stromal cells as an alternative stem cell source. *Cells Tissues Organs* **178:** 2-12.

Scherberich A, Galli R, Jacquiery C, et al., 2007; Three-dimensional perfusion culture of human adipose tissue-derived endothelial and osteoblastic progenitors generates osteogenic constructs with intrinsic vascularization capacity. *Stem Cells* **25:** 1823-1829.

Dégano IR, Vilalta M, Bagó JR, et al., 2008; Bioluminescence imaging of calvarial bone repair using bone marrow and adipose tissue-derived mesenchymal stem cells. *Biomaterials* **29:** 427-437.

De Girolamo L, Sartori MF, Arrigoni E, et al., 2008; Human adipose-derived stem cells as future tools in tissue regeneration: osteogenic differentiation and cell-scaffold interaction. *Int J Artif Organs* **31:** 467-479.

De Girolamo L, Lopa S, Arrigoni E, et al., 2009; Human adipose-derived stem cells isolated from young and elderly women: their differentiation potential and scaffold interaction during in vitro osteoblastic differentiation. *Cytotherapy* **11:** 793-803.

Haimi S, Gorianc G. 2009; Characterization of zinc-releasing three-dimensional bioactive glass scaffolds and their effect on human adipose stem cell proliferation and osteogenic differentiation. *Acta Biomater* **5:** 3122-3131.

Haimi S, Moimas L, Pirhonen E, et al., 2009; Calcium phosphate surface treatment of bioactive glass causes a delay in early osteogenic differentiation of adipose stem cells. *J Biomed Mater Res A* **91:** 540-547.

Haimi S, Suuriniemi N. 2009; Growth and osteogenic differentiation of adipose stem cells on PLA/bioactive glass and PLA/beta-TCP scaffolds. *Tissue Eng Part A* **15:** 1473-1480.

Gastaldi G, Asti A, Scaffino MF, et al., 2010; Human adipose-derived stem cells (hASCs) proliferate and differentiate in osteoblast-like cells on trabecular titanium scaffolds. *J Biomed Mater Res A* **94:** 790-799.

Marino G, Rosso F, Cafiero G, et al., 2010; Beta-tricalcium phosphate 3D scaffold promote alone osteogenic differentiation of human adipose stem cells: in vitro study. *J Mater Sci Mater Med* **21:** 353-363.

Muller AM, Mehrkens A. 2010; Towards an intraoperative engineering of osteogenic and vasculogenic grafts from the stromal vascular fraction of human adipose tissue. *Eur Cell Mater* **19:** 127-135.

Wang CZ, Chen SM, Chen CH, et al., 2010; The effect of the local delivery of alendronate on human adipose-derived stem cell-based bone regeneration. *Biomaterials* **31:** 8674-8683.

Lee JS, Lee JM. 2011; Electroporation-mediated transfer of Runx2 and Osterix genes to enhance osteogenesis of adipose stem cells. *Biomaterials* **32:** 760-768.

Bouler JM, LeGeros RZ, Daculsi G., 2000; Biphasic calcium phosphates: influence of three synthesis parameters on the HA/β-TCP ratio. *J Biomed Mater Res* **51:** 680–4.

Sun H, Wu C, Dai K, et al., 2006; Proliferation and osteoblastic differentiation of human bone marrow-derived stromal cells on akermanite-bioactive ceramics. *Biomaterials* **27:** 5651-5657.

Wu C, Chang J, Ni S, et al., 2006a; In vitro bioactivity of akermanite ceramics. *J Biomed Mater Res A* **76:** 73-80.

Wu C, Chang J, Zhai W, et al., 2006b; Porous akermanite scaffolds for bone tissue engineering: preparation, characterization, and in vitro studies. *J Biomed Mater Res B Appl Biomater* **78:** 47-55.

Wu C, Chang J, 2007; Degradation, bioactivity, and cytocompatibility of diopside, akermanite, and bredigite ceramics. *J Biomed Mater Res B Appl Biomater* **83:** 153-160.

Huang Y, Jin X, Zhang X, et al., 2009; In vitro and in vivo evaluation of akermanite bioceramics for bone regeneration. *Biomaterials* **30:** 5041-5048.

Gu H, Guo F, Zhou X, et al., 2011; The stimulation of osteogenic differentiation of human adipose-derived stem cells by ionic products from akermanite dissolution via activation of the ERK pathway. *Biomaterials* **32:** 7023-7033.

Agathopoulos S, Tulyaganov DU, Valerio P, et al., 2005; A new model formulation of the SiO2-Al2O3-B2O3-MgO-CaO-Na2O-F glass-ceramics. *Biomaterials* **26:** 2255-2264.

Chen X, Liao X, Huang Z, et al., 2010; Synthesis and characterization of novel multiphase bioactive glass-ceramics in the CaO-MgO-SiO(2) system. *J Biomed Mater Res B Appl Biomater* **93:** 194-202.

Liu Q, Cen L, Yin S, et al., 2008; A comparative study of proliferation and osteogenic differentiation of adipose-derived stem cells on akermanite and beta-TCP ceramics. *Biomaterials* **29:** 4792-4799.

Kneser U, Schaefer DJ, Polykandriotis E, et al., 2006; Tissue engineering of bone: the reconstructive surgeon's point of view. *J Cell Mol Med* **10:** 7-19.

Leong DT, Abraham MC, Rath SN, et al., 2006; Investigating the effects of preinduction on human adipose-derived precursor cells in an athymic rat model. *Differentiation* **74:** 519-529.

Leong DT, Nah WK, Gupta A, et al., 2008; The osteogenic differentiation of adipose tissue-derived precursor cells in a 3D scaffold/matrix environment. *Curr Drug Discov Technol* **5:** 319-327.

Zhang ZY, Teoh SH, Chong MS, et al., 2009; Superior osteogenic capacity for bone tissue engineering of fetal compared with perinatal and adult mesenchymal stem cells. *Stem Cells* **27:** 126-137.

Fabbri P, Bondioli F, Messori M, et al., 2010; Porous scaffolds of polycaprolactone reinforced with in situ generated hydroxyapatite for bone tissue engineering. *J Mater Sci Mater Med* **21:** 343-351.

Gimble JM, Bunnell BA, Guilak F, et al., 2011; Isolation and Growth of Stem Cells. In: Pallua. *Tissue Engineering* 643.

DiBartola SP, Willard MD. 2011; Disorders of phosphorous: Hypophosphatemia and hyperphosphatemia. *In:* DiBartola. *Fluid, Electrolyte, and Acid-Base Disorders in Small Animal Practice*. 4th Edition. Elsevier 195-212.

Levi B, James AW, Nelson ER, et al., 2010; Human adipose derived stromal cells heal critical size mouse calvarial defects. *PLoS One* **5:** e11177.

Chapter 6. Conclusions

The development of porous materials useful as scaffolds for the sustained 3D growth of hASC is of particular interest to facilitate healing after musculoskeletal injuries. While current scaffold materials facilitate the attachment of hASC by providing an interconnected pore structure to support cell migration, proliferation, differentiation and in some cases formation of blood vessels[40,47], the major limitations of pure ceramic scaffolds used today are their relatively poor mechanical properties and brittle behavior. As a consequence, the use of bioactive/bioabsorbable ceramics and bioabsorbable polymeric fiber reinforcement in the same composite structure are being explored as an alternative to address the mechanical limitations of pure ceramic scaffolds. To date, a clear trend towards the use of composite scaffolds can already be observed in current hASC-scaffolds bone tissue engineering models.

Of the bioactive ceramic materials current used in hASC bone tissue engineering, akermanite ($Ca_2MgSi_2O_7$), is the only biomaterial used entirely in its pure form. Compared to β-TCP and HA, akermanite scaffolds are believed to have a stable degradation rate and superior bone deposition. Moreover, the enhanced recruitment and osteogenic commitment of progenitor cells exposed to akermanite scaffolds, seems to be associated with the cells affinity for the Ca, Mg, and Si ions that makeup the akermanite scaffold backbone. Due to the enhanced biological and mechanical properties of akermanite in bone tissue engineering applications combined with hASC, we proposed in a series of hypotheses driven experiments the development of a novel composite scaffold suitable for hASC-assisted bone engineering.

In our first study, we characterized the scaffold properties (porosity, pore size, compressive strength and degradation) and hASC viability, attachment, proliferation and osteogenic differentiation to akermanite in the presence of PCL. As one of the most versatile synthetic

polymers currently used, PCL has been also proposed as composite scaffold in many hASC bone engineering studies. In our study, we determined that the combined mechanical, biological and osteogenic properties of 75:25 akermanite:PCL composite scaffolds should be further evaluated for bone repair applications combined with hASC.

As a result, in the next two *in vitro* studies, we characterized the osteogenic potential of hASC loaded to 75:25 akermanite:PCL scaffolds cultured in growth (control) and osteogenic media for 21 days; and we assessed the metabolic activity and osteogenesis of hASC loaded to 75:25 akermanite:PCL scaffolds in post-thawed scaffolds frozen at 5 different cooling rates in a PVP-serum free medium. According with these results, we observed that the metabolic activity and cell proliferation of hASC loaded to 75:25 akermanite:PCL scaffolds and cultured in growth (control) or osteogenic media proportionally decreased after 21 days, but were inversely proportional to the calcium deposition and expression of mature osteogenic marker (OCN) observed in 75:25 akermanite:PCL scaffolds cultured in osteogenic medium. For scaffolds frozen at different cooling rates, our results demonstrated that 75:25 akermanite:PCL scaffolds loaded with hASC can be cryopreserved with 10% PVP in serum-free medium. Moreover, after 10 days of culture, optimal hASC metabolic activity and osteogenesis were observed in scaffolds initially frozen at 40^{o}C/min. As a conclusion, the results of these two additional *in vitro* experiments indicated that hASC loaded to 75:25 akermanite:PCL scaffolds had enhanced bioactivity, which led us to further evaluate the biocompatibility of akermanite:PCL scaffolds *in vivo* using an immunodeficient murine model for ectopic bone formation.

Unexpectedly, within the first 48 hours of this *in vivo* experiment, we observed sudden death of all mice assigned to the akermanite and akermanite:PCL scaffolds. Based on the literature and the composition of the akermanite and akermanite:PCL scaffolds, we further evaluated the cause

of the mortality observed in this study. Results indicated comparable phosphorous content in all akermanite and akermanite:PCL scaffolds harvested 48 hours post-implantation. The results combined with the acute phosphorous depletion observed in the murine serum, confirmed the acute toxicity associated with akermanite-based scaffolds.

Over the past years, accumulative evidences have suggested that akermanite is biocompatible and can enhance adhesion, proliferation and osteogenic phenotype maintenance of adult/osteoprogenitor stem cells. However, we could not foresee the deleterious effects of akermanite overexposure in the animal model selected for this study, because a rabbit model for femur defect had been successfully proposed to study akermaninte osteogenesis. Therefore, the conclusion of this study is that further studies are needed to address the akermanite dose-dependent toxicity in murine models for akermanite-assisted bone regeneration.

Vita

Dr. Andrea S. Zanetti was born to Mr. Giuseppe Americo Zanetti and Ms. Marilene C. Serrano Zanetti in 1980. He was accepted into the School of Veterinary Medicine at Saint Paul State University (Unesp/Jaboticabal/Brazil) in 2001. After have received his Doctor of Veterinary Medicine in 2006 he came to the School of Veterinary Medicine at Louisiana State University in Baton Rouge to work as a D.V.M-postdoctoral researcher for one year before he was accepted into the Graduate School of the Louisiana State University to pursue his Master in Veterinary Medical Sciences in the department of Pathobiological Sciences of the School of Veterinary Medicine. He has a particular interest in surgery, clinical diagnoses and applied medical sciences and he plans to pursue a career as a surgeon to teach fundamental concepts of surgery and tissue engineering and regenerative medicine to veterinary students and to establish novel methods that will improve our understanding of disease pathology in veterinary as well as in comparative medicine. He is a LSU water polo player, plays tennis and lift weights.